University of Alberta

Selective Syntheses of Metal Nanoparticles and Characterization of the Interactions between Metal Nanoparticles and Blood

by

Yuan Gao 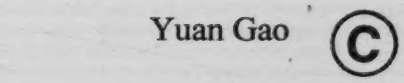

A thesis submitted to the Faculty of Graduate Studies and Research
in partial fulfillment of the requirements for the degree of

Master of Science

Department of Chemistry

Edmonton, Alberta

Fall, 2007

Library and Archives Canada

Published Heritage Branch

395 Wellington Street
Ottawa ON K1A 0N4
Canada

Bibliothèque et Archives Canada

Direction du Patrimoine de l'édition

395, rue Wellington
Ottawa ON K1A 0N4
Canada

Your file Votre référence
ISBN: 978-0-494-33245-0
Our file Notre référence
ISBN: 978-0-494-33245-0

NOTICE:
The author has granted a non-exclusive license allowing Library and Archives Canada to reproduce, publish, archive, preserve, conserve, communicate to the public by telecommunication or on the Internet, loan, distribute and sell theses worldwide, for commercial or non-commercial purposes, in microform, paper, electronic and/or any other formats.

The author retains copyright ownership and moral rights in this thesis. Neither the thesis nor substantial extracts from it may be printed or otherwise reproduced without the author's permission.

AVIS:
L'auteur a accordé une licence non exclusive permettant à la Bibliothèque et Archives Canada de reproduire, publier, archiver, sauvegarder, conserver, transmettre au public par télécommunication ou par l'Internet, prêter, distribuer et vendre des thèses partout dans le monde, à des fins commerciales ou autres, sur support microforme, papier, électronique et/ou autres formats.

L'auteur conserve la propriété du droit d'auteur et des droits moraux qui protège cette thèse. Ni la thèse ni des extraits substantiels de celle-ci ne doivent être imprimés ou autrement reproduits sans son autorisation.

In compliance with the Canadian Privacy Act some supporting forms may have been removed from this thesis.

While these forms may be included in the document page count, their removal does not represent any loss of content from the thesis.

Conformément à la loi canadienne sur la protection de la vie privée, quelques formulaires secondaires ont été enlevés de cette thèse.

Bien que ces formulaires aient inclus dans la pagination, il n'y aura aucun contenu manquant.

Canada

Dedication

To my parents and my sister Fu Xin

Abstract

This thesis describes some novel methods to synthesize metal nanoparticles with specific sizes and shapes, either in solution or on silicon surfaces. Generally, the metal nanoparticles can be obtained via thermal decomposition as well as galvanic displacement. We have also demonstrated the unique properties of amphiphilic block copolymers in size and shape selectivity and in surface patterning.

Since there are many possible routes for the nanoscale materials to enter the blood circulation system, we also investigated the interactions between metal nanoparticles and blood samples. The reactivity, stability, and aggregation state of such metal nanomaterials was examined both in simulated blood plasma solutions, with or without bovine serum albumin, and in real human blood samples, including blood plasma, blood serum, and whole blood.

Acknowledgements

It has been a great honor and opportunity for me to work with Professor Jillian M. Buriak, a knowledgeable, passionate and insightful chemist, for my graduate study. There are not enough words in my dictionary to express my sincere gratitude to her. She guided me into the brilliant palace of nanoscience and nanotechnology, giving me a chance to explore the beautiful world of materials chemistry. Her commitment and enthusiasm for chemistry, along with her dedication to excellence are a model that I will continue to live by and one day hope to achieve. Her openness to new ideas, trust without retention and encouragement throughout my graduate career help me find a way to develop myself into a truly independent researcher. I would not be able to complete this thesis without her consistent support and guidance. She will always be my role model for the rest of my life.

I would also like to thank Professor Bruce Ritchie for his supervising of the research entitled "Interactions between Metal Nanoparticles and Blood". The chance to work in his lab turned to be an extremely educational and highly rewarding experience for me. I would also like to extend my sincere gratitude to Professor Josef Takats for his consistent help and encouragement during my study in the Department of Chemistry at the University of Alberta, and especially for his helpful suggestions and valuable insight with regard to my thesis.

I am extremely grateful to the past and present members of the Buriak Group for their scientific involvement and extraordinary companionship. All of them made my

experience memorable, educational, rewarding and most importantly tolerable. Most notably, I want to express my great thanks to Dr. Jiguang Zhang as the collaborator for the work in Chapter 3. He has not only taught me a great deal about chemistry, but also shown me how to work successfully with others and enjoy yourself while doing it. I am also thankful to Dr. Dong Wang, Yinghong Qiao and Yunhui Li for their support in my research and thesis, as well as their invaluable friendships. I would like to acknowledge the contributions of Stephanie Bale. She is proof that we do not always learn from those that are more experienced than we are. Finally, I would like to thank Jennifer Bruce, Dr. Brian Daly, Dr. Vincent Wright, Dr. Masato Aizawa, Hidenori Mizuno, Sayed Nagy, Sean McClure, Steven Chai, Anne Copper, Xiaojiang Zhang, Jie Ru, Nicole Dehm, Xiang Xing, Dr. Kavithaa Loganathan, Dr. Lina Xu, Greg Nilsson, Xiangning Fan, Dr. Sang Sub Kim, and Kyle Park.

Most importantly I would like to thank the people who have supported me during my pursuit of a Master of Science. First and foremost, I give thanks to my parents and my sister Fu Xin. The never-ending support, patience and advice that they have given me throughout these years have allowed me to achieve my dream. I also thank Jie Sun, Hangqing Zhao, Hao Yuan, Bichu Cheng, Renzhuo Chen, Li Zhao, Rong Guo, Haiying Bie, Qingye Lv, Liya Cao, and Guibin Ma for going out of their way to provide me with some unimaginable friendships and memorable stories.

Financial support was provided by the NSERC Nano Innovation Platform.

Table of Contents

Chapter 1 Introduction 1

1.1 Research Objectives 1

1.2 Thesis Organization 2

Chapter 2 Literature Reviews 3

2.1 Introduction to Nanoscience and Nanotechnology 3

2.1.1 Definition 3

2.1.2 Unique Properties 4

2.1.3 Tools and Techniques 6

2.1.4 Typical Nanomaterials 12

2.2 Nanotoxicity 15

2.2.1 Introduction 15

2.2.2 Exposure Pathways 17

2.2.3 Interaction Mechanisms 20

2.2.4 Toxic Effects of Typical Nanomaterials 23

2.2.5 Summary 28

Chapter 3 Selective Syntheses of Metal Nanoparticles 29

3.1 Synthesis of Nanocrystalline Gold Octahedra Generated from Thermal Decomposition of $HAuCl_4$ in Block Copolymers 29

3.1.1 Introduction 29

3.1.2 Results 31

3.1.3 Conclusion 47

3.2 Block Copolymer Mediated Deposition of Metal Nanoparticles on Germanium Nanowires 49

3.2.1 Introduction 49

3.2.2 Results 53

3.2.3 Conclusion 62

Chapter 4 Interactions between Metal Nanoparticles and Blood 63

4.1 Interactions between Metal Nanoparticles and Simulated Blood Plasma 63

4.1.1 Introduction 63

4.1.2 Results 67

4.1.3 Conclusion 78

4.2 Interactions between Metal Nanoparticles and Human Blood 80

4.2.1 Introduction 80

4.2.2 Results 82

4.2.3 Conclusion 86

Chapter 5 Experimental Section 87

5.1 Synthesis of Nanocrystalline Gold Octahedra Generated from Thermal Decomposition of $HAuCl_4$ in Block Copolymers 87

5.2 Block Copolymer Mediated Deposition of Metal Nanoparticles on Germanium Nanowires 90

5.3 Interactions between Metal Nanoparticles and Simulated Blood Plasma 94

5.4 Interactions between Metal Nanoparticles and Human Blood..... 97

References..... 99

List of Figures

Figure 2.1 A series of quantum dots with different fluorescence. (Adapted from Prof. Moungi Bawendi, http://web.mit.edu/chemistry/nanocluster/; photographed by Felice Frankel) 5

Figure 2.2 Inverse relationship between particle size and number of surface expressed molecules. (Adapted from Nel, A.; Xia, T.; Madler, L.; Li, N. *Science* **2006**, *311*, 622-627). 6

Figure 2.3 Potential exposure pathways for nanomaterials to human body. (Adapted from Oberdorster, G.; Oberdorster, E.; Oberdorster, *J. Environ. Health Perspect.* **2005**, *113*, 823-839) 20

Figure 2.4 Possible interaction mechanisms between nanomaterials and biological issues. (Adapted from Nel, A.; Xia, T.; Madler, L.; Li, N. *Science* **2006**, *311*, 622-627) 23

Figure 3.1 a) Low magnification SEM image of gold nanoparticles formed on native oxide-capped Si(111) from a monolayer of PS-P2VP, with a loading of Au^{III}/pyridyl groups of 0.5. b-d) Higher magnification SEM images of gold octahedra. e) Histogram showing that the majority of nanoparticles formed under these conditions are octahedra. The y axis represents number of counts of nanoparticles). 32

Figure 3.2 XPS of a monolayer (40 nm thickness) of PS-P2VP block copolymer preloaded with $HAuCl_4$ (ratio AuIII/pyridyl = 0.5), heated at a) 250°C, and b) 350°C. 33

Figure 3.3 SEM images of gold nanoparticles formed upon heating a monolayer of PS-P2VP on the surface, loaded with 0.5 Au^{III}/pyridyl groups, at different

temperatures. 35

Figure 3.4 Histograms (measurements based on over 150 particles) of the composition of those gold nanoparticles formed upon heating a monolayer of PS-P2VP on the surface, loaded with 0.5 Au^{III}/pyridyl groups, at different temperatures. 36

Figure 3.5 X-ray diffraction data of gold nanoparticles on silicon. The intensities of the Au (111) features the two spectra were normalized to allow for simple comparison. a) XRD of Au nanocrystals on the native oxide of Si(111). This sample was prepared from a monolayer of PS-P2VP with a gold/pyridyl loading of 0.5 followed by 5 minutes of thermal treatment at 250°C for 5 minutes. b) This sample was prepared in the same manner as a) except that the sample was heated at 500°C for 5 minutes. The XRD patterns indicate that the nanoparticles are fcc gold (JCPDS, File No. 4-0784). 37

Figure 3.6 Histograms indicating the size distributions of nanoparticles of gold prepared from a monolayer of PS-P2VP on oxide-capped silicon. Loading = 0.5 Au^{III}/pyridyl group. a) 250°C, b) 300°C, c) 350°C, d) 400°C, e) 450°C, f) 500°C, g) 550°C, h) plot of the average size of the gold nanoparticles with respect to temperature, based on the histograms in a-g) 38

Figure 3.7 SEM image of gold deposits formed upon heating a 0.5 wt% $HAuCl_4$ solution in pyridine to 250°C for 5 minutes in air on a silicon wafer. 39

Figure 3.8 SEM images of gold nanoparticles formed on native oxide-capped Si(111). A monolayer of PS-P2VP on the surface was loaded with a) 0.1 Au^{III}/pyridyl groups and b) 0.7 Au^{III}/pyridyl groups, followed by a 5 minute thermal treatment at 250°C. 40

Figure 3.9 SEM data of gold nanoparticles prepared in a thick (5-8 μm) PS-P2VP sample on native oxide-capped Si(111). a-c) Low resolution SEM images of the gold nanoparticles imbedded within the polymer. d-e) Higher resolution SEM images of octahedra in the polymer matrix. 42

Figure 3.10 a) Transmission electron microscopy (TEM) image of an individual gold octahedron prepared through a bulk synthesis. b) Selected area electron diffraction (SAED) of the octahedron in a). 43

Figure 3.11 a) UV-Vis spectrum and optical photographs of a sample of gold octahedra prepared via the bulk synthesis route. b) SEM image of the sample used for the UV-Vis spectrum in a). 44

Figure 3.12 Lycurgus Cup (glass; British Museum; 4th century A.D.). This Roman cup is made of ruby glass. When viewed in reflected light, for example in daylight, it appears green. However, when a light is shone into the cup and transmitted through the glass, it appears red. (Adapted from Leonhardt, U. *Nat. Photon.* **2007**, *1*, 207-208.) 45

Figure 3.13 SEM images of gold nanoparticles formed upon heating a monolayer of PS-P4VP on the surface, loaded with 0.5 Au^{III}/pyridyl groups at 250°C. 46

Figure 3.14 a) TEM image of pristine Ge nanowires. b-d) Ge nanowires subjected to aqueous galvanic displacement for 60 s in ambient: b) TEM, 0.1 mM $AgNO_3$ (aq). c) TEM, 0.1 mM $HAuCl_4$ (aq). d) SEM, 1.0 mM $HAuCl_4$ (aq) 53

Figure 3.15 a-b) TEM images of oxide-capped Ge nanowires, prepared via method 1, with 0.5 wt% PS-P2VP (MW = 91,500-105,000) in toluene, loaded with $AgNO_3$ and $HAuCl_4$, respectively; ratio M^{n+}/pyridyl group = 0.5. c-d) Scanning Auger

microscopy of Ge nanowires prepared in the same manner as a-b)..... 55

Figure 3.16 XPS, Deposition method 1, HF etched Ge NWs, using PS-P2VP (MW = 91,500-105,000), 0.5 wt% polymer in toluene. 55

Figure 3.17 Results of deposition method 1, on oxide-capped (crude) Ge NWs. 56

Figure 3.18 Results of deposition method 1, on hydrogen terminated (etched) Ge NWs. 58

Figure 3.19 SEM images of silver nanoparticles on HF-etched Ge nanowires, formed via Method 1, using $AgNO_3$ and PS-P4VP (MW = 128,000-33,500). 58

Figure 3.20 TEM, Deposition method 1, HF etched Ge NWs, using PS-P2VP (MW = 91,500-105,000), $HAuCl_4$/pyridyl = 0.5, 1.0 wt% polymer in toluene..... 59

Figure 3.21 TEM, Deposition method 1, HF etched Ge NWs, using PS-P2VP (MW = 25,500-23,500), $HAuCl_4$/pyridyl = 0.5, 0.5 wt% polymer in toluene..... 59

Figure 3.22 SEM images of gold nanoparticles on crude Ge nanowires, prepared via method 2 with thermal treatment at 200°C for 5 min. Block copolymer is PS-P2VP (MW = 91,500-105,00), ratio of $HAuCl_4$/pyridyl = 0.5..... 60

Figure 3.23 SEM images (polymer left on) of deposition method 2 (thermal treatment) on oxide-capped (crude) Ge NWs, using PS-P2VP (MW = 91,500-105,000), 0.5 wt% polymer in toluene. a) 180°C; b) 190°C; c) 210°C; d) 220°C 61

Figure 3.24 Results of deposition method 2 (water treatment for 1 min), on oxide-capped (crude) Ge NWs, using PS-P2VP (MW = 91,500-105,000), 0.5 wt% polymer in toluene. 62

Figure 4.1 Au nanoparticles were synthesized via the CTAB-ascorbic acid reaction. The resultant nanoparticles were capped by a bilayer of CTAB and were purified by

centrifugation. SEM images of Au nanoparticles: a) short nanorods (1:3 aspect ratio); b) 10 nm nanoparticles; c) 60 nm nanoparticles; d) long nanorods (1:10 aspect ratio); e) UV-Vis spectra of the Au nanoparticles. 69

Figure 4.2 SEM images of Au nanoparticles from Figure 4.1, held in a pure water solution at 37°C for one week. 70

Figure 4.3 SEM images of short Au rods (a-c), 10 nm nanoparticles (d-f), and 60 nm nanoparticles (g-i) incubated in SBP solution at 37°C 72

Figure 4.4 FT-IR spectra of short gold nanorods capped with undisplaced CTAB bilayers after $HSCH_2CH_2OH$ treatment (a), and 10 nm gold nanoparticles capped with various thiol monolayers (b-d) after $HSCH_2CH_2OH$, $HSCH_2(CH_2)_4CH_2OH$, $HS(CH_2)_{15}COOH$ treatment, respectively 74

Figure 4.5 SEM images of 10 nm thiol functionalized gold nanoparticles in SBP solution for 7 days: a) $HSCH_2CH_2OH$-capped; b) $HSCH_2(CH_2)_4CH_2OH$-capped; c) $HSCH_2CH_2NH_2 \cdot HCl$-capped; d) $HS(CH_2)_{15}COOH$-capped; e) $HSCH_2COOH$ -capped; f) $HSCH_2CH_2N(CH_3)_2 \cdot HCl$-capped. 75

Figure 4.6 Studies demonstrating the effect of BSA on the stability of the CTAB-coated nanoparticles. The Au nanoparticles maintain their sizes and shapes in BSA containing (5 g/L) SBP solution at 37°C for 7 days. SEM images of Au nanoparticles in SBP & BSA: a-b) short nanorods immersed for 7 days; d-e) 10 nm nanoparticles immersed for 7 days; g-h) 60 nm nanoparticles immersed for 7 days. UV-Vis spectra of Au nanoparticles in SBP & BSA: c) nanorods immersed for 3 and 7 days; f) 10 nm nanoparticles immersed for 3 and 7 days; i) 60 nm nanoparticles immersed for 3 and 7 days. 76

Figure 4.7 The Ag nanoparticles involved in the experiments showed lower stability than the Au nanoparticles. SEM images of the Ag nanoparticles: a) newly prepared Ag nanoplates; b) Ag nanoplates in water for 7 days; c) Ag nanoplates in SBP solution for 1 day; d) in SBP and BSA (5 g/L) for 7 days. 77

Figure 4.8 UV-Vis spectra of Ag nanoplates in SBP solution with various BSA content (measuring time interval is 30 s): a) 5 g/L BSA; b) 40 g/L BSA; c) 80 g/L BSA.... 78

Figure 4.9 SEM images of various gold nanoparticles after 7 days incubation in human blood plasma at 37°C. a-b) short nanorods; c-d) 10 nm CTAB capped Au nanoparticles; e-f) long nanorods; g-h) 10 nm citrate capped Au nanoparticles. 84

Figure 4.10 TEM images, after 4 hour incubation between gold nanoparticles and blood cells. a-c) Some 10 nm citrate capped Au nanoparticles were internalized by the red blood cells; d-e) more nanoparticles remained outside of the red blood cells; f) Au nanorods did not enter the red blood cells at all, all the cells were empty..... 85

List of Schemes

Scheme 2.1 Photolithography 7

Scheme 2.2 Electron-beam lithography (EBL) 8

Scheme 2.3 Focused-ion beam (FIB) lithography 8

Scheme 2.4 a-c) Soft lithography; a) formation of an elastic stamp, b) microcontact printing, c) micromolding in capillaries; d) nanoimprint lithography (NIL). 9

Scheme 2.5 Dip-pen lithography 10

Scheme 2.6 Molecular beam epitaxy (MBE) 11

Scheme 3.1 The five Platonic solids 30

Scheme 3.2 Outline of galvanic displacement. A semiconductor substrate is in contact with a solution of sufficiently oxidizing metal ions (M^+) which oxidize the semiconductor and, in turn, will be reduce from M^+ to M^0 on the surface of the semiconductor. (Adapted from Porter, L. A.; Choi, H. C.; Ribbe, A. E.; Buriak, J. M. *Nano Lett.* **2002**, *2*, 1067-1071.) 49

Scheme 3.3 Outline of the block copolymer mediated delivery of reagents to semiconductor surfaces. The block copolymer micelles are shown in red (corona) and blue (core). The pyridine groups associate with metal ions in the core, which are then reduced by electrons from the semiconductor substrate via a galvanic displacement reaction. (Drawing courtesy of Dr. M. Aizawa) 52

Scheme 3.4 Summary of the two methods described here, utilizing block copolymers to controllably deliver metal ions to the Ge nanowire surface, leading to a galvanic displacement reaction and nanoparticle formation. 54

Scheme 4.1 Preparation of gold nanorods via the seed mediated growth method. 68

Scheme 4.2 Cartoon structure of gold nanorods capped by a bilayer of CTAB..... 68

Scheme 4.3 Structures of α,ω-terminal thiol functionalized 10 nm gold nanoparticles. 73

Scheme 4.4 Schematic image of the composition of blood, adapted from the Oxford Visual English Dictionary..... 80

List of Abbreviations

AFM	Atomic force microscopy
BSA	Bovine serum albumin
CBN	Carbon-based nanomaterial
CMD	Carboxymethyl dextran
CNT	Carbon nanotube
CTAB	Cetyltrimethylammonium bromide
DEP	Diesel exhaust particle
DMF	N,N-Dimethylformamide
DNA	Deoxyribonucleic acid
DPG	Diphenylgermane
EBL	Electron-beam lithography
EDTA	Ethylenediamine tetraacetic acid
FIB	Focused-ion beam
FT-IR	Fourier Transform Infrared Spectroscopy
HDF	High-density fraction
HBP	Human blood plasma
HF	Hydrofluoric acid
LSPR	Localized surface plasmon resonance
MBE	Molecular beam epitaxy
MRI	Magnetic resonance imaging
NIL	Nanoimprint lithography
PBMC	Peripheral blood mononuclear cell
PDMS	Polydimethylsiloxane
PEG	Poly(ethylene glycol)
PS-P2VP	Polystyrene-*block*-poly(2-vinylpyridine)
PS-P4VP	Polystyrene-*block*-poly(4-vinylpyridine)
PST	Plasma separator tube
PTFE	Polytetrafluoroethylene
PVP	Poly(vinyl pyrrolidone)
QD	Quantum dot

RNS	Reactive nitrite species
ROS	Reactive oxygen species
SAED	Selected area electron diffraction
SAM	Self-assembled monolayer
SBP	Simulated blood plasma
SCCNFP	Scientific Committee on Cosmetic and Non-food Products
SEM	Scanning electron microscopy
SFLS	Supercritical fluid- liquid-solid
STM	Scanning tunnel microscopy
SST	Serum separation tube
TEM	Transmission electron microscopy
Tris	Ttrishydroxymethylaminomethane
UV	Ultraviolet
UV-Vis	Ultraviolet-visible spectroscopy
VLS	Vapor-liquid-solid
XPS	X-ray photoelectron spectroscopy
XRD	X-ray diffraction

Chapter 1 Introduction

1.1 Research Objectives

Over the past decade, the scientific and engineering communities have shown extensive interest in the development of selective syntheses for metal nanocrystals due to the dependence of their properties on both shape and size. Exciting progress has been made towards strategies to selectively prepare anisotropic metal nanoparticles of gold, silver, platinum, and cobalt, for example, in the shape of cubes, rods, wires, prisms, and a range of other shapes. One goal of this research is the search for novel methods to synthesize metal nanoparticles in specific sizes and shapes, and to construct other complicated nanostructures as well.

We found, however, that despite the innumerable reports dealing with the applications of nanomaterials in different fields, particularly in biology and medicine, little is known about potential short- and long-term deleterious effects of such nanomaterials on human or environmental health. Furthermore, most published results have focused on the behavior of nanoparticles incubated with specific cell cultures or organisms, including cellular uptake and cytotoxicity. There is very little fundamental information about the physicochemical interactions between nanomaterials and the various components of the solvent of the body blood. Since there are many possible routes for the nanoscale materials to enter the blood system, we felt it important to understand the reactivity, stability, and potential aggregation properties of monodisperse

engineered metal and semiconductor nanomaterials in the complex environment of blood.

1.2 Thesis Organization

This thesis is presented in five chapters. Chapter 1 gives a brief description of the research objectives and thesis organization. A detailed literature review is given in Chapter 2. Chapter 3 describes shape-controlled syntheses of metal nanoparticles. This chapter includes two subsections; each describes one synthesis method for the preparation of metal nanoparticles and the related structures. Chapter 4 describes investigation on the interactions between the metal nanoparticles and blood samples, both in simulated blood plasma solution and human blood. Experimental procedures are addressed in Chapter 5. A full set of references is provided after Chapter 5.

Chapter 2 Literature Reviews

2.1 Introduction to Nanoscience and Nanotechnology

2.1.1 Definition

The prefix "nano-" comes from the Greek word "nanos", meaning "dwarf". A nanometer (nm) is one thousand millionth of a meter. For comparison, a single human hair is about 80,000 nm wide, a red blood cell is approximately 7,000 nm wide, a DNA double-helix has a diameter around 2 nm, and a water molecule is almost 0.3 nm across.

Whereas the application and related scientific research on nanoscale materials can be dated to centuries ago, the definition and description of nanoscience and nanotechnology only appeared in the late 20th century. It is well-known that the first mention of some of the distinguishing concept in nanoscience and nanotechnology were outlined in "There's Plenty of Room at the Bottom", a talk given by the Nobel Prize winner Richard Feynman at an American Physical Society meeting at Caltech on December 29, 1959.[1] Feynman suggested it might be possible to manipulate individual atoms and molecules, using one set of precise tools to build and operate another proportionally smaller set, down to the needed scale. He also noted that scaling issues would arise from the changing magnitude of various physical phenomena: gravity would become less important, surface tension and Van der Waals attraction would become more important, etc. In 1974, Tokyo Science University Professor Norio Taniguchi defined the term "nanotechnology" in an engineering paper as follows, "Nanotechnology mainly consists of the processing of,

separation, consolidation, and deformation of materials by one atom or one molecule".[2] In the 1980s, the basic idea of this definition was explored in much more depth by Dr. K. Eric Drexler, who promoted the technological significance of nanoscale phenomena and devices through speeches and the books, and so the term acquired its current sense.[3]

Today, the definition of nanoscience and nanotechnology has been explored in much more depth and width. For example, the following three-part definition given by Chad A. Mirkin of Northwestern University is regarded as distinguishing the field from other initiatives; "Nanoscience and technology is a field that focuses on: 1) the development of synthetic methods and surface analytical tools for building structures and materials, typically on the sub-100 nanometer scale, 2) the identification of the chemical and physical consequences of miniaturization, and 3) the use of such properties in the development of novel and functional materials and devices."[4] Here, we define nanoscience as the study of phenomena and manipulation of materials at atomic, molecular and macromolecular scales, where properties differ significantly from those at a larger scale; and nanotechnology as the design, characterization, production and application of structures, devices and systems by controlling shape and size at the nanometer scale.

2.1.2 Unique Properties

A unique aspect of nanoscience and nanotechnology is that the nanoscale materials usually exhibit quite different properties when compared to macroscopic systems. For instance, gold and silver nanoparticles exhibit vivid colors in solution,[5] while the semiconductor nanoparticle solutions can fluorescence strongly under UV light (Figure

2.1);[6] materials such as gold and platinum, which are chemically inert at normal scales, can serve as potent chemical catalysts at the nanoscale;[7] copper nanoparticles smaller than 50 nm are considered super hard materials that do not exhibit the same malleability and ductility as bulk copper.[8]

Figure 2.1 A series of quantum dots with different fluorescence. (Adapted from Prof. Moungi Bawendi, http://web.mit.edu/chemistry/nanocluster/; photographed by Felice Frankel)

The properties of nanomaterials significantly differing from other materials are mainly due to the following two main reasons. First, as a particle decreases in size, a greater proportion of atoms are found at the surface compared to those inside (Figure 2.2). For example, a particle of size 30 nm has 5% of its atoms on its surface, at 10 nm, 20% of its atoms, and at 3 nm, 50% of its atoms. Thus nanomaterials have a relatively larger surface area when compared to the same mass of material produced in a larger form. This can make materials more chemically reactive, since many chemical reactions (for example, catalytic reactions, etc.) occur at surfaces, and affect their strength or electrical properties.[7,8] Second, quantum effects can begin to dominate the behavior of matter at the nanoscale, affecting the optical, electrical and magnetic behavior of materials. These effects become particularly noticeable as the structure or particle size approaches the smaller end of the nanoscale. Materials that exploit these effects include quantum dots, and quantum well lasers for optoelectronics.[9]

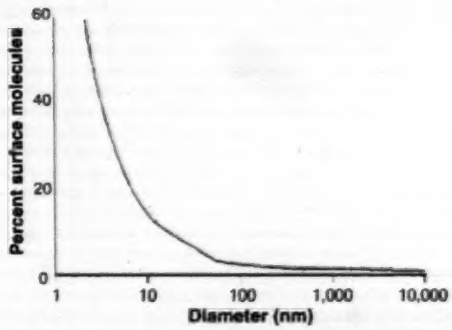

Figure 2.2 Inverse relationship between particle size and number of surface expressed molecules. (Adapted from Nel, A.; Xia, T.; Madler, L.; Li, N. *Science* **2006**, *311*, 622-627).

For other materials such as crystalline solids, as the size of their structural components decreases, there is a much greater interface area; this can greatly affect both mechanical and electrical properties. For example, most metals are made up of small crystalline grains; the boundaries between the grain slow down or arrest the propagation of defects when the material is stressed, thus giving it strength. If these grains can be made very small, or even nanoscale in size, the interface area within the material greatly increases, which enhances its strength.[10] The super hard copper nanoparticles mentioned above are good example of the interface effect.

2.1.3 Tools and Techniques

Much of nanoscience and many nanotechnologies are concerned with producing new or enhanced nanomaterials and devices. The "top-down" and "bottom-up" techniques are generally used as two main approaches for their assembly. Top-down methods start with patterns made on a large scale and reduce its lateral dimensions before forming nanostructures. On the other hand, bottom-up methods begin with atoms or molecules to build up nanostructures, in some cases through smart use of self-organization.[11]

The top-down approach has been conventionally used in the semiconductor industry for making microelectronic and other devices for decades. The most used top-down technique is photolithography, through which a beam of light (typically ultraviolet light) passes through a mask and a lens, which focuses an image on photoresist (photosensitive coating of organic polymer) placed on a surface of a silicon wafer or a film; the parts that are exposed to the photoresist can be removed, leaving the desired pattern on the silicon wafer or film (Scheme 2.1).[11c] Such technique has been extended into the nanoscale fabrication in recent years. The current development of the photolithography at 193 nm is pushing the limit of 32 nm (half pitch). Dimensions smaller than 32 nm are generally viewed as beyond the capabilities of photolithography at 193 nm wavelength unless high-index fluids, high-index lens materials, and higher-index resist can be developed.[11b]

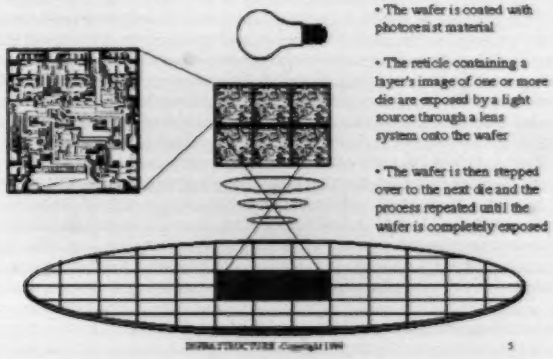
• The wafer is coated with photoresist material
• The reticle containing a layer's image of one or more die are exposed by a light source through a lens system onto the wafer
• The wafer is then stepped over to the next die and the process repeated until the wafer is completely exposed

Scheme 2.1 Photolithography (http://www.infras.com/Tutorial/sld005.htm)

Therefore, instead of masks, lithography technologies based on focused beams are used as an alternative, such as electron-beam lithography (EBL) and focused-ion beam (FIB) lithography (typically using Ga ions) to create nanostructures. Features of 10 nm in scale can be achieved by both of these methods. In the case of EBL, the pattern is written in the photoresist with a beam of electrons (Scheme 2.2), whereas FIB directly

machines the film or substrate (Scheme 2.3).[11a,c]

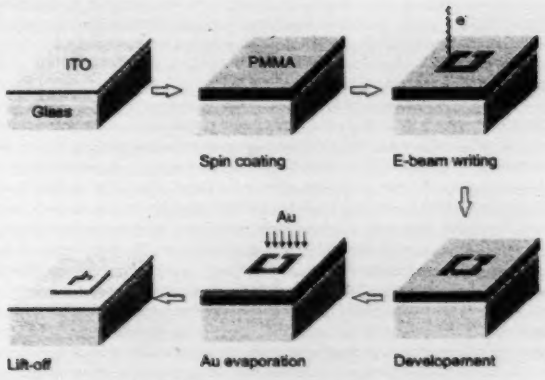

Scheme 2.2 Electron-beam lithography (EBL) (http://www.cfn.uni-karlsruhe.de/web/index.php?tabId=312)

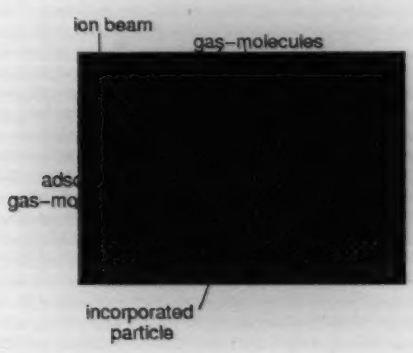

Scheme 2.3 Focused-ion beam (FIB) lithography (http://nchrem.tnw.tudelft.nl/microscopes/fib.html)

There are also certain mold-based top-down techniques employed in the nanoscience research, for example the soft lithography and nanoimprint lithography (NIL) (Scheme 2.4). In soft lithography, the mold is usually made by producing a pattern (master) in a layer of photoresist on the surface of the silicon wafer by photolithography or electron-beam lithography. A liquid precursor, polydimethylsiloxane (PDMS), is then poured over it and cured into the resulting rubbery solid. The peeled PDMS stamp will then be used to transfer materials and molecules onto a surface, for example transferring thiols onto gold surfaces.[12] The peeled PDMS stamp can be also used for micromolding

of capillaries, in which the PDMS stamp is placed on a hard surface and a liquid polymer, flown into the recesses between the surface and the stamp by capillary forces, solidifies into the given pattern.[13] Differently, in NIL, a rigid mold is pressed into the resist. After removing the mold, the pattern can be transferred to a surface by etching.

In addition, our group has recently developed a top-down method to chemically etch silicon wafers, mediated by block copolymers, such as polystyrene-*block*-poly(2- or 4-vinylpyridine) (PS-P2VP or PS- P4VP, respectively). The core-shell structures of such polymers on silicon surfaces provide the etching selectivity, since the etchant (HF) can only penetrate the PVP cores which are hydrophilic. By changing the silicon substrates and reaction conditions, the sizes and shapes of the resulted holes could be well tuned.[14]

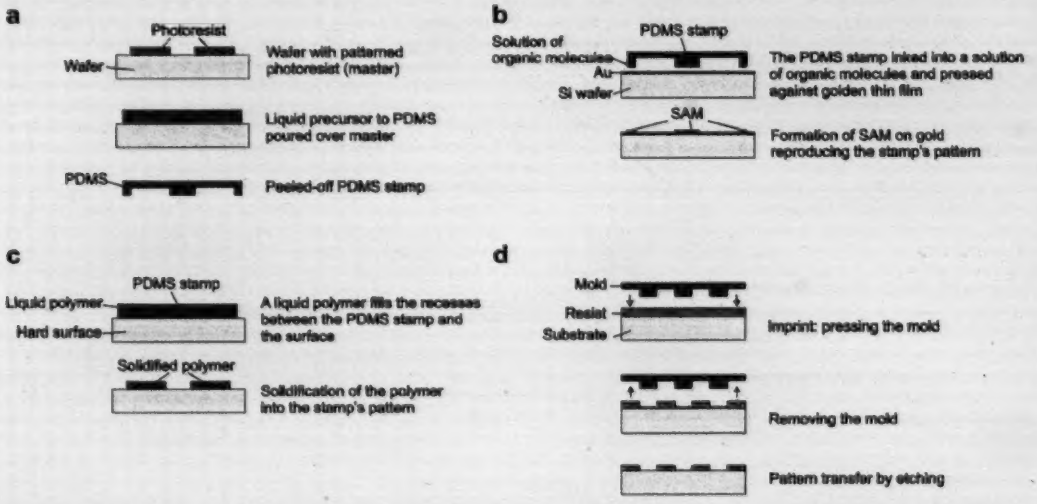

Scheme 2.4 a-c) Soft lithography; a) formation of an elastic stamp, b) microcontact printing, c) micromolding in capillaries; d) nanoimprint lithography (NIL). (Adapted from Mijatovic, D.; Eijkel, J. C. T.; van den Berg, A. *Lab Chip*, **2005**, *5*, 492–500)

The development of scanning probe devices provides another top-down fabrication possibility. The tip on the AFM can be used to physically move atoms or nanoparticles around on surfaces and to arrange them in patterns. It can also be used to make

scratches in a surface (or more commonly, in monolayer films of atoms or molecules that coat the surface). Similarly, if researchers increase the current flowing from the tip of the STM, the microscope becomes a very small source for an electron beam, which can be used to write nanometer-scale patterns. The STM tip can also push individual atoms around on a surface to build rings and wires that are only one atom wide.[11a] The scanning probe devices can also be used for the lithography, such as dip-pen lithography (Scheme 2.5). The chemical molecules are first coated on the AFM tips and then transferred to the fabricating surfaces to form certain patterns.[15]

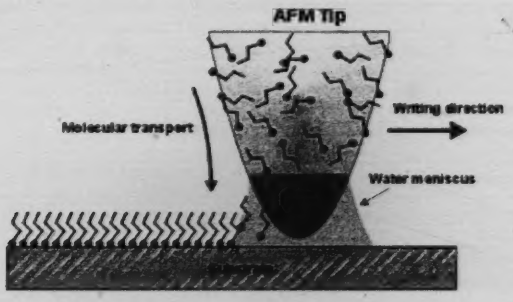

Scheme 2.5 Dip-pen lithography (http://coen.boisestate.edu/MSE/spotlight.asp)

Bottom-up approaches, in contrast, seek to build nanodevices from the atomic or molecular components. Generally, the atoms and molecules are assembled into the smallest nanostructures (dimensions of typically 2 to 10 nm) by carefully controlled chemical reactions, which make this technique much less expensive and highly parallel, as compared to the lithographical methods. Crystal growth of nanoparticles (metals or semiconductors), provides an excellent example of those approaches, as does the chemical synthesis of large molecules.[16] The exhibition of the bottom-up approaches in larger scales falls in the areas of self-assembly and the supermolecular chemistry. In nature, there are innumerable structures fabricated by these approaches; for example the DNA double helix is constructed via the enzymatic assembly of four nucleotides.

Similar assemblies are constructed by scientists with certain biological molecules or building blocks with similar structures, utilizing noncovalent interactions, such as hydrogen bonding, metal coordination, hydrophobic interactions, van der Waals forces, pi-pi interactions, and electrostatic effects. Examples of the self-assembly and the supermolecular chemistry include the catenanes and rotaxanes,[17] the self-assembling dendritic dipeptides,[18] and the host-guest complex based on crown ethers or cyclodextrins.[19]

Another variation of the bottom-up approach is molecular beam epitaxy (MBE), which was developed and implemented by researchers at Bell Telephone Laboratories like John R. Arthur and Alfred Y. Cho in the late 1960s and 1970s.[20] The most important aspect of MBE is the slow deposition rate (0.001 to 0.3 micrometers per minute), which allows the films to grow epitaxially (Scheme 2.6). It helps scientists to lay down atomically-precise layers of atoms and, in the process, build up complex structures. Important for research on semiconductors, MBE is also widely used to make samples and devices for the newly emerging field of spintronics.

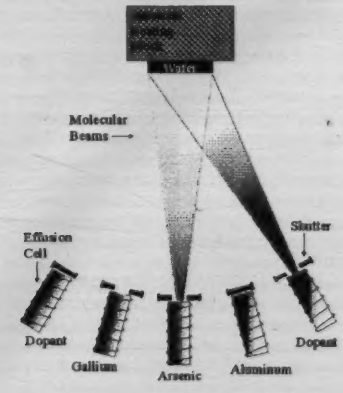

Scheme 2.6 Molecular beam epitaxy (MBE)
(http://www.nber.org/~tanwinc/DissertationDefense/1_Introduction/mbe.html)

2.1.4 Typical Nanomaterials

Although a broad definition, we categorize nanomaterials as those which have structured components with at least one dimension less than 100 nm. Materials that have one dimension in the nanoscale (and are extended in the other two dimensions) are layers, such as a thin films or surface coatings. Materials that are nanoscale in two dimensions (and extended in one dimension) include nanowires and nanotubes. Materials that are nanoscale in three dimensions are particles, for example metal nanoparticles and quantum dots.

One-dimensional nanomaterials, such as thin films and engineered surfaces, have been developed and used for decades in fields such as electronic device manufacture, chemistry and engineering. In the silicon integrated-circuit industry, for example, many devices rely on thin films for their operation, and control of film thicknesses approaching the atomic level is routine. Self-assembled monolayers (SAM) that are one molecule thick are also widely made and used in chemistry.[21] The formation and properties of these layers are reasonably well understood from the atomic level upwards, even in quite complex layers (such as lubricants). Advances are being made in the control of the composition and smoothness of surfaces, and the growth of films.

Nanowires and carbon nanotubes are the most important species among the two dimensional nanomaterials. They have generated considerable interest among the scientific community in recent years because of their novel electrical and mechanical properties. Carbon nanotubes (CNTs), which are regarded as extended tubes of rolled

graphene sheets, were first observed by Sumio Iijima in 1991.[22] There are two types of CNT, single-walled and multi-walled, both of which are typically a few nanometres in diameter and several micrometres to centimetres long. Generally, CNTs are mechanically strong (their Young's modulus is over 1 terapascal, making them as hard as diamond), flexible (about their axis), and some can conduct electricity extremely well.[10] All of these remarkable properties give CNTs a range of potential applications: for example, in reinforced composites, sensors, nanoelectronics and display devices.[23]

Nanowires are ultrafine wires or linear arrays of dots, formed by self-assembly. They can be made from a wide range of materials, from metals to semiconductors. Nanowires made of silicon, germanium and gallium nitride have demonstrated remarkable optical, electronic and magnetic characteristics (for example, silica nanowires can bend light around very tight corners), providing them with potential applications in high-density data storage (either as magnetic read heads or as patterned storage media) and electronic and opto-electronic nanodevices.[24]

Nanoparticles are often defined as particles of less than 100 nm in diameter. They exhibit significant different properties compared with larger particles of the same materials. The nanoparticles exist widely in the natural world: for example as the products of photochemical and volcanic activity, and are created by plants and algae. They have also been created for thousands of years as products of combustion and food cooking, and more recently from vehicle exhausts.[10] Deliberately manufactured nanoparticles, such as metal and semiconductor nanoparticles, are by comparison in the

minority. Nanoparticles have a range of potential applications: in the short-term in new cosmetics, textiles and paints; in the longer term, in methods of targeted drug delivery where they could be to used deliver drugs to a specific site in the body. Nanoparticles can also be arranged into layers on surfaces, providing a large surface area and hence enhanced activity, relevant to a range of potential applications such as catalysts.

Besides the metal nanoparticles being discussed in the next two chapters, nanoparticles of semiconductors (quantum dots) acquire intensive interest. If semiconductor particles are made small enough, quantum effects come into play, which limit the energies at which electrons and holes (the absence of an electron) can exist in the particles.[9a] As energy is related to wavelength, this means that the optical properties of the particle can be finely tuned depending on its size. Thus, particles can be made to emit or absorb specific wavelengths of light, merely by controlling their size.[6] Recently, quantum dots have found applications in composites, solar cells and fluorescent biological labels (for example to trace a biological molecule) which use both the small particle size and tuneable energy levels.[25] Advances in chemistry have resulted in the preparation of monolayer-protected, high-quality, monodispersed, crystalline quantum dots as small as 2 nm in diameter, which can be conveniently treated and processed as a typical chemical reagent.

2.2 Nanotoxicity

2.2.1 Introduction

Over the past decade, the scientific and engineering communities have witnessed an explosion of interest and investment in the field of nanoscience and nanotechnology. Yet despite the innumerable reports on the application of nanomaterials in different fields, particularly in biology and medicine,[26] little is known about potential short- and long-term deleterious effects of such nanomaterials on human or environmental health. Fortunately, the situation has changed in recent years. There are increasing concerns about the potential impacts of nanoscale materials on the health and safety of humans, non-human biota and ecosystems. Some preliminary data has been collected, showing that nanotoxicity is emerging as a new research area that is attracting intense interest.[27]

Although nanoscience and nanotechnology involve a broad range of research areas as described in the previous sections, not all of them necessarily require nanotoxicity research. For instance, the IT industry also uses nanotechnologies, for example fabricating computer chips by light lithography. However, compared to the engineered nanomaterials which will be the main focus in the nanotoxicity research, the above nanotechnologies do not present any unique hazard. Although a computer chip with 100 million nanostructures presents a potential hazard for manufacture, disposal and recycling, these effects are related to the bulk materials which make up the chips, rather than to the nanostructures within them. As a result, the possible harmful exposure to a range of chemical substances and materials, other than the nanoscale materials themselves are

covered by existing regulation.[10] There is a significant distinction between manufactured nanostructures on large objects (generally through the top-down approaches) and the nanoscale materials which are made as powders, including nanowires, nanotubes, and nanoparticles (generally through the bottom-up approaches).

The ambient ultrafine particles which have similar sizes as the nanomaterials are derived from both natural sources and human activities, for example as the products of photochemical and volcanic activity, created by combustion and food cooking, and more recently from vehicle exhausts. Humans have been exposed to those particles for millennia. Such exposure has been connected to adverse health effects in the respiratory tract as well as in extrapulmonary organs in recent years.[27d] For instance, several epidemiologic studies have found an association between ambient ultrafine particles and adverse respiratory and cardiovascular effects, resulting in a variety of diseases in susceptible people.[28] In addition, studies in animals using ambient ultrafine particles showed that they consistently induced mild yet significant pulmonary inflammatory responses as well as effects in extrapulmonary organs.[29] Major differences between the ambient ultrafine particles and the nanomaterials are their disperse natures, as well as the particle morphologies. The former are polydisperse and often with branched structures, whereas the latter normally have monodisperse size distributions with controlled shapes such as spheres, wires, tubes, and planes. However, the similarity of particle sizes and surface area between the ambient ultrafine particles and nanoscale materials suggests that the exposure pathways, the bio-kinetics, and the possible cell interactions will most likely be similar for both of them. Thus the research on the health effects of ambient ultrafine

particles has built a solid foundation for the nanotoxicity on nanomaterials, making it possible to extrapolate the results on the former ones to the latter ones.[10]

2.2.2 Exposure Pathways

From the research on ambient ultrafine particles, it is postulated there are several possible pathways for the entry of nanomaterials (Figure 2.3). For all those routes, humans may take up the nanomaterials intentionally or unintentionally.[27d,e] If a material is released into the air, it may be inhaled directly. This is the dominant pathway for humans exposed to manufactured nanoparticles released in the workplace, and for all organisms exposed to nanoparticles from sources such as combustion. In addition to inhalation, exposure to nanoparticles could occur via surface contact (for example in cosmetic skin preparations) or from ingestion (if nanoparticles are to be added to food or drink in the future). In the future, medicinal applications may result in nanoparticles being injected into the body. Other organisms such as bacteria and protozoa may take in nanoparticles through their cell membranes, and thus allow the particles to enter a biological food chain.

So far, inhalation is the most investigated route for the entry of nanomaterials. Inhaled nanoparticles are efficiently deposited by diffusional mechanisms in all regions of the lung, while the depth of deposition is actually controlled by the particle sizes. For example, 90% of inhaled 1 nm particles are deposited in the nasopharyngeal region, while the rest are in the etracheobronchial region. Particles that penetrate more deeply reach the pulmonary alveoli, which are located at the ends of the lung bronchioles. For instance, about 50% of 20 nm particles are deposited in the alveolar region; to the

contrary, the deposition efficiency is only 15% in nasopharyngeal and etracheobronchial regions.[30]

Once deposited, the nanomaterials are able to translocate to extrapulmonary organs by different transfer routes and mechanisms. Most materials in microscale are effectively cleared by the alveolar translocation, in which these materials are absorbed by alveolar macrophages through the phagocytosis of them.[31] However, when the particle sizes decrease to the nanoscale, such phagocytosis becomes less efficient.[32] The lower efficiency for nanoscale materials is caused by their small size, which may not induce a sufficiently strong stimulus at the site of their deposition, and thus the macrophages do not sense those nanomaterials. In addition, the alveolar epithelial surfactant layer increases contact of the nanoscale materials with epithelial cells, facilitating an alternative mechanism of epithelial cell uptake.[33] Results from several studies have confirmed such translocation of nanomaterials from the deposited respiratory tract to epithelial interstitial sites,[34] followed with further translocation into the regional lymph nodes as well as the blood circulation, either as free particles or after phagocytosis by interstitial macrophages. The nanomaterials can then be distributed throughout the body during the blood circulation, such as to the vasculature, liver and heart. Such processes have already been associated with cardiovascular events, including heart attacks and cardiac rhythm disturbances.[35]

Alveolar translocation, followed with interstitial translocation, is not the only pathway for nanomaterial clearance, especially for small nanoparticles. Nanomaterials

could be cleared form the respiratory tract via the mucociliary escalator, and subsequently be ingested into the gastrointestinal tract.[27d] Another translocation route involves the neuronal axon specific to nanomaterials. If materials are deposited on olfactory fibers in the nasal mucous membrane, they may proceed directly to the olfactory center of the brain via the nerve cells in the nose.[36]

Another potentially important uptake route is through dermal exposure, which occurs regularly during the use of sunscreen products. For example, TiO_2 nanoparticles are used in sunscreen creams, since they are transparent to visible light while acting as absorbers and reflectors of UV light. It is believed in healthy skin, the epidermis, consisting of the outer horny layer (stratum corneum), the prickle cell layer (stratum spinosum), and the basal cell layer (stratum basale), provides excellent protection against particle penetration. However, damaged skin is regarded to provide a readily available access even for micrometer-size particles.[37] Moreover, flexing of normal skin also facilitates the particle penetration.[38] Previous *in vivo* imaging on intradermally injected near-infrared quantum dots in animals revealed that the nanomaterials, once in dermis, will localize to regional lymph nodes, leading to potential toxic effects on the immune system.[39]

As described above, nanomaterials could be ingested in the gastrointestinal tract from the mucociliary escalator in the respiratory tract. Alternatively, they can be ingested directly via the gastrointestinal tract as well. Although most research demonstrated the nanomaterials were eliminated from the gastrointestinal tract rapidly, there were some

results revealing possible absorption there.[32a] It is postulated again that the particle size and the surface chemistry play important roles in such absorption.

When used for medical applications, nanomaterials might be injected directly into humans. Once injected, such nanomaterials would easily be transported throughout the body by blood circulation. The process is much faster than other absorption pathways, potentially leading to rapid adverse effects on human health. It is necessary to apply more attention to this area before the putting nanomaterials into applications.

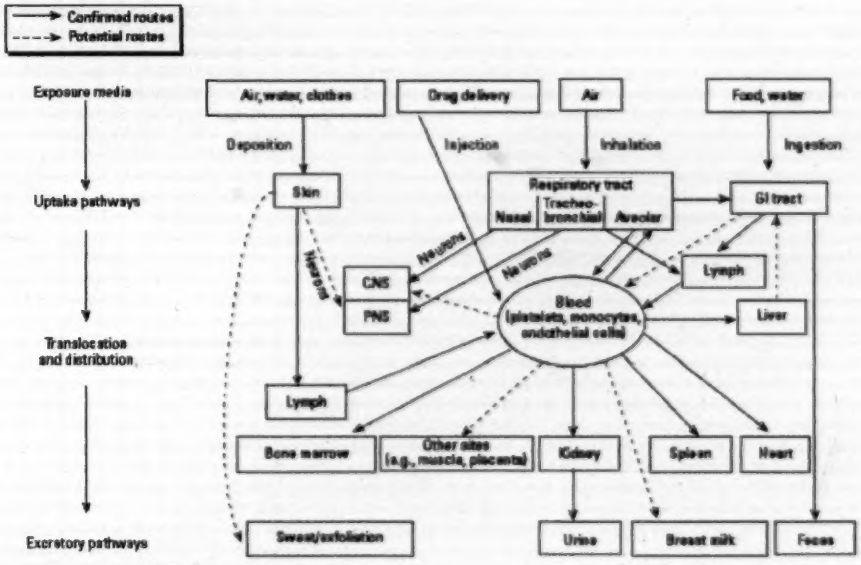

Figure 2.3 Potential exposure pathways for nanomaterials to human body. (Adapted from Oberdorster, G.; Oberdorster, E.; Oberdorster, J. *Environ. Health Perspect.* **2005**, *113*, 823-839)

2.2.3 Interaction Mechanisms

Being taken up into the human body, nanomaterials could exert a series of effects on human health due to their unique properties that are significantly different from the corresponding bulk materials(Figure 2.4). The mechanisms for the biological

interactions are thus regulated by those properties, including particle size, shape, chemical composition, surface chemistry, aggregation state and solubility.

From a chemical viewpoint, the small particle size corresponds to a large surface area per unit mass, which greatly increases the reactivity of the nanomaterials. Thus, when taken up into the human body, same highly reactive nanomaterials can generate reactive oxygen species (ROS), such as free radicals, leading to oxidative stress, inflammation, and subsequent damage to proteins, membranes and DNA.[27d,e] It is likely that this surface activity is one of the primary mechanisms of the toxicity of nanomaterials which might vary considerably between different types of materials. Another consequence of such small nanoparticles sizes is the extraordinarily high concentrations of nanomaterials per given mass. As a result, even if the same material is relatively inert in bulkier form, the corresponding nanoscale form may cause disease to the organism, because the number of particles is sufficiently large. In addition, when the internalized nanomaterials mobilize to mitochondria, the redox active organelles, there is an increase of ROS production, resulting in overwhelming of the accepted loading for the lung defenses.[40]

There are also other toxicological effects that could be related to nanoparticle size. For instance, a particle with nanoscale size normally contains a number of structural defects due to insufficient growth of crystal planes, rendering disruption of the normal structured electronic configuration of the material. Such structural changes result in an altered electronic property, and consequently provide possible reactive sites for the

oxidative damage.[41]

Another determining influence on particle toxicity is the particle chemistry, especially surface chemistry. It is well known that surface coating of nanomaterials plays an important role in nanomaterial uptake. For example, proteins, such as albumin, can enhance nanoparticle uptake into cells, whereas polyethylene glycol inhibits the nanoparticle uptake into the liver.[42] One direct example about effect of surface chemistry on toxicity is related to polytetrafluoroethylene (PTFE) fume which exhibits high toxicity both on animals and humans. By aging such PTFE fume particles for 3 min, which changes the surface chemistry of the particles, a loss of toxicity was observed.[43] In addition, some transition metal impurities in nanomaterials (Fe in carbon nanocubes), and in particular on the surface, have been found to participate in the formation of certain electron donor or acceptor active sites (chemically or physically activated) which could interact with oxygen (O_2). Electron capture can lead to the formation of the superoxide radical ($O_2^{\cdot -}$) through Fenton chemistry. The latter product is related to the amplification of chemical changes in the bio-environment. Similarly, some organic molecules, such as quinones, can generate additional ROS through a redox cycling as well.[27e]

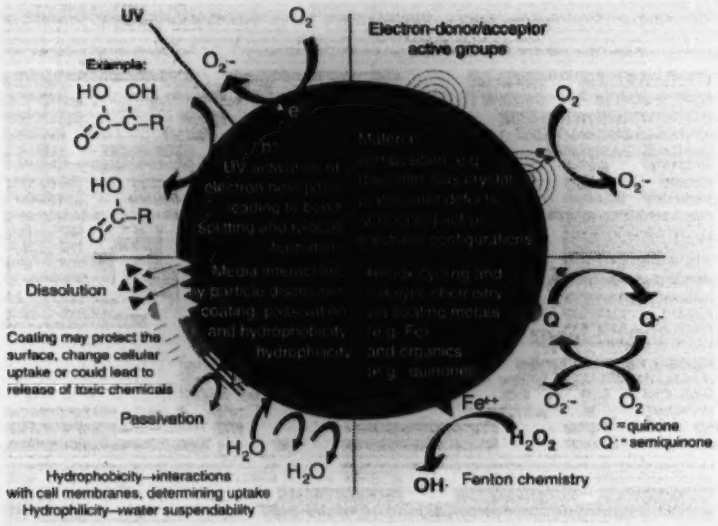

Figure 2.4 Possible interaction mechanisms between nanomaterials and biological issues. (Adapted from Nel, A.; Xia, T.; Madler, L.; Li, N. *Science* **2006**, *311*, 622-627)

2.2.4 Toxic Effects of Typical Nanomaterials

Compared to the ambient ultrafine particles which have been intensively studied, the synthesized nanomaterials have been subjected to much less toxicity testing. It is necessary to investigate the effect of size, shape, and surface chemistry on the bioavailability, uptake, subcellular distribution, metabolism, and degradation of those nanomaterials. Progress toward this goal has been reported in recent years.[44-47]

Carbon-based nanomaterials (CBNs) are currently one of the most attractive nanomaterials due to their diversity of forms, such as fullerenes, single- and multiple-walled carbon nanotubes, carbon nanoparticles, nanofibers, and so forth. Recent studies demonstrated that CBNs also aggregate in combustion streams of fuel gas and air commonly used in our everyday life, indicating that we are already strongly exposed to CBNs in the atmospheric environment both in and outdoor and there is urgent

need to know their toxicity.[44e] Cytotoxicity of water-soluble fullerene species towards HDF and HepG2 cells was recently reported to be sensitive to surface functionalization.[44a] Under ambient conditions in water, all investigated fullerene species can generate $O2^{-}$ anions which are responsible for membrane damage, lipid oxidation and subsequent cell death. However, the lethal dose changes over 7 orders of magnitude with relatively minor alterations in fullerene structures. Specifically, the nanoscale aggregated form of C_{60} is toxic at the 20 ppb level, the highly derivatized species, such as $Na^{+}_{2-3}[C_{60}O_{7-9}(OH)_{12-15}]^{(2-3)-}$ and $C_{60}(OH)_{24}$, show cytotoxicity only at relatively high concentrations. Moreover, modification of the fullerene surface by attachment of malonyl groups yields nanoparticles with biologically useful antioxidant activity, showing the determining effect of surface chemistry.[44b] Similar investigation has been performed with carbon nanotubes. *In vitro* incubation of keratinocytes and bronchial epithelial cells with high doses of single-walled nanotubes results in ROS generation, lipid peroxidation, oxidative stress, mitochondrial dysfunction, and changes in cell morphology.[44c] Multi-walled nanotubes also elicit proinflammatory effects in keratinocytes.[44d] It has been reported the surface chemistry can change the nanotube cytotoxicity in various ways. While the biomimetic polymer coated carbon nanotubes are much less cytotoxic than the unmodified ones, the carbonyl, carboxyl, and hydroxyl groups on surfaces increases the toxicity, which is opposite to the results for fullerenes.[44c,f] Another concern about the toxicity of carbon nanotubes is their structural resemblance to asbestos. Inhalation of asbestos fibers is known to induce asbestosis (a progressive fibrotic disease of the lung), lung cancer, and malignant mesothelioma of the pleura. Corresponding research reveals the carbon nanofibers indeed exhibit high

toxicity than the normal nanotubes.[44e]

Titanium dioxide (TiO_2) and zinc oxide (ZnO) nanoparticles are currently used for cosmetic purposes commercially. They are usually used as additives in some sunscreens to absorb or reflect ultraviolet light. Other practical examples involve iron oxide which is used as a base in some products, including lipsticks. It is declared by the Scientific Committee on Cosmetic and Non-food Products (SCCNFP) that the use of titanium dioxide containing cosmetics on healthy skin is safe no matter the particle size orsurface chemistry.[10] Research also shows that although the uncoated titanium dioxide nanoparticles might be photoactive, the coatings used on titanium dioxide in sunscreens to prevent agglomeration also reduce the formation of free radicals. Therefore, even if the titanium dioxide used in sunscreens were able to penetrate the skin, it would probably not exacerbate free radical damage.[10] Similar assessment of zinc oxide used as UV filters in cosmetic products met with some difficulties due to the lack of relevant information from the manufacturers. Potential hazards of those metal oxide nanoparticles by other absorption ways were also reported. For example, inhalation of ZnO fumes can cause metal fume fever (fatigue, chills, fever, cough, dyspnea, leukocytosis, and salivation).[45] And intratracheal instillation of TiO_2 nanoparticles in rodents demonstrates that they can induce a severer inflammatory response than particles in larger forms.

Semiconductor quantum dots (QDs) show great promise as alternatives to organic dyes for biological labeling and imaging, due to their bright fluorescence, narrow

emission, broad UV excitation, and high photostability. On the other hand, they also draw intensive concern about the potential dangers in such applications, not only because of their small particle sizes which may cause adverse effects to the organisms, but also because the compositions, for example Cd^{2+} and Pb^{2+}, are well known as toxic materials. Research verified the cytotoxicity of CdSe QDs through investigation of their effects on primary hepatocyte cells, which are the main cells in the liver involved in metal detoxification.[46a] Release of Cd^{2+} ions was observed on the QD surfaces, and the concentration of the Cd^{2+} ions was found to correlate directly with observed cytotoxic effects. Such ion release is enhanced by oxidation, either through illumination with UV light or exposure to excess hydrogen peroxide, but is suppressed by coating the quantum dots with appropriate shells, such as ZnS. For the CdSe/ZnS particles, the main source of cytotoxicity is not the cadmium content, but rather the interaction between the particle surfaces with the cells. The study was further extended to QDs with different organic shells. While mercaptopropionic acid coated CdSe and CdSe/ZnS nanoparticles still exhibited Cd^{2+} release, PEG-silica coated CdSe and CdSe/ZnS particles provided good protection of the Cd^{2+} ions, showing much less toxicity.[46b] Furthermore, cytotoxic effects are different in the case when particles are ingested by the cells, compared to the case when particles are just present in the medium surrounding the cells. Lastly, it was reported that ROS, which can be formed via Cd^{2+}-specific cellular pathways or photoxidative processes involving singlet oxygen or electron transfer from excited QDs to oxygen, also contribute the cytotoxicity for QDs.[46c]

Finally, metal nanoparticles, in particular gold nanoparticles, have shown promising

potential in biological applications, including cell imaging, biosensing, and DNA/drug delivery. At the same time, cytotoxic research on those nanoparticles has been carried out as well. The results show that the cytotoxicity of gold nanoparticles depends on the characteristics of the molecules adsorbed on the nanoparticle surface; and in most cases, such particles appear to be biologically inert. For instance, gold nanoparticles coated with lysine demonstrate biocompatible properties such as nontoxicity, nonimmunogenicity, and high tissue permeability in RAW264.7 macrophage cells. Surprisingly, at higher concentrations, they can even show the ability to inhibit the production of ROS and reactive nitrite species (RNS).[47a] Similarly, citrate or biotin modified nanoparticles did not appear to be toxic at concentrations up to 250 μM (gold atoms). Cetyltrimethylammonium bromide (CTAB) capped gold nanoparticles turn out to be cytotoxic when excess CTAB remains in solution. However, the nanoparticles themselves are not necessarily detrimental to cellular functions, as verified by the fact that removing excess CTAB by centrifugation results in the nontoxicity of those particles.[47b] In addition, replacing CTAB coatings with phospholipids by extraction using a chloroform phase can permanently eliminate the possibility of releasing the surface bonded CTAB, and assure the nontoxicity of such gold nanoparticles.[47c]

The intracellular uptake of gold nanoparticles is widely investigated in almost all cases. While the highest uptake efficiency was observed for the intermediate sized gold nanoparticles, the high aspect ratio for gold nanorods resulted in a low cellular uptake.[47d] In addition, displacing the CTAB layers with chemisorptive surfactants, particularly by the conjugation of poly(ethylene glycol) (PEG) chains onto nanorods can greatly reduce

the nonspecific uptake.[47e]

2.2.5 Summary

As a newly emerged research area, nanotoxicity research has attracted intense interest, because it investigates the toxicity of synthesized nanomaterials, such as nanoparticles, nanotubes, and nanowires, which already exhibit the potential to cause adverse effects on human or environmental health. Based on the research of ambient ultrafine particles, it is postulated that synthesized nanomaterials could be taken up into human body via inhalation, via ingestion, through dermal exposure, or via direct injection. The absorbed nanomaterials could then be distributed throughout the body via circulation. Studies showed the small particle size and surface chemistry render nanomaterials more active than the same materials in bulk form. They are able to generate ROS, which are always related to the nanomaterials induced inflammation and oxidation. Progress on toxicity research of specific nanomaterials, including carbon-based nanomaterials, metal oxide nanoparticles, quantum dots, and metal nanoparticles, has been reported in recent years.

Chapter 3

Selective Syntheses of Metal Nanoparticles

3.1 Synthesis of Nanocrystalline Gold Octahedra Generated from Thermal Decomposition of $HAuCl_4$ in Block Copolymers

3.1.1 Introduction

As described in the previous chapter, the development of selective syntheses for metal nanocrystals is an area of intense interest due to the dependence of their properties on both shape and size.[48] Exciting progress has been made towards strategies to selectively prepare anisotropic metal nanoparticles of gold,[49] silver,[50] platinum,[51] and cobalt,[52] for example, in the shape of cubes,[49c,50] rods,[53] wires,[54] prisms,[55] and a range of other shapes.[49c,56] Among these synthetic approaches, the polyol process has been widely used for preparing gold and silver nanoparticles because it provides exceptional shape control.[49a,50] The surface regulating polymer, poly(vinyl pyrrolidone) (PVP), plays an important role in the crystallization due to the selective interaction between the PVP and the different surface planes of the metal nanocrystals. In addition, the high temperature for the polyol process also promotes the crystal growth. At over 160°C, Ostwald Ripening dominates the growth process, facilitating the anisotropic growth of the gold and silver nanoparticles.

So far, different sized nanocrystalline gold cubes, icosahedra, tetrahedra, and silver

nanocubes, nanowires can all be successfully prepared by the polyol process at high yield. However, gold octahedra, one of the Platonic solids (Scheme 3.1), having eight equilateral triangle faces,[49a,57] remain elusive as they have only been observed previously as minor side-products in the polyol synthesis of tetrahedra and icosahedra; about 10% of the shapes were a mix of decahedra (5 fold twinned structures) and octahedra.[49a] It was recently reported that replacing polyol with DMF as the reducing agent and carrying out the reaction at a high temperature (~150°C) will produce gold octahedral nanoparticles, although full characterization and determination of the yield of octahedra with respect to other shapes in the mixture are lacking.[49b]

The Five Convex Regular Polyhedra (Platonic solids)				
Tetrahedron	Hexahedron or Cube	Octahedron	Dodecahedron	Icosahedron
		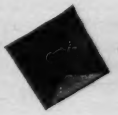		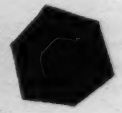

Scheme 3.1 The five Platonic solids

In addition, the organic media for the polyol process has certain drawbacks. First, the surface regulating polymer has a strong interaction with the synthesized nanoparticles, but also hinders any subsequent surface modification. Unfortunately, surface modification is always critical for transferring nanoparticles into aqueous solutions and other applications. Second, in recent years, there has been increasing interest in the selective patterning of nanoparticles on surfaces, but direct transfer of nanoparticles in solution onto surfaces with certain patterns is not easy to achieve. On the other hand, amphiphilic diblock copolymers have been widely used for two dimensional patterning of nanoparticles owning to the following unique properties: (a) the polymer molecules can

self-assemble into micelles in selective solvent for one block, which makes them good nanoreactors for inorganic nanoparticles; (b) those micelles can further self-assemble into two dimensional close packed arrays.[58] Even though various types of nanoparticle arrays have been prepared this way, the shapes of these particles were generally spherical and their crystallinities were not elucidated. Moreover, the inter-particle distances by this method were restricted by the size of polymer micelles, generally tens of nanometers, which could not be used for any optical-based single particle study. It is necessary to find a method to prepare shape-controlled nanoparticles, and to pattern them on surfaces simultaneously.

Here we describe a solvent-free, selective synthesis of nanocrystalline gold octahedra that can be carried out on an interface, or in bulk. Under the reaction conditions described in this thesis, at least 70% of the products are crystalline gold octahedra, permitting detailed analysis by electron microscopy and surface spectroscopy of these nanomaterials.

3.1.2 Results

Gold octahedral nanoparticles were synthesized in high yields by thermal treatment of $HAuCl_4$-loaded polystyrene-*block*-poly(2-vinylpyridine) (PS-P2VP, MW = 91500-105000) with a ratio of 1:2 Au^{III}/pyridyl groups, at a temperature of 250°C in air for 5 minutes. The block copolymer solution (0.5% in toluene) was loaded with the predefined amount of $HAuCl_4$ (s), and spin-coated onto a native oxide-capped silicon surface to form a monolayer of block copolymer micelles, followed by brief heating. Scanning electron microscopy (SEM) images of sub-100 nm gold octahedra are shown in

Figure 3.1a-d. The corresponding geometric models for those octahedra are also presented in the same figure for illustration.

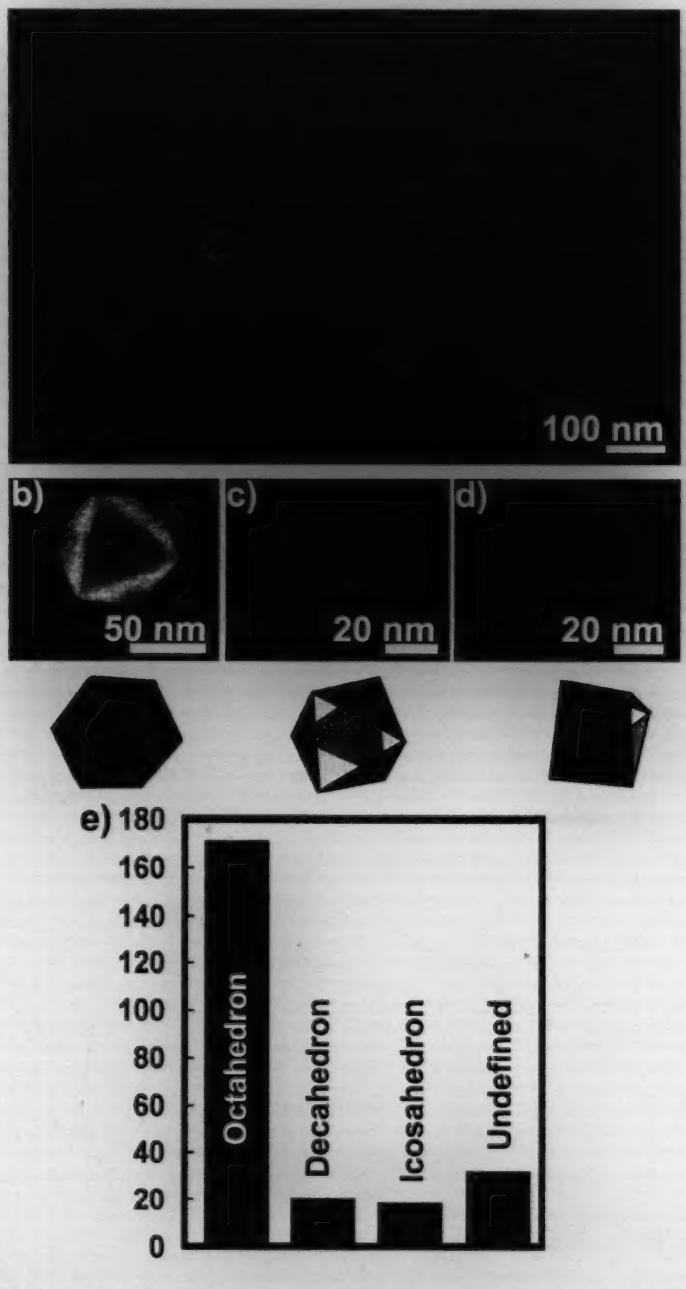

Figure 3.1 a) Low magnification SEM image of gold nanoparticles formed on native oxide-capped Si(111) from a monolayer of PS-P2VP, with a loading of Au^{III}/pyridyl groups of 0.5. b-d) Higher magnification SEM images of gold octahedra. e) Histogram showing that the majority of nanoparticles formed under these conditions are octahedra. The y axis represents number of counts (of nanoparticles).

The histogram (measurement based on over 250 particles) in Figure 3.1e summarizes the evaluation of the composition of the metal products, and reveals that the majority of metal nanoparticles formed under these conditions are octahedra (~71%). Other shapes include decahedra (~8%), icosahedra (~7%), and particles whose shapes were ill-defined, or too small to identify with certainty (~14%). Because it is possible that some of the smaller particles with undiscernable geometry have octahedral morphology, the 71% octahedral composition represents the lower limit. The sizes of the octahedra are just under 50 nm across under these conditions, on average. X-ray photoelectron spectroscopy (XPS) reveals that the reaction is quantitative, that all of the Au^{III} has been reduced to Au^0 (Figure 3.2). Gold nanoparticle synthesis in a thin polymer film has been carried out previously, using polyvinylalcohol that acts simultaneously as a reducing agent and polymer thin film support.[59] However, recent work suggests that pyridyl groups do not have sufficient reducing power to produce Au^0, so in the case described here, there is no obvious reducing agent present and therefore, thermal decomposition of $HAuCl_4$ is the most probable route towards gold nanoparticle nucleation and growth.[60]

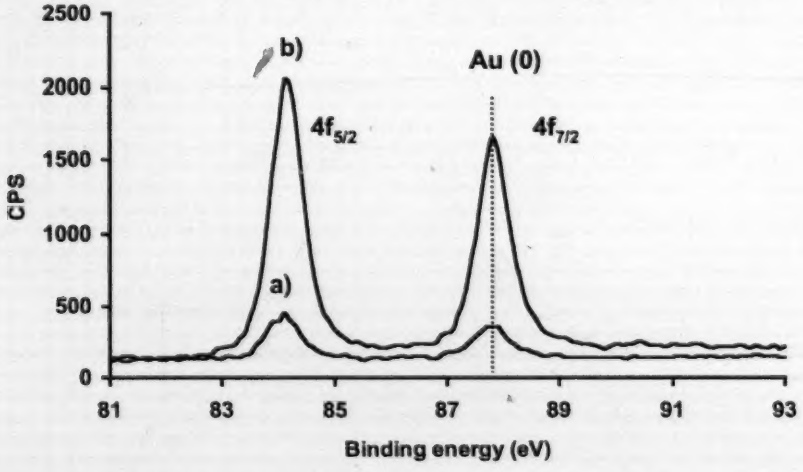

Figure 3.2 XPS of a monolayer (40 nm thickness) of PS-P2VP block copolymer preloaded with $HAuCl_4$ (ratio Au^{III}/pyridyl = 0.5), heated at a) 250°C, and b) 350°C.

The first investigated influence on such thermal decomposition is the temperature effect, since the nucleation and growth of nanocrystals is a thermodynamic process depending heavily on the reaction temperature.[61] As such, there is a strong temperature dependence, with no obvious formation of Au^0 noted below 200°C, based upon SEM analysis, and a lack of color when the reaction is carried out on a glass slide. This is consistent with solution decomposition studies of $HAuCl_4$ that suggest that Au^0 formation takes place only above 200°C.[62] With the highest octahedra yield, 250°C turns to be the optimum temperature for the gold nanoparticle preparation. In addition, at 250°C, there are the least ill-defined nanoparticles found in the SEM images comparing to the other temperatures. At intermediate temperatures of 300-350°C, there is a decrease in the percentage of octahedra, and an increase in the number of icosohedra. At 300-350°C, ~30-35% of the gold nanoparticles are octahedra, and ~40-50% are icosahedra, with some unidentifiable shapes (~20%). Upon a further increase of temperature to 400°C, the majority of particles appear as truncated octahedra with 3-fold symmetry which look like steering wheels. Finally, at 500°C, most particles appear to be spherical, although the occasional octahedron or other regular shape is noted. SEM images of gold octahedra prepared under those temperatures are shown in Figure 3.3.

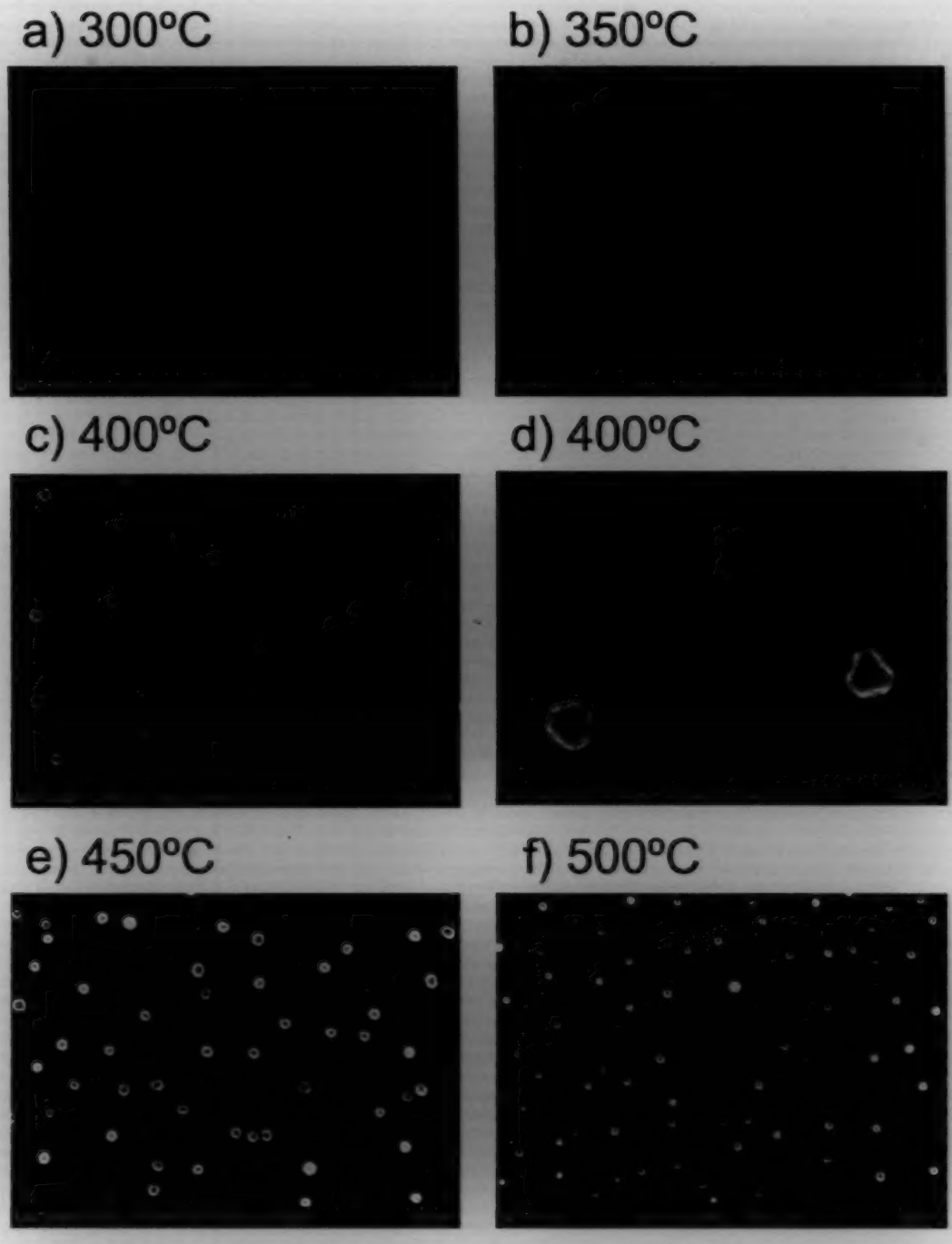

Figure 3.3 SEM images of gold nanoparticles formed upon heating a monolayer of PS-P2VP on the surface, loaded with 0.5 Au^{III}/pyridyl groups, at different temperatures.

In addition, the histograms (measurements based on over 150 particles) of the

composition of those gold nanoparticles are shown in Figure 3.4.

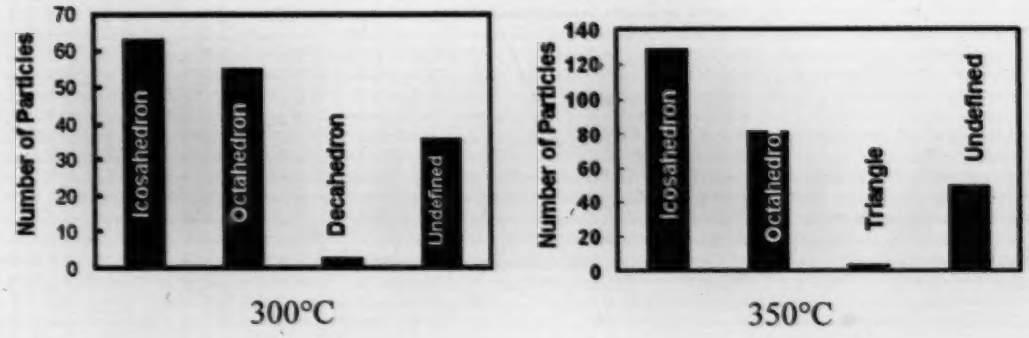

Figure 3.4 Histograms (measurements based on over 150 particles) of the composition of those gold nanoparticles formed upon heating a monolayer of PS-P2VP on the surface, loaded with 0.5 Au^{III}/pyridyl groups, at different temperatures.

While the electron microscopy samples only a small portion of the products, X-ray diffraction (XRD) in Figure 3.5 is used to assess the overall quality and purity of these facetted nanoparticles.[49a,50c] Two XRD patterns in this figure were recorded for the nanoparticles produced under different reaction temperatures, with the peaks assigned to the (111), the (200), and the (220) diffractions of fcc gold respectively (JCPDS, File No. 4-0784). It is worth noting that, in the XRD pattern for the 250°C reaction, the intensity ratio between the (111) and the (200) diffractions is 0.27, which is significantly smaller than the conventional bulk intensity ratio (~0.53). This is a clear indication that the faces of these nanoparticles, primarily composed of {111} planes, tend to preferentially orient parallel to the supporting substrates, thus giving a significantly high (111) diffraction intensity.[63] When the reaction temperature increased to 500°C, the intensity ratio between the (111) and the (200) diffractions increased to 0.44, which is close to the bulk value, since the dominant products at this temperature have spherical shapes. This set of XRD patterns unambiguously demonstrates our capability of synthesizing with a

high degree of selectivity, crystalline gold nanoparticles via this route.

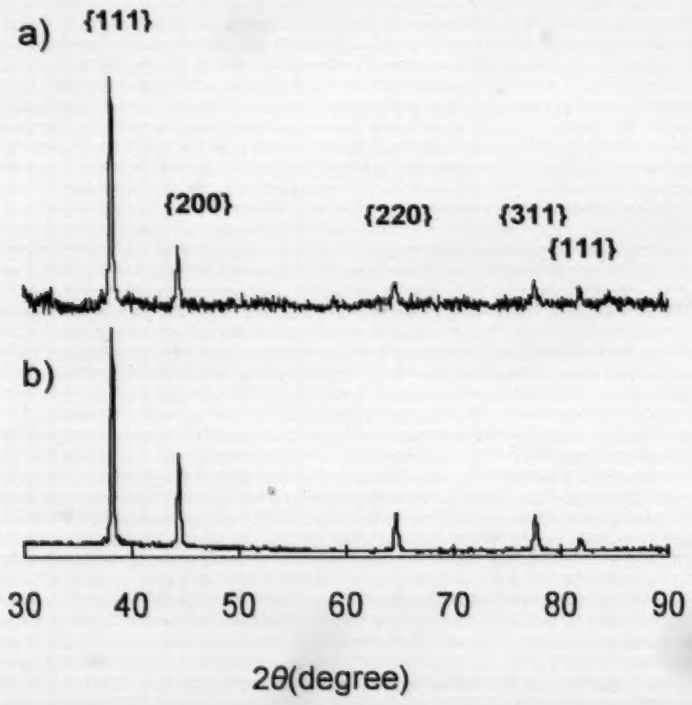

Figure 3.5 X-ray diffraction data of gold nanoparticles on silicon. The intensities of the Au (111) features the two spectra were normalized to allow for simple comparison. a) XRD of Au nanocrystals on native oxide of Si(111). This sample was prepared from a monolayer of PS-P2VP with a gold/pyridyl loading of 0.5 followed by 5 minutes of thermal treatment at 250°C for 5 minutes. b) This sample was prepared in the same manner as a) except that the sample was heated at 500°C for 5 minutes. The XRD patterns indicate that the nanoparticles are fcc gold (JCPDS, File No. 4-0784).

It is believed that the surface energies of different crystallographic planes determine the crystal growth.[64] In our case, the {111} planes have a lower surface energy than the {100} planes, and therefore the octahedra and icosahedra represent the thermodynamic products below 400°C. When the reaction temperature is increased to 400°C and above, the particles attain the higher energy crystallographic planes, such as the {100} planes, and the truncated octahedra and spheres are formed. As the temperature increases from 250°C to 500°C, the size distribution of the nanoparticle mixture narrows, as shown in Figure 3.6 (measurement based on over 150 particles). The wider distribution of sizes at

lower temperatures may be due to concurrent nucleation and growth since the former may be slow and prolonged; at higher temperatures, however, the nucleation is expected to be fast and therefore complete before growth commences, leading to simultaneous growth of the nanoparticles that results in a tighter range of product sizes.[60]

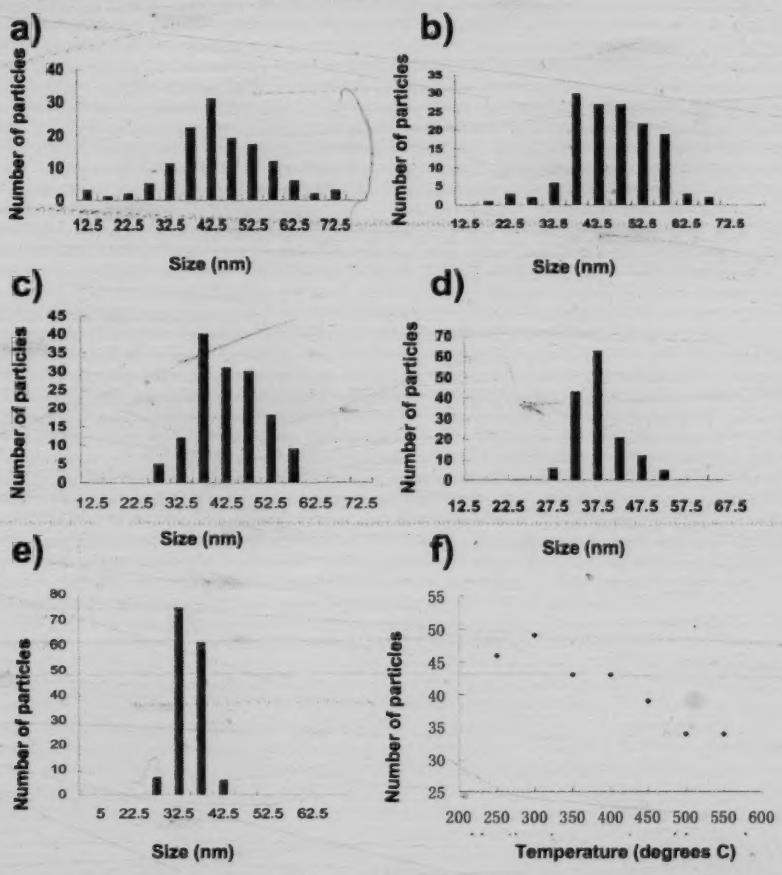

Figure 3.6 Histograms indicating the size distributions of nanoparticles of gold prepared from a monolayer of PS-P2VP on oxide-capped silicon. Loading = 0.5 Au^{III}/pyridyl group. a) 250°C, b) 300°C, c) 350°C, d) 400°C, e) 550°C, f) plot of the average size of the gold nanoparticles with respect to temperature, based on the histograms in a-g).

The following experiments reveal that the ratio of Au^{III}/pyridyl units (in the P2VP block) has an important effect on the average size of the octahedra and polydispersity, at 250°C (5 min heating time). Attempts to produce gold octahedra through thermal

decomposition of the auric acid precusor solution (pyridine, 0.5 wt%) at 250°C on a silicon wafer yielded only random gold nanoparticles, with no octahedra (Figure 3.7). Obviously, the pyridyl units in the PS-P2VP block copolymer play a crucial role in the synthesis of the gold octahedra.

Figure 3.7 SEM image of gold deposits formed upon heating a 0.5 wt% $HAuCl_4$ solution in pyridine to 250°C for 5 minutes in air on a silicon wafer.

At a Au^{III}/pyridyl ratio of 0.1, the majority of nanoparticles are small octahedra with an average size of ~20 nm (Figure 3.8a). A ratio of 0.5 corresponds to the images in Figure 3.1, with an average size of ~50 nm, while at a ratio of 0.7 the products were dominated by icosahedra (~60%) with a broad size distribution, ranging from 10 nm to 100 nm (Figure 3.8b). The ratio of metallic precursors to polymer repeating units has been observed to play an important role in nanoparticle shape in previous work by other groups. For example, the shape of Pt nanoparticles varied from cubic to prismatic as the $[PtCl_4]^{2-}$ to polyacrylic acid ratio increased.[51a] Both the Xia and Yang groups have demonstrated control over the shape of Ag or Au nanocrystals simply by changing the metal to polymer ratio in their polyol syntheses.[49a,50]

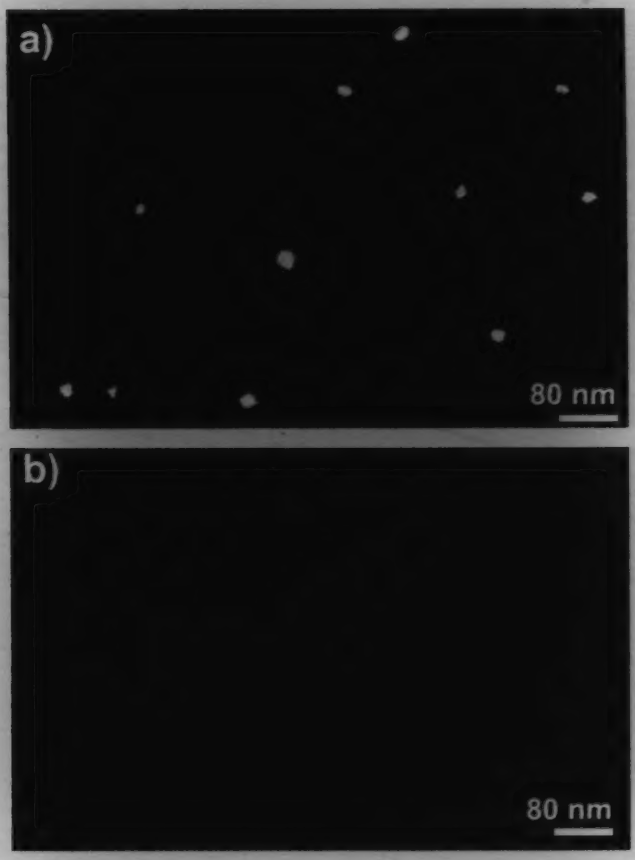

Figure 3.8 SEM images of gold nanoparticles formed on native oxide-capped Si(111). A monolayer of PS-P2VP on the surface was loaded with a) 0.1 Au^{III}/pyridyl groups and b) 0.7 Au^{III}/pyridyl groups, followed by a 5 minute thermal treatment at 250°C.

To investigate the scalability of the synthesis of gold octahedra, a bulk preparation was carried out with a thick film, prepared by evaporation deposition of a 0.5 wt% polymer solution in toluene on a silicon substrate, followed by thermal treatment at 250°C for 5 minutes in air. The ratio of $HAuCl_4$/PS-P2VP was kept constant at 0.5 Au^{III}/pyridyl group. Figure 3.9 shows the morphology of Au nanoparticles generated in this thick polymer film. At low magnification, the block copolymer strips are conspicuous in the SEM images, and all the gold nanoparticles are found imbedded within such polymer strips, which also suggests that the PS-P2VP block copolymer

works as a microreactor for the decomposition reaction.[65] Inspection of the higher magnification SEM images in Figures 3.9c-e reveals that the majority of gold particles are octahedral in shape, although icosahedra, decahedra and truncated tetrahedra are also present as minor products. Compared with the thin film products, the gold nanoparticles prepared in the thick films are better defined, since the thick polymer films provide a better environment for the shape development improving the nucleation and particle growth. In addition, in the thick films, the average size of the nanoparticles increased significantly: the average size reaches ~120 nm with moderate size dispersity for loadings of 0.5 Au^{III}/pyridyl group, in contrast to an average of ~50 nm in thin film samples, at the same loading of auric acid. Lowering the loading of auric acid to 0.1 Au^{III}/pyridyl group leads to particles with an average size of 70 nm, which is ~50 nm larger compared with monolayer samples where the particles are about 20 nm in diameter. Therefore, the average sizes of the gold nanocrystals under different conditions can be tuned over a wide range, from ~20 nm (monolayer, with 0.1 Au^{III}/pyridyl group loading) to above 120 nm (bulk sample, with 0.5 Au^{III}/pyridyl group loading).

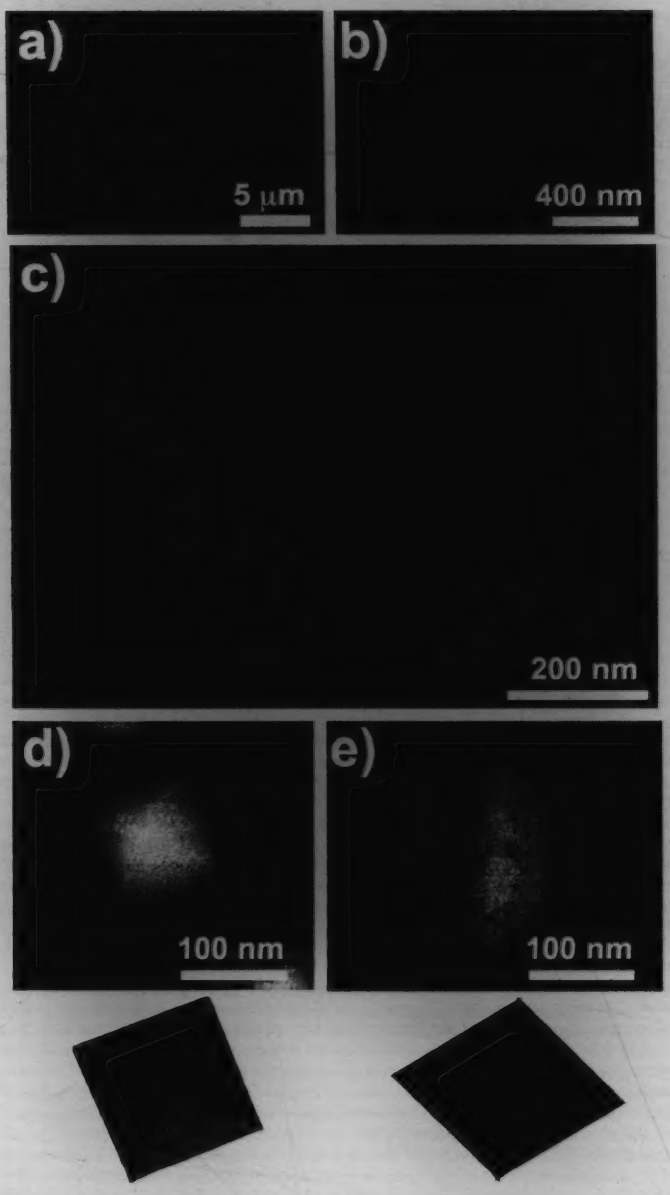

Figure 3.9 SEM data of gold nanoparticles prepared in a thick (5-8 μm) PS-P2VP sample on native oxide-capped Si(111). a-c) Low resolution SEM images of the gold nanoparticles imbedded within the polymer. d-e) Higher resolution SEM images of octahedra in the polymer matrix.

Selected area electron diffraction (SAED) of a single ~120 nm gold octahedron prepared via a bulk synthesis, taken by transmission electron microscopy (TEM), is shown in Figure 3.10 and is characteristic of a single crystalline gold nanoparticle with

(111) faces (perpendicular to the beam); the hexagonal diffraction pattern can be assigned to the (220) plane of the gold fcc crystal.[50c,55a,66] Due to the difficulty of clearly observing the gold nanoparticles within the polymer, a detailed statistical analysis was not carried similar to that shown in Figure 3.1e.

Figure 3.10 a) Transmission electron microscopy (TEM) image of an individual gold octahedron prepared through a bulk synthesis. b) Selected area electron diffraction (SAED) of the octahedron in a).

The gold nanoparticles prepared in bulk with a 250°C thermal treatment can be readily dispersed in a non-polar solvent such as chloroform or toluene. Higher temperatures result in lower fractions of gold octahedral nanoparticle products, and apparent degradation of the polymer makes dispersal difficult.[67] In order to remove excess polymer from the 250°C thermal treatment material, four cycles of centrifugation and dispersion in chloroform were carried out to minimize interference during the surface plasmon acquisition. It is assumed that a residual layer of block copolymer prevents aggregation of the nanoparticles in solution. Figure 3.11 shows optical photographs and the localized surface plasmon resonance (LSPR) of 120 nm Au nanoparticles in chloroform as well as the corresponding SEM image of the purified sample. The solution appears a green/blue color when placed in front of a white light due to absorption, while under ambient light, the solution is red-pink due to strong Rayleigh scattering.

Such bicolor appearance is widely observed for the metal nanoparticles with sizes above 30-50 nm.[68]

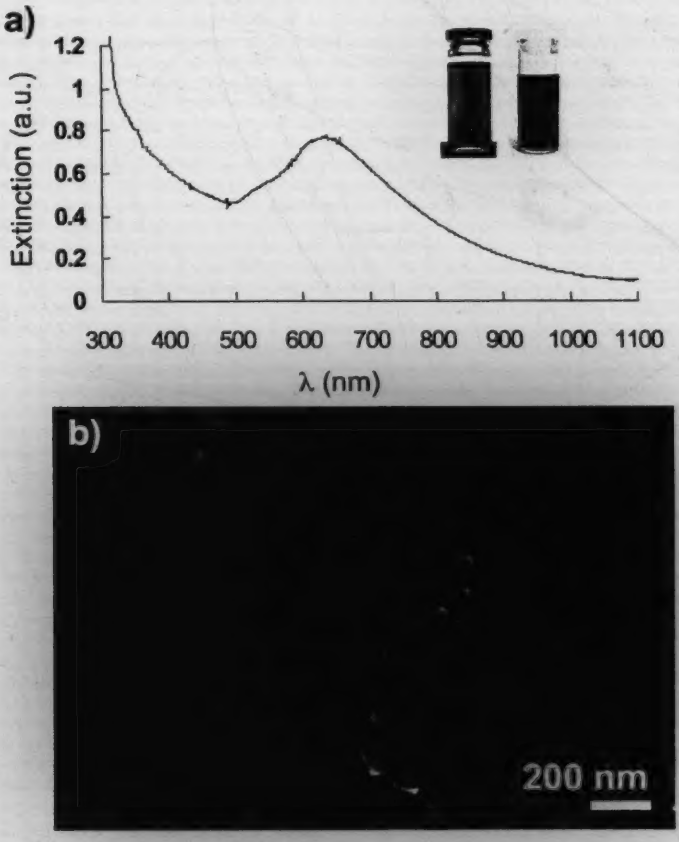

Figure 3.11 a) UV-Vis spectrum and optical photographs of a sample of gold octahedra prepared via the bulk synthesis route. b) SEM image of the sample used for the UV-Vis spectrum in a).

The exquisite Lycurgus Cup (glass; British Museum; 4th century A.D.) is a perfect example for this phenomenon. Octahedral nanoparticles present a LSPR maximum at 625 nm, similar to that of gold icosahedra of similar size.[49a]

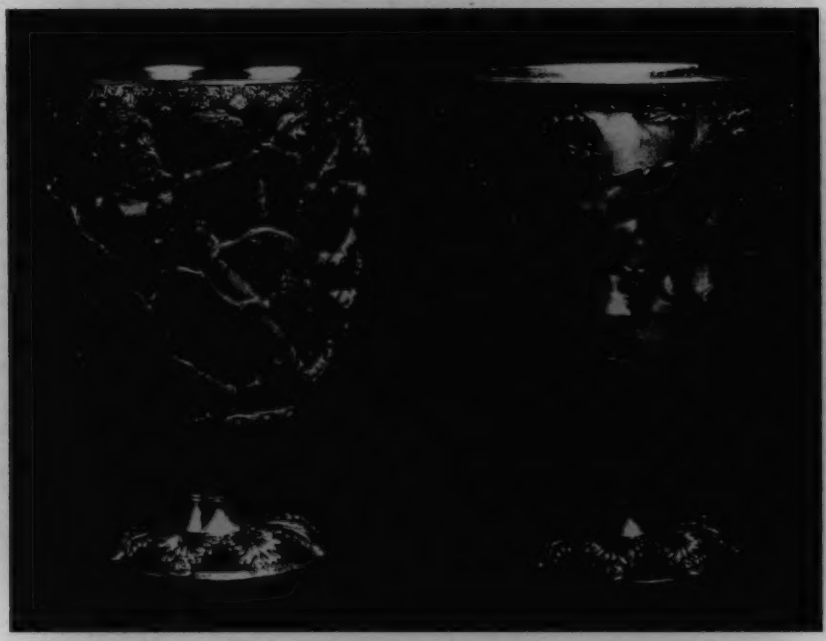

Figure 3.12 Lycurgus Cup (glass; British Museum; 4th century A.D.). This Roman cup is made of ruby glass. When viewed in reflected light, for example in daylight, it appears green. However, when a light is shone into the cup and transmitted through the glass, it appears red. (Adapted from Leonhardt, U. *Nat. Photon.* **2007**, *1*, 207-208.)

Replacement of PS-P2VP with polystyrene-*block*-poly(4-vinylpyridine) (PS-P4VP MW = 128400/33500) in a bulk synthesis (0.5 Au^{III}/pyridyl group loading) requires higher temperatures (300°C or greater) to observe metal deposition (Figure 3.13). Furthermore, the thermal decomposition products have a much broader size distribution than those from PS-P2VP, ranging from to 25 nm to over 175 nm. These results suggest that in case of PS-P4VP, the formation of gold nanoparticles requires additional energy, which necessitates the higher temperature and results in concurrent nucleation and growth. It appears that the polymer morphology and/or the strength of the interaction between the protonated pyridinium group of the pyridine and the $[AuCl_4]^-$ anion are important.

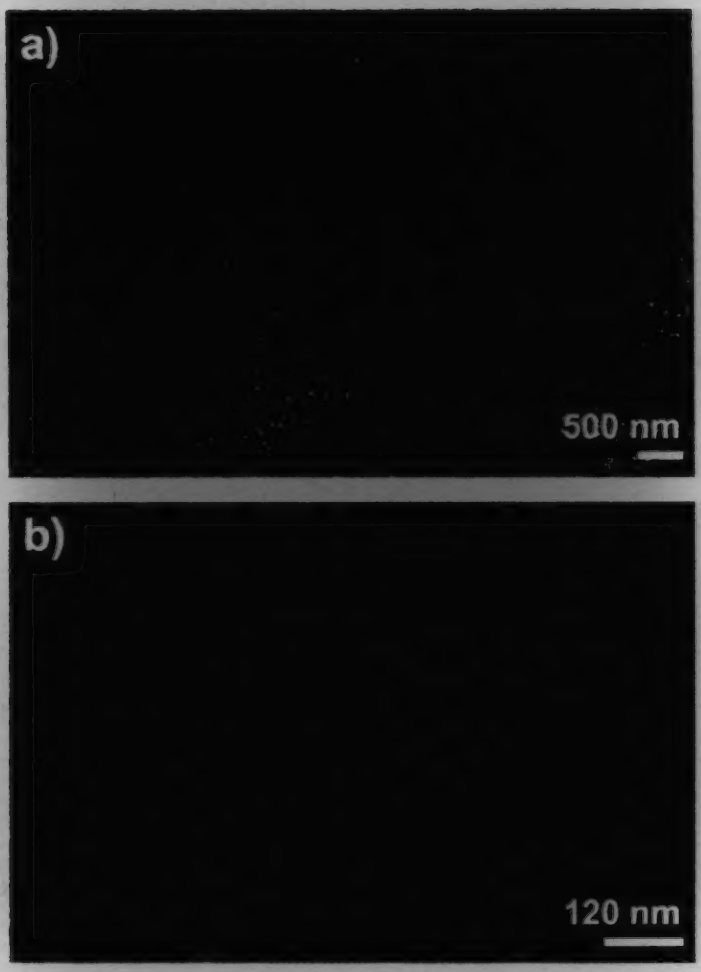

Figure 3.13 SEM images of gold nanoparticles formed upon heating a monolayer of PS-P4VP on the surface, loaded with 0.5 Au^{III}/pyridyl groups at 250°C.

Another feature of this thermal synthesis is its ability to simultaneously form diverse patterns of gold nanoparticles on surface due to the dewetting of the block copolymer films, which is usually caused by the thermal instability of the polymers above the glass transition temperature.[69] In our case, the glass transition temperatures for the two polymer blocks are 100°C (PS) and 138°C (PVP), both of which are well below the reaction temperatures.[70] Therefore dewetting occurs in order to lower the solid-polymer interface energy. According to the different thickness of polymer films, the polymer

morphology after dewetting could be tuned into holes, polygonal networks, bicontinuous structures and droplet structures.[69b] When the reactions were performed at 250°C with thin polymer films, the coverage and average density of the nanoparticles per unit area on the surface is acquired under different auric acid loading. At Au^{III}/pyridyl loadings of 0.1, 0.5 and 0.7, the average density of nanoparticles is approximately 36/μm^2, 32/μm^2, and 19/μm^2, respectively; these numbers indicate that the block copolymer is not directly mediating spacing since the average distances between the gold nanoparticles become independent of the observed room temperature patterning and thus verify that the dewetting is the most possible patterning mechanism: the thin polymer films form droplet structures through dewetting. The large inter-particle distance for this patterning makes it a possible substrate for single particle study, since the nanoparticles can be taken as isolated ones and their optical properties are not affected by interference by surrounding particles.[71] In case of bulk reactions, the bicontinuous structures of the PS-P2VP were formed with gold octahedra embedded inside. This metal/polymer hybrid structures might be useful as optical filters or nonlinear optical devices.

3.1.3 Conclusion

In conclusion, a one-step preparation route was developed to selectively produce octahedral gold nanoparticles. The $HAuCl_4$ loaded within thin or thick block PS-P2VP copolymer films undergoes thermal decomposition at a relatively low temperature of 250°C, in 5 minutes in air, to produce gold nanoparticles of different sizes, depending upon parameters such as $HAuCl_4$ loading, film thickness, and others. Higher temperatures lead to greater percentages of icosohedra and other shapes at the expense of

octahedra. Bulk samples of octahedra can be solubilized and analyzed by SEM, TEM and surface plasmon spectroscopy.

3.2 Block Copolymer Mediated Deposition of Metal Nanoparticles on Germanium Nanowires

3.2.1 Introduction

A very efficient approach to semiconductor metallization is galvanic displacement, an electrochemical reaction whereby a sufficiently oxidizing metal ion is reduced to its metallic state, and is accompanied by oxidation of the semiconductor.[72] The reactions do not require either an external electron source or a chemical reducing agent; on the other hand, the reducing electrons are derived from the valence band or bonding electrons of the solid. (Scheme 3.2)

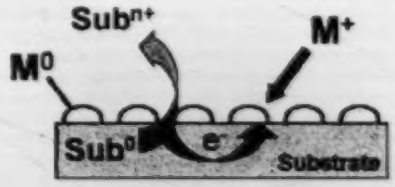

Scheme 3.2 Outline of galvanic displacement. A semiconductor substrate is in contact with a solution of sufficiently oxidizing metal ions (M^+) which oxidize the semiconductor and, in turn, will be reduce from M^+ to M^0 on the surface of the semiconductor. (Adapted from Porter, L. A.; Choi, H. C.; Ribbe, A. E.; Buriak, J. M. *Nano Lett.* **2002**, *2*, 1067-1071.)

Galvanic displacement reactions of noble metals on flat germanium surfaces are particularly intriguing due to the apparent formation of an intermetallic metal-germanium interface, leading to a strongly bound metal film, and potentially, an electronically active interface.[73] For example, a dip-and-rinse galvanic displacement approach to synthesizing complex, highly regular crystalline silver inukshuk architectures directly on germanium surfaces, with only three ingredients: silver nitrate, water, and germanium, has been described previously. In this case, germanium-germanium bonds in the crystal

lattice acted as the reducing agent for the Ag^{+} ions in solution, leading to Ag(s) and concomitant oxidation of Ge(s) to Ge^{4+} in the following spontaneous redox reaction.

While galvanic displacement on flat germanium surfaces has been investigated, little is known as to whether galvanic displacement reactions on nanostructured germanium surfaces could lead to interesting composite materials, controllably linking metal nanoparticles to this technologically important semiconductor material. Generally, integration of semiconductor nanowires with extant devices is a critical challenge that requires addressing for many applications.[74] The traditional solution uses lithographically defined metal electrodes having a width of ~1 μm. These metal contacts define a size scale that is much larger than the nanometer-scale building blocks, thus limiting many potential advantages of applications using nanowires as, for example, high density logic and memory arrays.[74b] Because metal nanoparticles interfaced directly to a nanowire provides a means of "wiring in" via metallic interconnects and possibly molecules, it is becoming an increasingly relevant approach.[75] For instance, electroless deposition of metal nanoparticles on carbon nanotubes has been reported, although the oxidation product of the reaction remains obscure.[76]

The syntheses of germanium nanowires in high yield via supercritical fluid-liquid-solid (SFLS) processes, as well as by vapour-liquid-solid (VLS) processes have been demonstrated in recent years.[77] For example, in the SFLS processes, the Ge nanowires were synthesized by a gold nanocrystal-seeded process in supercritical hexane using the organo-germane precursor, diphenylgermane (DPG), as the Ge source. The

resulting nanowires are single crystals with few crystallographic defects. They exhibit a predominant <110> growth direction with diameters ranging from 7 to 25 nm. The accessibility to such germanium nanowires makes it possible to investigate the related galvanic displacement.

Galvanic displacement of gold nanoparticles has recently been demonstrated on silicon nanowires (prepared by VLS) in the presence of dilute HF (aq), and the reaction leads to consistent coverage of gold nanoparticles along the length of the Si nanowires.[75a,b] With germanium nanowires, on the other hand, attempts to carry out galvanic displacement with either gold or silver ionic precursors, $HAuCl_4$ (aq) and $AgNO_3$ (aq), lead to significant corrosion of the nanowire structures; little control of the etching process is possible, and variability is seen from wire-to-wire within the same sample batch. The difference between germanium and silicon is related to the oxide coating: germanium oxide is water soluble, whereas the silicon oxide is not.[73] The rate of oxide etching in the case of silicon is at least partially controlled by the HF concentration; with germanium, however, no such restraint exists in aqueous solution; and undercutting is a severe problem. A new, non-aqueous method to control both metal ion reduction and concomitant germanium oxidation, and germanium oxide dissolution was required. Ideally, the approach should be a simple, solution processable approach permitting large scale functionalization reactions.

Block copolymer micelles that contain polystyrene (PS) and poly(2- or 4-vinylpyridine) (P2VP or P4VP) blocks have been demonstrated to deliver metal ions to

semiconductor surfaces for galvanic displacement reactions, leading to deposition of metal nanoparticles.[58] (Scheme 3.3) The micellar cores can be loaded with the metal precursor salt ($AgNO_3$ or $HAuCl_4$) in a quantifiable fashion.[78] The block copolymer can be therefore utilized to provide a point of restriction with respect to the passage of reagents to the semiconductor interface. As previously demonstrated on flat semiconductor surfaces, the size of formed metal nanoparticles can be controlled at the nanoscale, and the obtained structures, arrays of sub 20 nm metal nanoparticles, are vastly different than the much larger, irregular metal deposits observed in absence of block polymer.[73] In addition, in the previous section, we have demonstrated that block copolymers have specific interactions with the metal surface. Therefore, it is expected that the introduction of PS-P2VP or PS-P4VP will bring certain shape selectivity into the galvanic displacement reactions.

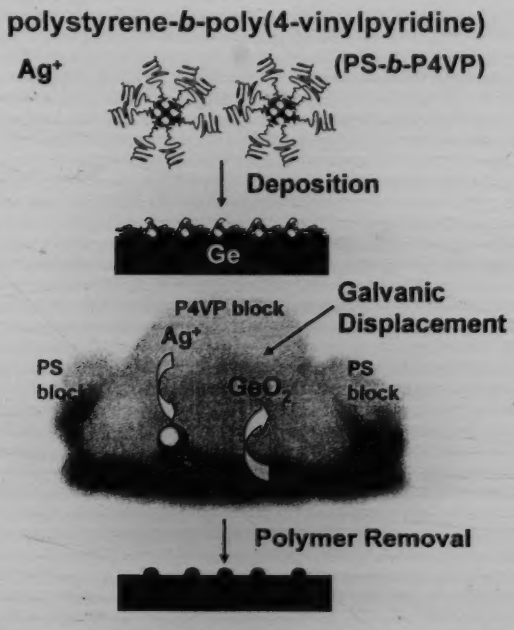

Scheme 3.3 Outline of the block copolymer mediated delivery of reagents to semiconductor surfaces. The block copolymer micelles are shown in red (corona) and blue (core). The pyridine groups associate with metal ions in the core, which are then reduced by electrons from the semiconductor substrate via a galvanic displacement reaction. (Drawing courtesy of Dr. M. Aizawa)

Here we describe a non-aqueous controllable galvanic displacement on germanium nanowires. Mediated by block copolymers, metal ions can be delivered to the germanium surface in a mild way, producing metal nanoparticles on germanium nanowires, thereby avoiding problems of uncontrolled wire etching and undercutting in standard aqueous solution-based galvanic displacement chemistry. By changing the reaction conditions, the sizes, coverage, and even the shapes of resulted metal nanoparticles can be controlled in a wide range.

3.2.2 Results

As described above, the attempts of performing galvanic displacement on germanium nanowires in aqueous solutions only resulted in corrosion on nanowires. As shown in Figure 3.14, the wires are obviously corroded, cleaved, or entirely dissolved, and the metal deposition is irregular, even at different metal ion concentrations.

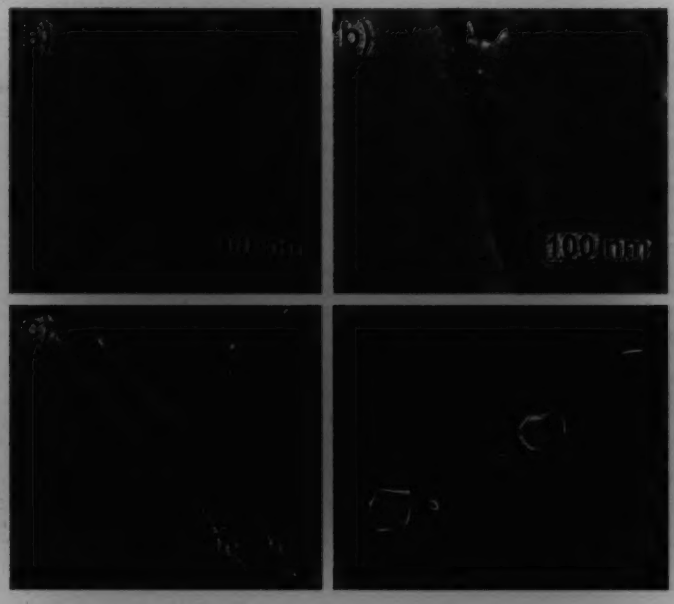

Figure 3.14 a) TEM image of pristine Ge nanowires. b-d) Ge nanowires subjected to aqueous galvanic displacement for 60 s in ambient: b) TEM, 0.1 mM $AgNO_3$ (aq). c) TEM, 0.1 mM $HAuCl_4$ (aq). d) SEM, 1.0 mM $HAuCl_4$ (aq).

The two approaches of galvanic displacement detailed in this study are summarized in Scheme 3.4.

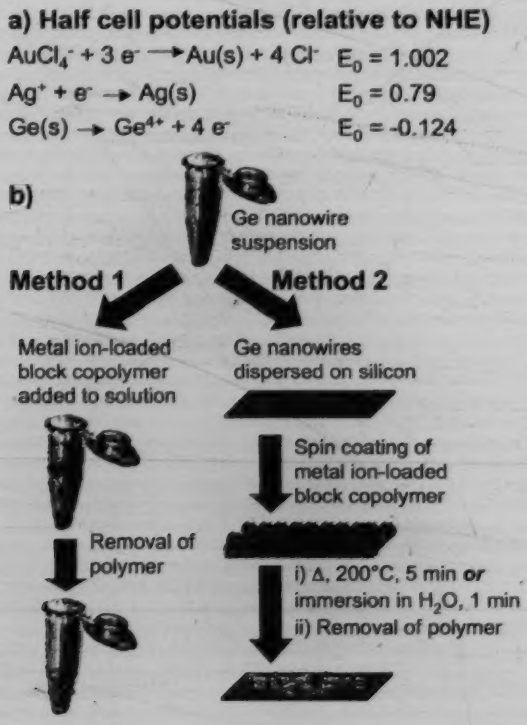
a) Half cell potentials (relative to NHE)
$AuCl_4^- + 3\ e^- \rightarrow Au(s) + 4\ Cl^-$ $E_0 = 1.002$
$Ag^+ + e^- \rightarrow Ag(s)$ $E_0 = 0.79$
$Ge(s) \rightarrow Ge^{4+} + 4\ e^-$ $E_0 = -0.124$
b)
Ge nanowire suspension
Method 1
Method 2
Metal ion-loaded block copolymer added to solution
Ge nanowires dispersed on silicon
Spin coating of metal ion-loaded block copolymer
Removal of polymer
i) Δ, 200°C, 5 min or immersion in H_2O, 1 min
ii) Removal of polymer

Scheme 3.4 Summary of the two methods described here, utilizing block copolymers to controllably deliver metal ions to the Ge nanowire surface, leading to a galvanic displacement reaction and nanoparticle formation.

Germanium nanowires, prepared from a supercritical fluid-liquid-solid (SFLS) synthesis,[77a-c] were either used as untreated (oxide capped) or etched (hydrogen terminated) via short treatment with dilute HF [10% (aq)], to remove the external oxide coating, rendering the nanowires hydrophobic.[77d] In method 1 of Scheme 3.4, 0.5 mL of a 0.5 wt% solution of polystyrene-*block*-poly(2- or 4- vinylpyridine) (PS-P2VP or PS-P4VP, respectively), preloaded with 0.2-0.6 molar equivalents of metal ion precursor ($HAuCl_4$ or $AgNO_3$) per pyridyl group, was mixed with 0.5 mL of a suspension of germanium nanowires (derived from a stock suspension of 0.3 mg of nanowires in 20 mL

toluene) in a standard eppendorf, at ambient conditions. The mixture was allowed to react for one minute before centrifugation to form a visible dark pellet. The toluene was replaced with fresh toluene, the nanowires redispersed with brief ultrasonication, and the centrifugation process repeated twice. As shown in Figure 3.15a-d, sparse deposition of gold and silver nanoparticles is observed on the oxide-capped Ge nanowires, using PS-P2VP (MW = 91,500-105,000), with a ratio of M^{n+}/pyridyl of 0.5. Scanning Auger microscopy (Figure 3.15c-d) confirms the elemental identity of gold and silver deposits.

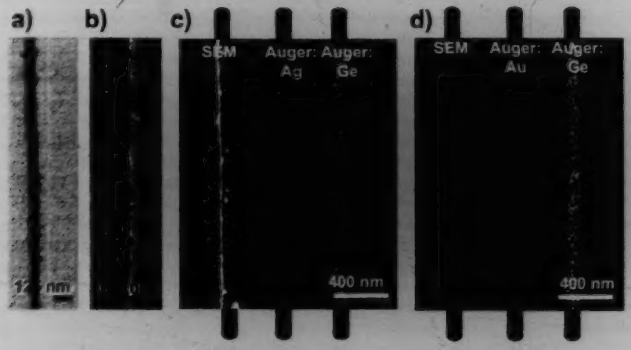

Figure 3.15 a-b) TEM images of oxide-capped Ge nanowires, prepared via method 1, with 0.5 wt% PS-P2VP (MW = 91,500-105,000) in toluene, loaded with $AgNO_3$ and $HAuCl_4$, respectively; ratio M^{n+}/pyridyl group = 0.5. c-d) Scanning Auger microscopy of Ge nanowires prepared in the same manner as a-b).

XPS verifies that the deposited nanoparticles are indeed Au^0 or Ag^0 (Figure 3.16).

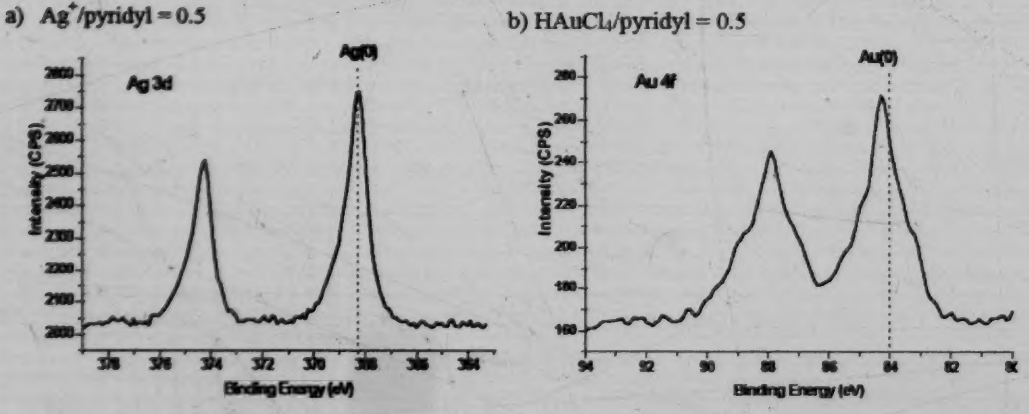

Figure 3.16 XPS, Deposition method 1, HF etched Ge NWs, using PS-P2VP (MW = 91,500-105,000), 0.5 wt% polymer in toluene.

Such sparse deposition on the nanowires reveals that the oxide layer has hindered the displacement reactions on the surface to a certain degree. A pair of low metal loading reactions was carried out to verify it. (Figure 3.17) In this case, the M^{n+}/pyridyl ratio was reduced from 0.5 to 0.2, resulting much less deposition on the germanium nanowires. For some nanowires, there was no visible deposition at all.

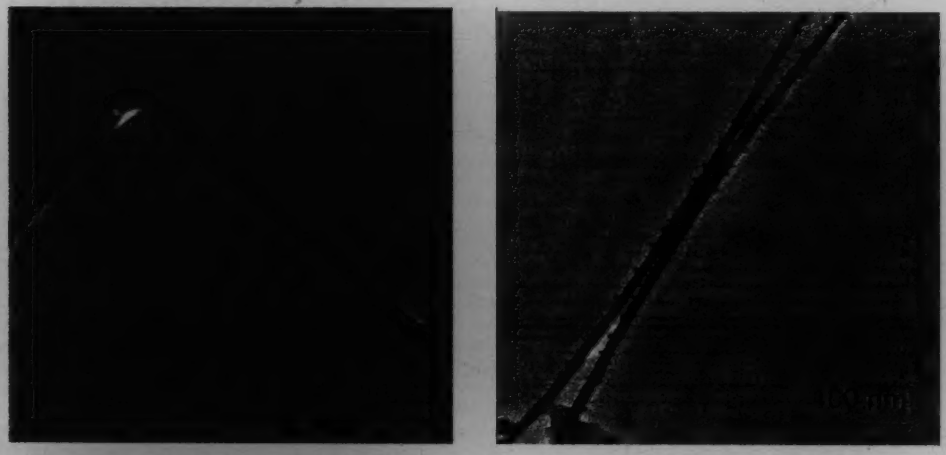

a) TEM image, $AgNO_3$-loaded PS-P2VP (MW = 91,500-105,000), at a ratio of 0.2 Ag^+/pyridyl.

b) TEM image, $HAuCl_4$-loaded PS-P2VP (MW = 91,500-105,000), at a ratio of 0.2 Au^{III}/pyridyl.

Figure 3.17 Results of deposition method 1, on oxide-capped (crude) Ge NWs.

Much greater deposition was observed, however, when the Ge nanowires were etched with HF (aq). As demonstrated with PS-P2VP (MW = 91,500-105,000, 0.5 wt%

in toluene), both the high (0.5) and low (0.2) metal ions loading resulted in the full coverage of metal nanoparticles on the nanowires. (Figure 3.18)

a) TEM, $AgNO_3$-loaded PS-P2VP (MW = 91,500-105,000), Ag^+/pyridyl = 0.2, 0.5 wt% polymer in toluene.

b) TEM, $AgNO_3$-loaded PS-P2VP (MW = 91,500-105,000), Ag^+/pyridyl = 0.5, 0.5 wt% polymer in toluene.

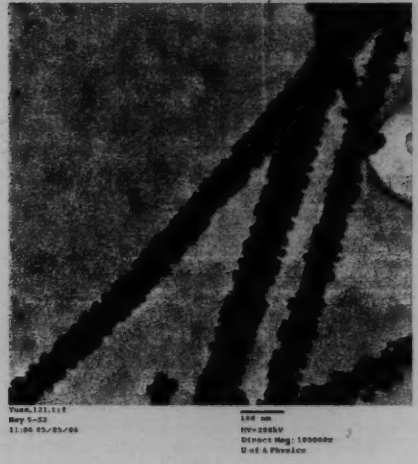

c) TEM, $HAuCl_4$-loaded PS-P2VP (MW = 91,500-105,000), $HAuCl_4$/pyridyl = 0.2, 0.5 wt% polymer in toluene.

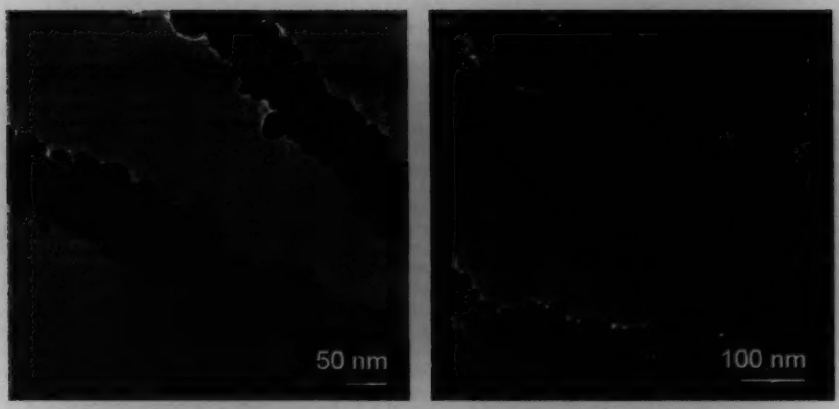

d) TEM, $HAuCl_4$-loaded PS-P2VP (MW = 91,500-105,000), $HAuCl_4$/pyridyl = 0.5, 0.5 wt% polymer in toluene.

Figure 3.18 Results of deposition method 1, on hydrogen terminated (etched) Ge NWs.

The replacement of PS-P2VP with PS-P4VP gives the similar galvanic displacement results. As shown in Figure 3.19 for silver using 0.5 wt% PS-P4VP (MW = 128,000-33,500) in toluene, with a ratio of Ag^+/pyridyl groups of 0.6, even coatings of metal nanoparticles over the entirety of the nanowire length are observed.

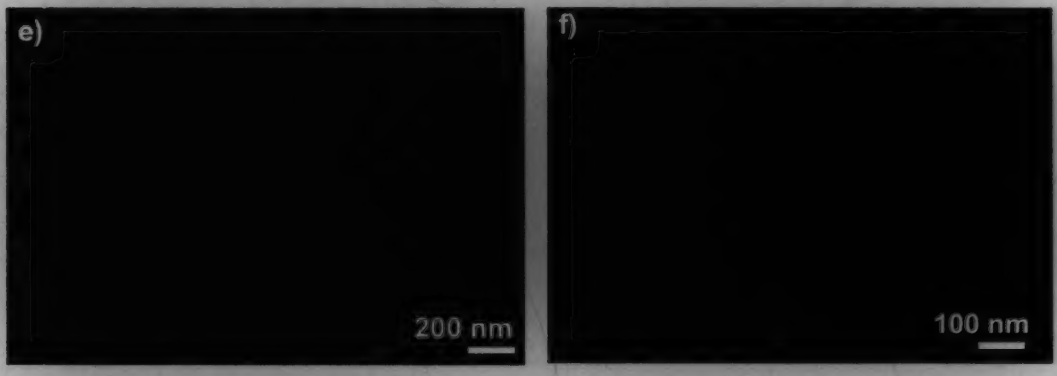

Figure 3.19 SEM images of silver nanoparticles on HF-etched Ge nanowires, formed via Method 1, using $AgNO_3$ and PS-P4VP (MW = 128,000-33,500).

While no control over particle spacing on the nanowires was observed, the choice of block copolymer molecular weight and other experimental parameters influenced the metal deposition outcome. For instance, increasing the $HAuCl_4$/pyridyl ratios from 0.2 to 0.5 resulted in an increase in particle size from ~10 nm to ~20-40 nm. Increasing the

wt% in toluene of PS-P2VP from 0.5 to 1, keeping the metal loading constant ($HAuCl_4$/pyridyl = 0.5), also predictably led to an increase in particle size, and an increase of the nanoparticle density as well (Figure 3.20).

Figure 3.20 TEM, Deposition method 1, HF etched Ge NWs, using PS-P2VP (MW = 91,500-105,000), $HAuCl_4$/pyridyl = 0.5, 1.0 wt% polymer in toluene.

Smaller molecular weights for PS-P2VP (MW = 25,500-23,500) resulted in smaller particles (~10 nm), keeping all other parameters constant ($HAuCl_4$/pyridyl = 0.5, 0.5wt% polymer in toluene) (Figure 3.21). It is clear that modulation of these experimental conditions can afford some degree of control over nanoparticle uniformity when deposited on the germanium nanowires.

Figure 3.21 TEM, Deposition method 1, HF etched Ge NWs, using PS-P2VP (MW = 25,500-23,500), $HAuCl_4$/pyridyl = 0.5, 0.5 wt% polymer in toluene.

In order to provide an alternative to the solution method (Method 1), a second approach was developed that utilizes the propensity of the nanowires to physisorb on a native-oxide capped silicon wafer. Method 2 as outlined in Scheme 1, involves dispersal of hydride- or oxide-terminated Ge nanowires on flat, native oxide-capped Si, followed by spin coating of a monolayer of $HAuCl_4$-loaded PS-P2VP block copolymer micelles over the entire surface (MW = 91,500-105,000, 0.5 wt% in toluene, $HAuCl_4$/pyridyl = 0.5). At room temperature in air, little deposition of gold is noted. Deposition is initiated, however, with brief heating to 200°C in air (5 min), followed by polymer removal with warm toluene; the results are shown in Figure 3.22.

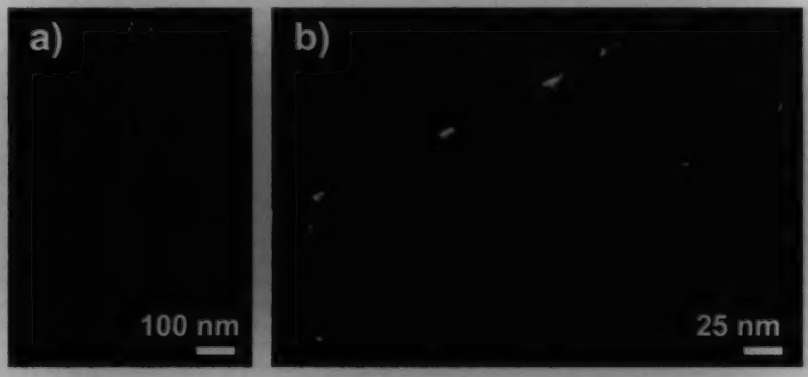

Figure 3.22 SEM images of gold nanoparticles on crude Ge nanowires, prepared via method 2 with thermal treatment at 200°C for 5 min. Block copolymer is PS-P2VP (MW = 91,500-105,00), ratio of $HAuCl_4$/pyridyl = 0.5

Arrays of trianglular plates and other anisotropic gold nanoparticles are clearly seen on the surface of germanium nanowires. Thin polymer films gave better results in this reaction; there were almost no noticeable nanoparticles formed when a very thick polymer film was applied. The size distribution of those nanoparticles is quite narrow and the sizes are well below 20 nm. The ability to synthesize such small gold nanoparticles with specific shapes on semiconductor nanowires surfaces makes this method unique. Little difference is noted between hydride- or oxide- termination, most

likely due to in-situ oxidation of the Ge-H_χ interface under these conditions. The temperature to which the Ge nanowires are heated is critical: 180°C and 190°C led to little metal deposition, and 210°C and above resulted in $HAuCl_4$ thermal decomposition throughout the block copolymer micelles on the silicon surface (Figure 3.23).[79] It remains to be determined if the Au^{III} to Au^0 conversion is in fact due to galvanic displacement or thermal decomposition of $HAuCl_4$, or both. What we can speculate here, however, is that the intermediate temperature (200°C) is suitable to melt the block copolymer, increasing contact between $HAuCl_4$ and germanium nanowires, and bringing water vapor in the air to dissolve the germanium oxide as well.

Figure 3.23 SEM images (polymer left on) of deposition method 2 (thermal treatment) on oxide-capped (crude) Ge NWs, using PS-P2VP (MW = 91,500-105,000), 0.5 wt% polymer in toluene. a) 180°C; b) 190°C; c) 210°C; d) 220°C

A second variation that leads to metal deposition involves immersion of the same

polymer-coated nanowires on silicon in water at room temperature (1 min). The galvanic displacement reaction occurs quickly but with a much higher degree of uncontrolled, random metal growth (Figure 3.24); the role of the water is presumably to dissolve the formed germanium oxides, allowing the galvanic displacement reaction to continue. The thermal method is preferable if a tighter range of nanoparticle sizes is desired.

Figure 3.24 Results of deposition method 2 (water treatment for 1 min), on oxide-capped (crude) Ge NWs, using PS-P2VP (MW = 91,500-105,000), 0.5 wt% polymer in toluene.

3.2.3 Conclusion

To summarize, metal ion delivery, mediated by block copolymers, is an effective method of producing metal nanoparticles on germanium nanowires, thereby avoiding problems of uncontrolled wire etching and undercutting in standard aqueous solution-based galvanic displacement chemistry.

Chapter 4

Interactions between Metal Nanoparticles and Blood

4.1 Interactions between Metal Nanoparticles and Simulated Blood Plasma

4.1.1 Introduction

Nanotoxicity, as a new developing discipline, has been the focus of intensive interests in recent years. Research about the potential adverse effects on human health has been summarized in a previous chapter. So far, most published results have focused on the behavior of nanoparticles incubated with specific cell cultures or organisms, including cellular uptake and cytotoxicity.[44-47] There is, however, very little fundamental information about the physicochemical interactions between nanomaterials and the various components of blood.[86]

Intentional and unintentional uptake of nanoscale materials in the blood via different routes is highly likely. For instance, as described in a previous chapter, once the inhaled nanomaterials reach the alveolar region, they could be translocated into the pulmonary interstitial sites, followed by further transcytosis to regional lymph nodes. Some particles, after accumulation in lymph nodes, will also translocate into post-nodal lymph and then enter the blood circulation.[27d] Collectively, the studies indicate that particle size and surface chemistry, and possibly charge govern translocation. Albumin, the

most abundant protein in plasma and interstitium, appears to facilitate nanomaterials translocated via caveolae, which is normally a pathway only for larger particles (~500 nm) without surface coating;[87] so does lecithin, a phospholipid.[88] For nanomaterials below 200 nm, internalization via clathrin-coated pits may be involved as well.[89] Furthermore, particles cleared via the mucociliary escalator and swallowed into the gastrointestinal tract could also be taken into the blood circulation across the intestinal epithelium.[29d]

In addition to the above unintentional uptake of nanoscale materials in the blood, there exists the possibility of intentional absorption, due to the many biomedical applications envisioned based upon nanoparticles for sensing, drug delivery, and imaging, among others. One widely studied example is the use of fluorescent quantum dots (QDs) for *in vivo* targeting and imaging via intravenous or intradermal injection.[26d,e] The fluorescence emission wavelength (from the UV to near IR) of QDs can be tuned by varying the particle size and composition and thus they have the potential to revolutionize imaging of live cells, tissue, and whole organs. Other examples involve gold nanoparticles; an example is the application of gold nanoparticles in inhibiting the proliferation of multiple myeloma, a monoclonal malignant plasma cell, without affecting the proliferation of normal peripheral blood mononuclear cells (PBMCs).[86e] Magnetic iron oxide nanoparticles are under investigation for use as contrast agents in magnetic resonance imaging (MRI), as they cause changes in the spin-spin relaxation times of neighboring water molecules, to monitor gene expression or detect pathologies such as cancer, brain inflammation, arthritis, or atherosclerotic plaques.[90] Furthermore, carboxymethyl dextran (CMD) coated magnetic particles can be used for the separation

of tumor cells from the peripheral blood cells.[86d] Polymer-nanoparticle composites containing drugs designed to be transported are being widely studied, but at present, the lack of understanding between the influence of surface chemistry and materials in the blood has made this research challenging.[91]

Because of the wide variety of routes for the uptake of nanomaterials in the blood, and the potential long term existence of these particles in blood circulation, a detailed physicochemical study of the reactivity, stability, and potential aggregation of nanomaterials in the blood is an absolute necessity. Current research on this topic remains limited.[86] It was reported that 60 nm polystyrene particles could be related to the resulting thrombus formation in a hamster model after intravenous and intratracheal injection.[86a] While the unmodified particles had no effect on thrombosis, the carboxylate- polystyrene particles significantly inhibited thrombus formation, and the amine- polystyrene particles significantly enhanced thrombosis, indicating the surface chemistry of such polystyrene particles has a significant influence on the results. Such *in vivo* prothrombotic tendency results, at least in part, from platelet activation by positively charged amine-polystyrene particles. The results were then extended to the intratracheal injected diesel exhaust particles (DEPs), which not only led to the rapid induction of pulmonary inflammation but also enhanced both arterial and venous thrombosis after minor vessel injury, in association with circulating platelet activation.[86b] Recently, engineered and combustion-derived carbon nanoparticles, including single-walled nanotubes, multi-walled nanotubes, fullerenes, and mixed carbon nanoparticles, were employed in similar investigations. Research showed that these

carbon nanomaterials, except fullerenes, were able to induce aggregation of human platelets and to enhance vascular thrombosis in rats.[86c]

In our research, we want to gain a fundamental understanding of the physicochemical interactions between nanomaterials and the various components of the blood. We began such research from a chemical perspective, focusing up on the fate of nanomaterials in the complex environment of blood. How the material size, shape, composition, and surface chemistry affect the reactivity, stability, and potential aggregation of monodisperse engineered metal and semiconductor nanomaterials in the blood attracted our attention. With sufficient results on this chemical topic, we would like to extend our research to the biology area, investigating possible biological effects that the nanomaterials may exert on the blood components. Ultimately, we anticipate that systematic research on nanomaterials and blood could provide guidelines to avoid negative outcomes in the much anticipated biological and medical applications.

In this thesis, we selected metal (gold and silver) nanoparticles as the model system for such studies; the rationale being that gold and silver nanoparticles can be synthesized with a broad range of sizes (1-200 nm diameter) and shapes (nanorods,[49c,56,84b] 1:1 to 1:10 aspect ratio; triangle nanoplates[92]). Surface functionalized metal nanoparticles are also easy to characterize via the techniques of UV-Vis spectrophotometry, FT-IR spectrometry,[93] scanning electron microscopy (SEM), and transmission electron microscopy (TEM). Furthermore, gold nanoparticles have recently been demonstrated in cell imaging, targeted drug delivery,[94] and cancer diagnostics[95] and therapeutic

applications.[96] These studies appear to be representative of the initial applications of metal nanoparticles in biology and medicine.

Before commencing with human blood products, we worked initially with the widely studied simulated blood plasma (SBP) solution which was developed by Kokubo and coworkers.[97] The solution mimics the inorganic ion concentration in human blood plasma (HBP) with a composition of 1.0 mM K_2HPO_4, 4.2 mM $NaHCO_3$, 2.5 mM $CaCl_2$, 1.5 mM $MgCl_2$, 3.0 mM KCl, and 134.8 mM NaCl, and is buffered at the physiological pH (~7.4) with trishydroxymethylaminomethane (Tris) and HCl. Applications of SBP solutions include the stability evaluation of derivatized mesoporous silicon and *in vitro* simulation of biological mineralization.[98] Although a revised SBP solution was reported a few years ago with an increased amount of $NaHCO_3$, which is exactly equal to the amount of HCO_3^- in HBP,[98b-d] we chose to use the original recipe to avoid the possible [HCO_3^-] change in the revised one. In addition, bovine serum albumin (BSA) was added into the SBP solution later to better mimic the 7-8% of proteins present in the HBP.[99] It is expected the addition of BSA would be quite important for the stability of metal nanoparticles, since previous reports showed that albumin could act as the surfactant in nanoparticle synthesis.[100]

4.1.2 Results

The gold nanoparticles used for this research were generally synthesized via the seed mediated growth method in the presence of cetyltrimethylammonium bromide (CTAB), shown in the Scheme 4.1.

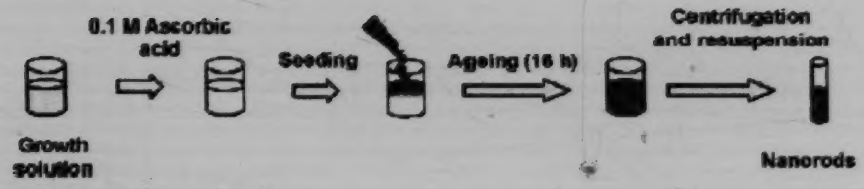

Scheme 4.1 Preparation of gold nanorods via the seed mediated growth method. [48g]

Both 10 and 60 nm facetted spheres were prepared in a one step growth procedure by altering the reaction conditions, while a three step growth method is employed to prepare the long nanorods (20x200 nm, 1:10 aspect ratio). When a small amount of silver ions were introduced into the growth solution, the aspect ratio could be significantly reduced to 1:3, and thus short nanorods were made in a high yield.[56] The resultant gold nanoparticles were capped by a bilayer of CTAB, and were purified by centrifugation.[93a,101] SEM images in Figure 4.1 show four kinds of gold nanoparticles prepared via this CTAB-ascorbic acid reaction. UV-Vis spectra of the solutions of these nanoparticles are also presented (Figure 4.1e), revealing size and shape information as well. Due to the large aspect ratio, the longitudinal surface plasma absorbance of long nanorods falls into the near-IR range, so the spectrum for such nanorods is not included.[84b]

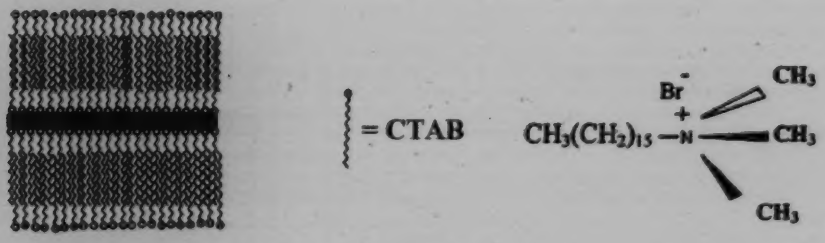

Scheme 4.2 Cartoon structure of gold nanorods capped by a bilayer of CTAB. [48g]

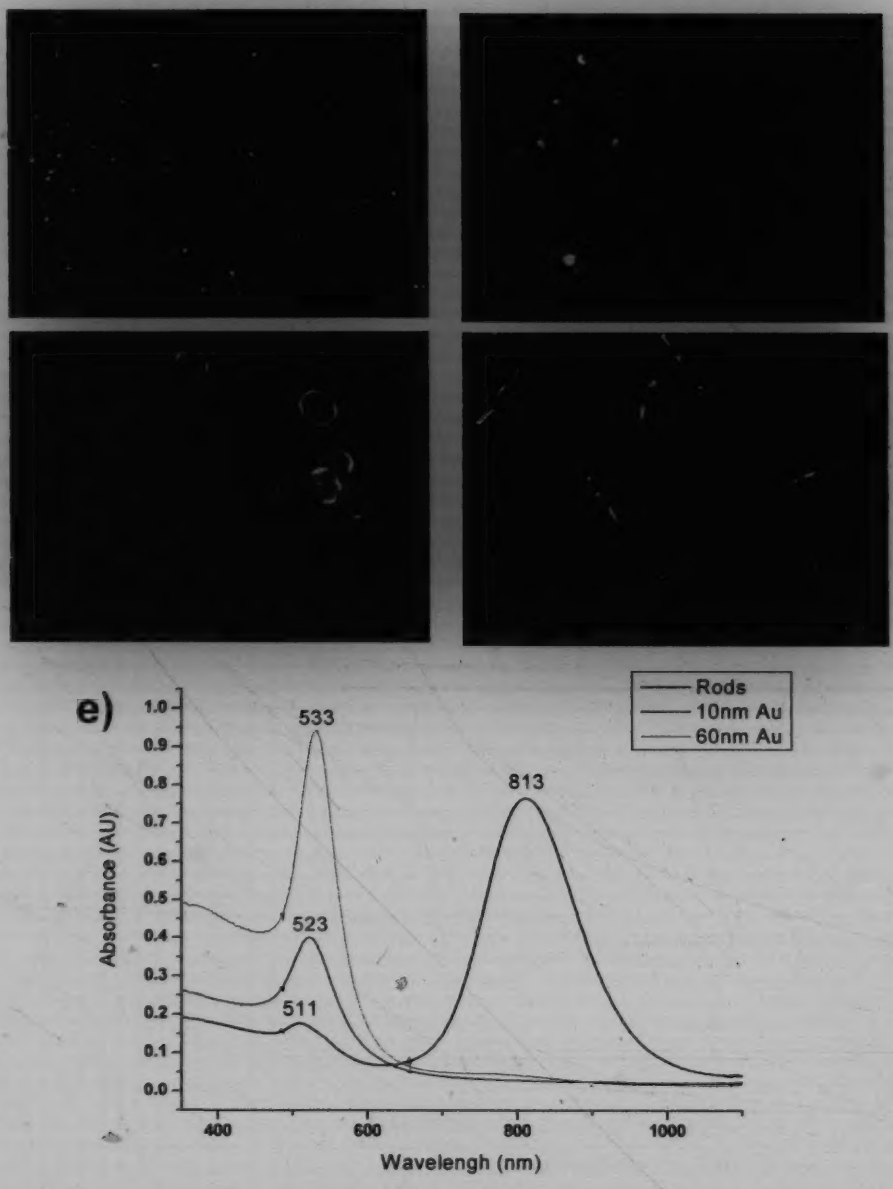

Figure 4.1 Au nanoparticles were synthesized via the CTAB-ascorbic acid reaction. The resultant nanoparticles were capped by a bilayer of CTAB and were purified by centrifugation. SEM images of Au nanoparticles: a) short nanorods (1:3 aspect ratio); b) 10 nm nanoparticles; c) 60 nm nanoparticles; d) long nanorods (1:10 aspect ratio); e) UV-Vis spectra of the Au nanoparticles.

As a control experiment, after centrifugation, some nanoparticles from Figure 4.1 were first dissolved in water with no added salts, and allowed to sit at 37°C for 7 days,

with no extra additives. As shown in Figure 4.2, the shapes of the particles are visible, and only slight changes have occurred. To be more specific, in Figure 4.2b, some fusion of the 10 nm particles is clear, but most remain intact and separated. The 60 nm particles in Figure 4.2c do not present any difference whatsoever when compared to the starting nanoparticles. Previous research has demonstrated that the CTAB bilayer would not be removed from nanoparticles after a few cycles of centrifugation.[102] Our results here reveal that the remaining surfactant layers can sufficiently prevent the gold nanoparticles from aggregation or agglomeration in aqueous solution, especially for large particles.

Figure 4.2 SEM images of Au nanoparticles from Figure 4.1, held in a pure water solution at 37°C for one week.

Incubation of such gold nanoparticles in the SBP solution without albumin was performed following the blank experiments. Instead of water, 1 mL SBP solution was used to disperse the centrifuged gold nanoparticles, and was preserved at 37°C. It is important to note that these cationic particles lost their original vivid colors in solution immediately after the addition of SBP solution. They appeared to precipitate in the SBP solution and form a dark powder at the bottom of the reactor eppendorf. This phenomenon described here clearly points to the great change of the aggregation state of gold nanoparticles in the high salt environment of the SBP solution. More detailed information was provided by the SEM images in Figure 4.3, showing a different picture

of events for 2 days, 7 days, and 22 days. The short nanorods, in Figures 4.3a-c show evidence of fusion after 2 days, becoming completely fused at 7 days; little additional change is observed following this 7 day immersion. Figures 4.3d-f show rapid fusion for the 10 nm particles, with large conglomerates visible at 7 days. The 60 nm nanoparticles appear to be the most stable, showing some fusion until 7 days; after the elongated 22 days period, more concrete fusion was observed. The long nanorods exhibit a similar stability to the 60 nm nanoparticles, showing incomplete fusion after 7 days (images not shown). On a qualitative basis, the 10 nm particles are the most reactive, followed by the short rods, followed by the much more stable long nanorods and 60 nm gold particles. The salt induced aggregation of gold nanoparticles has been described several times previously, but most of the results are based on the citrate capped gold nanospheres,[103] whereas the gold nanoparticles in our case are capped with CTAB. Although it is believed that the CATB capped nanoparticles have a higher stability than the citrate capped ones, our results show such stability is still insufficient in SBP solution. The aggregation and following agglomeration can be explained as the result of the high salt environment of the SBP solution. The anions with high concentration would effectively neutralize the positive surface charges, lower the ζ-potential, and thus facilitate the formation of aggregation and fusion.[103] Thus, the high radius of curvature of the 10 nm nanoparticles results in packing of the CTAB layer of lower quality, resulting in greater fusion. On the other hand, the 60 nm nanoparticles and the long nanorods have large flat surface areas. The CTAB molecules can then closely pack into a dense bilayer, which can resist the "ionic erosion" to a certain degree, providing relative higher stabilities.[93a,101]

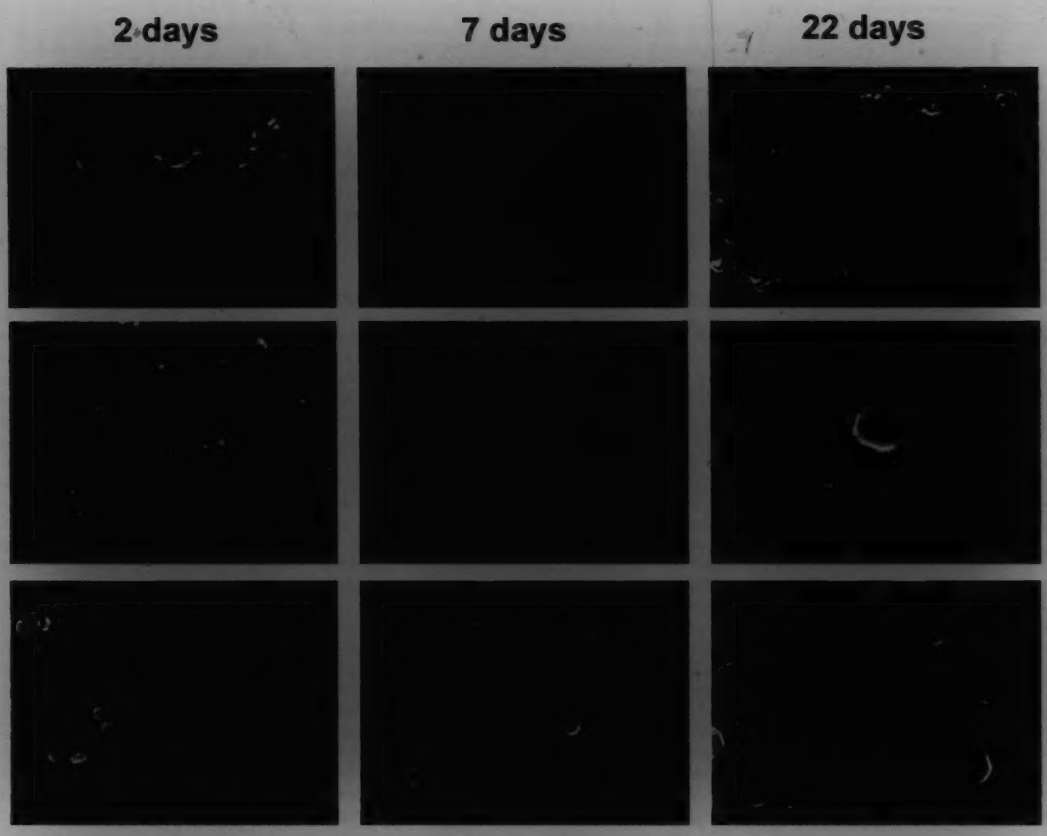

Figure 4.3 SEM images of short Au rods (a-c), 10 nm nanoparticles (d-f), and 60 nm nanoparticles (g-i) incubated in SBP solution at 37°C.

Since the insufficient stability of CTAB capped nanoparticles in SBP solution is mainly due to the destruction of the CTAB bilayer coating, it is expected that the replacement of the CTAB coverage with thiol termination might result in much higher stability, due to the covalent bonding between the gold and thiolate.[104] To verify our speculation, surface functionalization with α,ω-thiols was performed by dispersing the centrifuged gold nanoparticles in the thiol solutions. Terminations ranging from hydroxy (-OH), to ammonium ($-NH_3^+Cl^-$ and $-N(CH_3)_2H^+Cl^-$), to carboxylic acid (-COOH, certainly ionized to $-COO^-$ in the pH 7.4 SBP) were employed in the investigation.

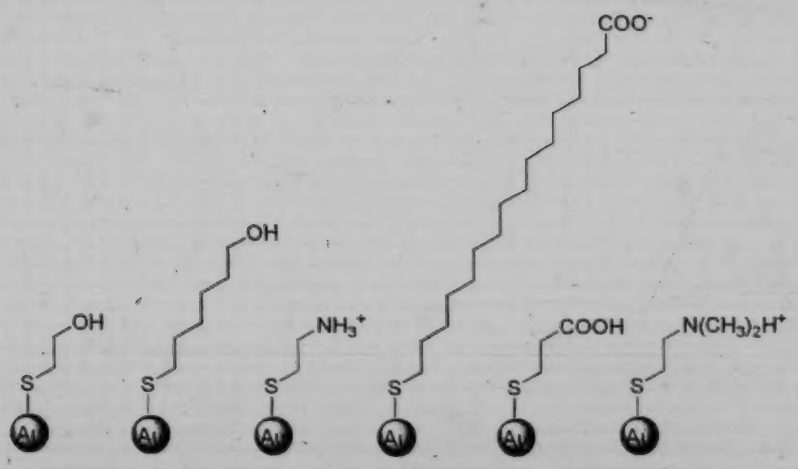

Scheme 4.3 Structures of ω-terminal thiol functionalized 10 nm gold nanoparticles.

The solutions were stored overnight to ensure completion of the reactions. Several recent publications showed that thiols were unsuccessful at displacing the CTAB bound to the length of the gold nanorods, and that they preferentially bound to the {111} ends of the rods.[105] In our research, the FT-IR spectra of those surface functionalized nanoparticles confirmed this result. For example, in the case of $HSCH_2CH_2OH$ (Figure 4.4a), the peak at ~2953 cm^{-1} is assigned to ν_{asym}(C-H) of the CH_3 terminal group of the methylene chain and ν_{sym}(C-H) of CH_3-N^+, providing evidence to the existence of unchanged CTAB bilayers.[93a] On the other hand, the 10 nm nanoparticles, the most reactive ones, were found to react with all investigated thiols probably due to the low quality packing of the CTAB layers. As shown in Figure 4.4b-d, the noticeable CH_3 peak in the former case does not exist here, revealing that the CTAB coatings on 10 nm nanoparticles can be readily displaced by the α,ω-thiols. In addition, there is a significant increase of the relative intensities of peaks at 2850 (ν_{sym}(C-H)) and 2920 cm^{-1} (ν_{asym}(C-H)) from spectra b to d, corresponding to a increase of numbers of CH_2 groups from $HSCH_2CH_2OH$ to $HS(CH_2)_{15}COOH$.[93a] Therefore, we decide to investigate the

stability of the thiol functionalized 10 nm nanoparticles in SBP solution to examine the influence of surface chemistry.

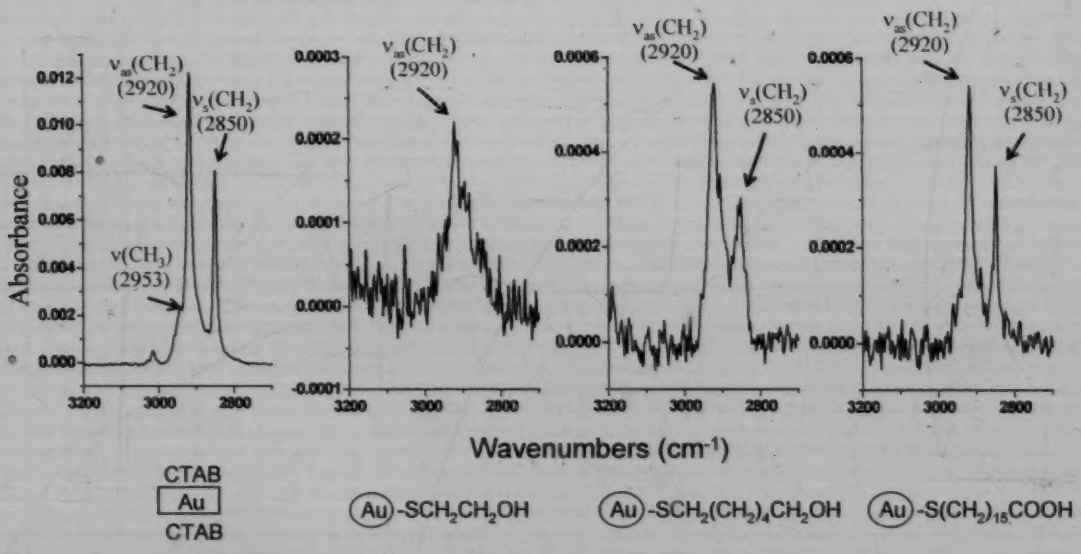

Figure 4.4 FT-IR spectra of short gold nanorods capped with undisplaced CTAB bilayers after $HSCH_2CH_2OH$ treatment (a), and 10 nm gold nanoparticles capped with various thiol monolayers (b-d) after $HSCH_2CH_2OH$, HS $CH_2(CH_2)_4CH_2OH$, $HS(CH_2)_{15}COOH$ treatment, respectively.

SEM images were taken after 7 days incubation of these thiol functionalized 10 nm gold nanoparticles in SBP solution at 37°C, and are shown in Figure 4.5. While rapid aggregation and precipitation was noted for most of the terminations, probably due to the weak repulsion between the original neutral terminal groups (-OH) as well as the charged terminal groups ($-NH_3^+$, $-N(CH_3)_2H^+$, and $-COO^-$) which were neutralized by the counter ions in solution, little fusion of the metallic nanoparticle cores was observed. These results point to a much higher stability of the thiol termination, most likely due to covalent bonding between the gold and thiolate, which matches our previous prediction. Still, oxidation of the thiolate would be expected, especially for the thiols with short methylene chains, such as $HSCH_2COOH$ and $HSCH_2CH_2NH_2 \cdot HCl$, and thus some fusion was predicted in such cases. The formation of some big particles in Figure 4.5 c,e

confirms this prediction.

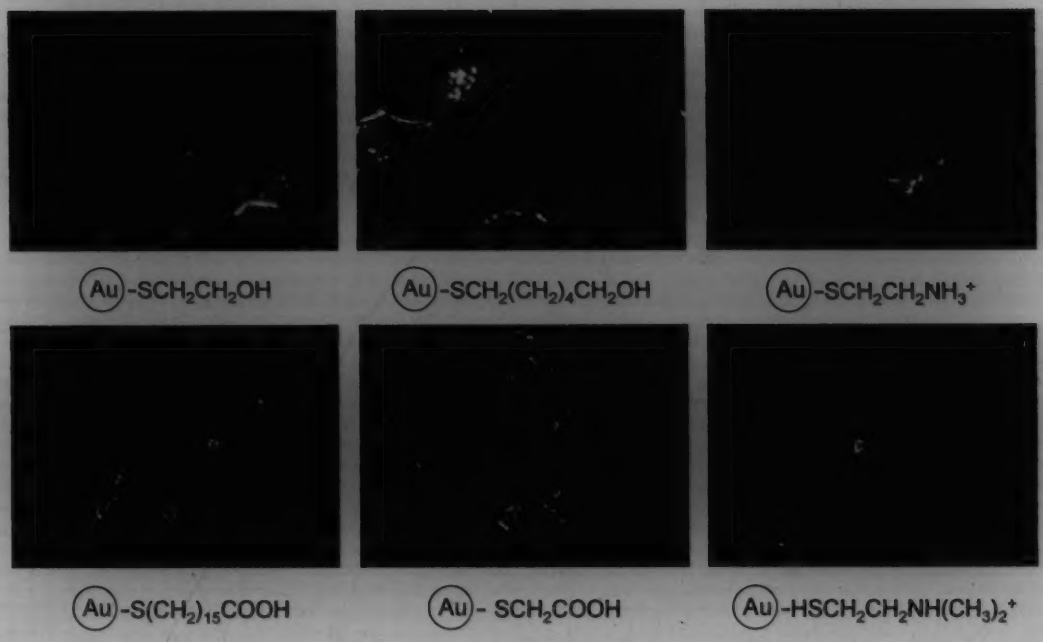

Figure 4.5 SEM images of 10 nm thiol functionalized gold nanoparticles in SBP solution for 7 days: a) $HSCH_2CH_2OH$-capped; b) $HSCH_2(CH_2)_4CH_2OH$-capped; c) $HSCH_2CH_2NH_2 \cdot HCl$-capped; d) $HS(CH_2)_{15}COOH$-capped; e) $HSCH_2COOH$-capped; f) $HSCH_2CH_2N(CH_3)_2 \cdot HCl$-capped.

Albumin is the major protein in blood plasma with a concentration of 40 g/L (~0.6 mM), which represents about half of the total proteins in blood plasma.[106] Therefore, the role of proteins in HBP was simulated by adding BSA to SBP solutions (5 g/L).[99] As outlined in Figure 4.6, the BSA obviously has a stabilizing effect on the gold short nanorods, and on the 10 nm and 60 nm nanoparticles. Neither the SEM images nor the UV-Vis spectra reveal any major change whatsoever. It is worth to note, in the high resolution SEM images, that all the gold nanoparticles are found to be capped with a thin protein layer, which seems to increase their stability greatly. Since the isoelectric point, pI, of BSA is 4.7,[100] the protein will have an overall negative charge at pH 7.4, and thus it is expected that electrostatic interactions between the cationic CTAB-terminated nanoparticles and the anionic BSA provide additional cushion to stabilize the particles

either via further electrostatic interactions or by the steric effect coming from the capped bulky protein, preventing fusion events from occurring. To summarize the effects of BSA, these results and others conducted within our laboratories suggest that amphiphilic proteins may have a strong stabilizing effect on charged nanoparticles.

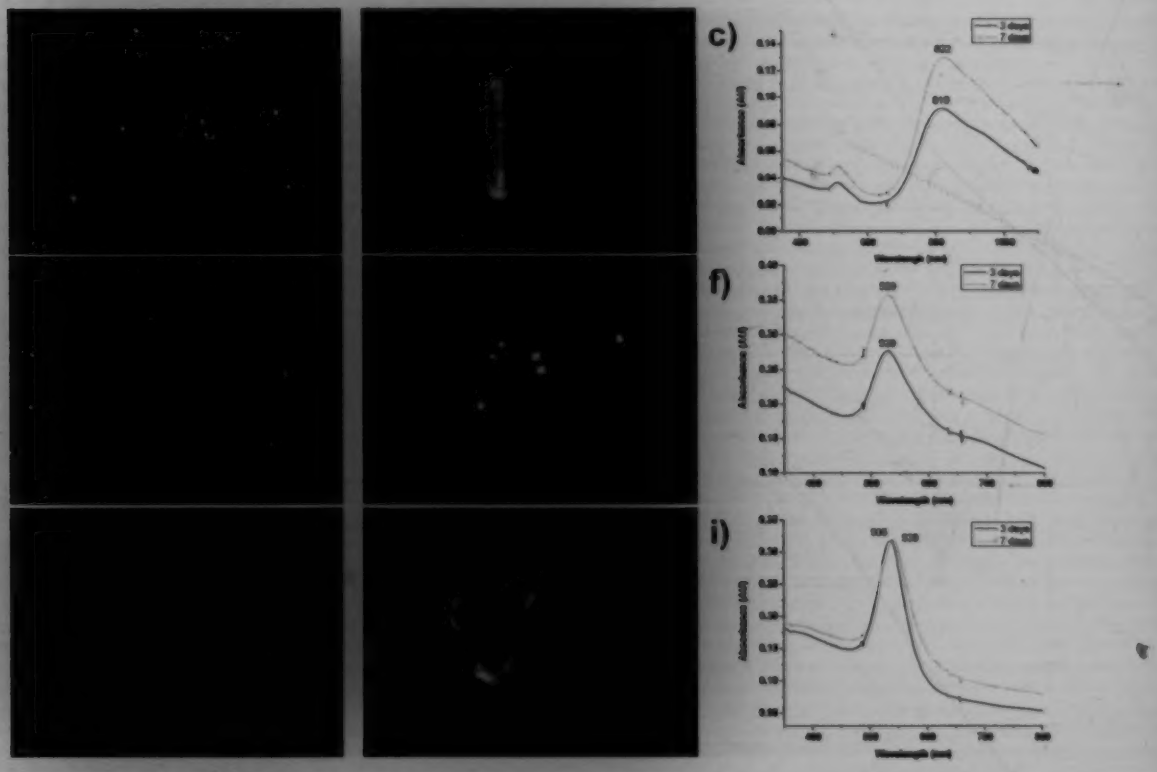

Figure 4.6 Studies demonstrating the effect of BSA on the stability of the CTAB-coated nanoparticles. The Au nanoparticles maintain their sizes and shapes in BSA containing (5 g/L) SBP solution at 37°C for 7 days. SEM images of Au nanoparticles in SBP & BSA: a-b) short nanorods immersed for 7 days; d-e) 10 nm nanoparticles immersed for 7 days; g-h) 60 nm nanoparticles immersed for 7 days. UV-Vis spectra of Au nanoparticles in SBP & BSA: c) nanorods immersed for 3 and 7 days; f) 10 nm nanoparticles immersed for 3 and 7 days; i) 60 nm nanoparticles immersed for 3 and 7 days.

To examine the influence of nanoparticle composition, silver nanoparticles were employed in similar investigation to compare their stability with gold nanoparticles. The attempts to synthesize monodisperse shape-controlled CTAB capped silver nanoparticles were not satisfying, and therefore we chose to prepare silver nanoplates by

reducing silver ions in the presence of sodium citrate and polyvinylpyrrolidone (PVP).[92] Preliminary studies, as highlighted in Figure 4.7, suggest that silver is more reactive.

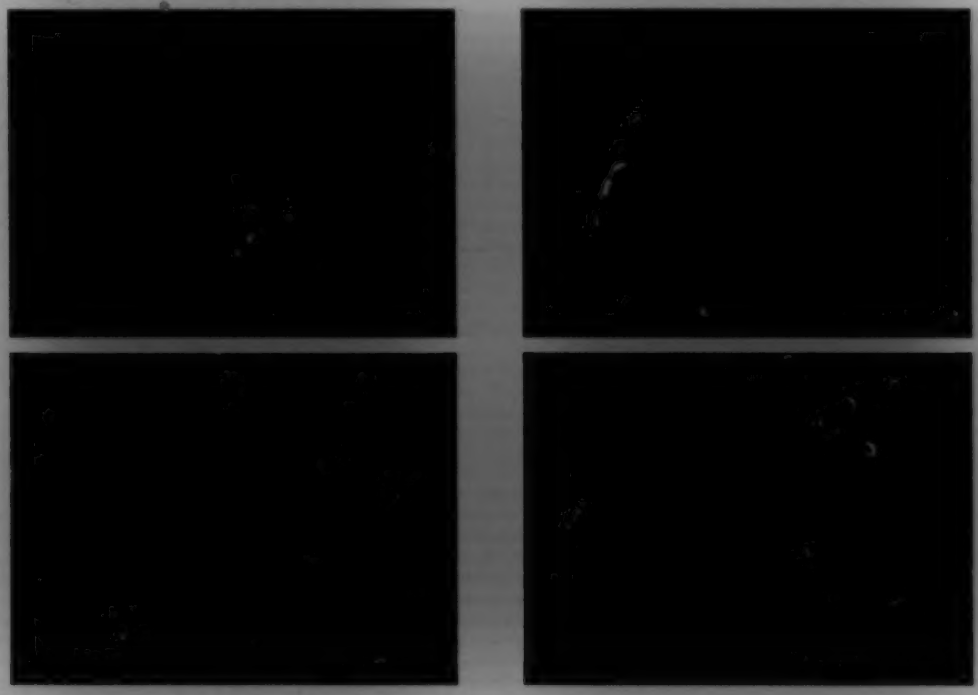

Figure 4.7 The Ag nanoparticles involved in the experiments showed lower stability than the Au nanoparticles. SEM images of the Ag nanoparticles: a) Newly prepared Ag nanoplates; b) Ag nanoplates in water for 7 days; c) Ag nanoplates in SBP solution for 1 day; d) In SBP and BSA (5 g/L) for 7 days.

More studies are required to tease out the many variables at play, but moderate agglomeration of silver nanoplates, capped with a PVP polymer, is observed after 7 days incubation in water (Figure 4.7b). In SBP solution, however, complete fusion is observed even after 1 day incubation, as shown in Figure 4.7c. The effect of protein addition in the form of BSA (5 g/L) does have a stabilizing influence, as shown in Figure 4.7d, but the obvious change of shape of the silver particles indicates that this system is more reactive. Figure 4.8 shows the shift of the UV-Vis maxima during 30 min at different BSA concentrations (5 g/L to 80 g/L). It is still unclear why the absorbance peaks shift to the shorter wavelength, which becomes more significant at high BSA

concentration, but such shifts obviously reveal certain changes on the silver nanoplates, probably corresponding to the formation of tiny silver nanoparticles (less than 10 nm) observed in Figure 4.7d. Because both shape and surface composition are different from the gold nanoparticle cases, more work is required to understand the important factors at play in this case.

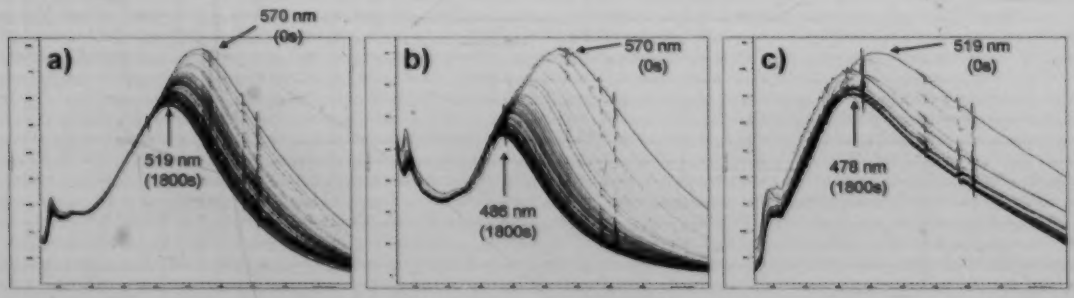

Figure 4.8 UV-Vis spectra of Ag nanoplates in SBP solution with various BSA content (measuring time interval is 30 s): a) 5 g/L BSA; b) 40 g/L BSA; c) 80 g/L BSA.

4.1.3 Conclusion

While incubating in the simulated blood plasma with or without bovine serum albumin, the gold and silver nanoparticles, of various sizes, shapes and surface chemistries, showed different stabilities. Particles of large sizes (~60 nm and above) and flat crystalline surfaces usually exhibited strong abilities to resist the SBP solution. Replacement of the capping reagents with α,ω-terminal thiols which formed covalent bonds with the gold surface atoms could largely increase the nanoparticles' stabilities. When albumin was added, the gold nanoparticles could be well preserved due to the strong interaction between BSA and gold nanoparticles. Compared to gold nanoparticles, silver nanoparticles exhibited much less stability in almost all cases. Even if albumin was added, the silver nanoparticles experienced significant

agglomeration and shape changes. The UV-Vis spectra of those particles also confirmed such results.

4.2 Interactions between Metal Nanoparticles and Human Blood

4.2.1 Introduction

In humans, blood is a fluid pumped by the heart which circulates throughout the body via the arteries, veins, and capillaries. An adult male normally has about 5 liters of blood. It carries oxygen and nutrients to the body tissues and removes carbon dioxide and other wastes as well. Blood also helps to keep our body temperature steady by controlling the loss of body heat through the skin. White blood cells and some components of blood plasma play an essential role in the body's defense against disease.

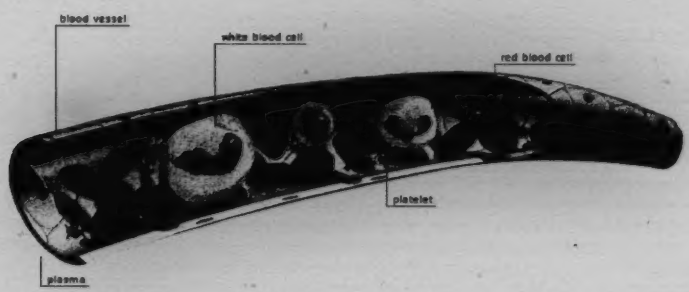

Scheme 4.4 Schematic image of the composition of blood, adapted from the Oxford Visual English Dictionary

Blood plasma is the liquid component of blood, in which the blood cells are suspended. It is a yellow colored liquid, making up about 55% of total blood volume. Essentially, blood plasma is an aqueous solution containing 92% water, 8% blood plasma proteins, and trace amounts of other materials, like hormones and inorganic electrolytes. Many vital proteins are found in blood plasma, including fibrinogen, globulins and human serum albumin.[107] Sometimes blood plasma may contain viral impurities which must be extracted through viral processing. The main functions of plasma are to serve

as transport medium for nutrients, waste materials, and hormones; to provide an appropriate environment for different blood cells; to ensure that the chemical composition of the body fluids, both outside and inside cells, remains within normal, physiological concentrations; and to ensure that blood loss is prevented promptly after injury by carrying the coagulation proteins.[107] A simple way to separate plasma from blood cells in a blood sample is by centrifugation.[108] If the blood is allowed to clot spontaneously prior to isolating the liquid component, the soluble protein fibrinogen in blood plasma is converted to insoluble fibrin. In this case, the clear liquid after centrifugation is known as blood serum, which can be regarded as blood plasma without the fibrinogen.

The other 45% of the whole blood by volume is constituted of several kinds of blood cells, such as red blood cells, white blood cells, and blood platelets. The red blood cells are the most common type of blood cells. They are biconcave disks: flattened and depressed in the center, with a dumbbell-shaped cross section. The diameter of a typical human red blood cell disk is 6-8 μm, much smaller than most other human cells. In addition, mature red blood cells lack a nucleus and other organelles, including their mitochondria and insulin receptor. As a result, the property of red blood cells is much different from other cells.[109] A typical red blood cell contains about 270 million hemoglobin molecules, with each carrying four heme groups. It is these hemoglobin molecules that provide red blood cells the ability to transport O_2 and CO_2 through the human body. White blood cells are cells of the immune system which destroy and remove old or aberrant cells and cellular debris, as well as attack infectious agents (pathogens) and foreign substances. The blood platelets are small disc-shaped bodies

about 3 μm long and occur in large numbers in circulating blood. They are responsible for blood clotting (coagulation) by changing fibrinogen into fibrin. The fibrin creates a mesh onto which red blood cells collect and clot. This clot stops more blood from leaving the body and also helps to prevent bacteria from entering the body. It is worth noting that both white blood cells and blood platelets are much less abundant than the red blood cells in blood, and thus the cell behavior in our research can be regarded basically belonging to the red blood cells.[107]

Although the SBP solution together with BSA could mimic the human blood plasma to a certain degree, it is important to carry out parallel experiments in real blood plasma to examine the nanoparticle stability and other properties in biology environment. In addition to the blood plasma, blood serum is also used as the incubation media in our research. Furthermore, in order to investigate the interaction between gold nanoparticles and blood cells, we carry out the incubation of different sized and shaped nanoparticles in whole blood as well as in blood cells alone to examine any possible uptake activity of such nanoparticles.

4.2.2 Results

In addition to the CTAB capped gold nanoparticles described in the previous section, we introduced 10 nm citrate capped gold nanoparticles to see the influence of surface charge and surface chemistry. The blood plasma was separated from donated blood by 10 min centrifugation. Four different collection tubes were used to treat the blood prior to the centrifugation, either to inhibit or facilitate clot formation. For instance, EDTA tubes, sodium citrate tubes, and plasma separator tubes (PST) are able to prevent blood

from coagulation, while the serum separation tubes (SST) contain clot activator and serum separator gel. As a result, we could obtain blood plasma from the first three tubes and get blood serum from the last ones.

Gold nanoparticles were then dispersed in the above blood plasma and blood serum and stored at 37°C for 7 days. No significant difference is found in the SEM images between the different incubation media, showing certain plasma or serum treatments did not have direct different effects on the stability of gold nanoparticles. Figure 4.9 shows the incubation results for various gold nanoparticles in the PST as examples. Again, as shown in Figures 4.9a-f, the 10 nm CTAB capped nanoparticles and both short and long nanorods exhibit their stability in the blood plasma or serum, which is similar to the results in SBP with BSA. To our surprise, slight differences were observed in case of 10 nm citrate capped nanoparticles. It was recently reported that BSA has a strong electrostatic interaction with citrate capped gold nanoparticles, greatly increasing their stability.[110] This was confirmed by our results, as most particles remained unchanged in the SEM images (Figure 4.9g). However, very occasional agglomeration and fusion has been observed as well, shown in Figure 4.9h. It is still preliminary to draw a conclusion that the ionic components of blood plasma might slightly affect the electrostatic interaction between serum albumin and citrate capped nanoparticles at the current stage, and thus more detailed investigation would certainly be helpful. We also attempted to record the UV-Vis spectra to identify the possible changes on the nanoparticles. However, the relative strong absorbance from the plasma and serum media provides a great deal of interference on the nanoparticle surface plasma spectra.

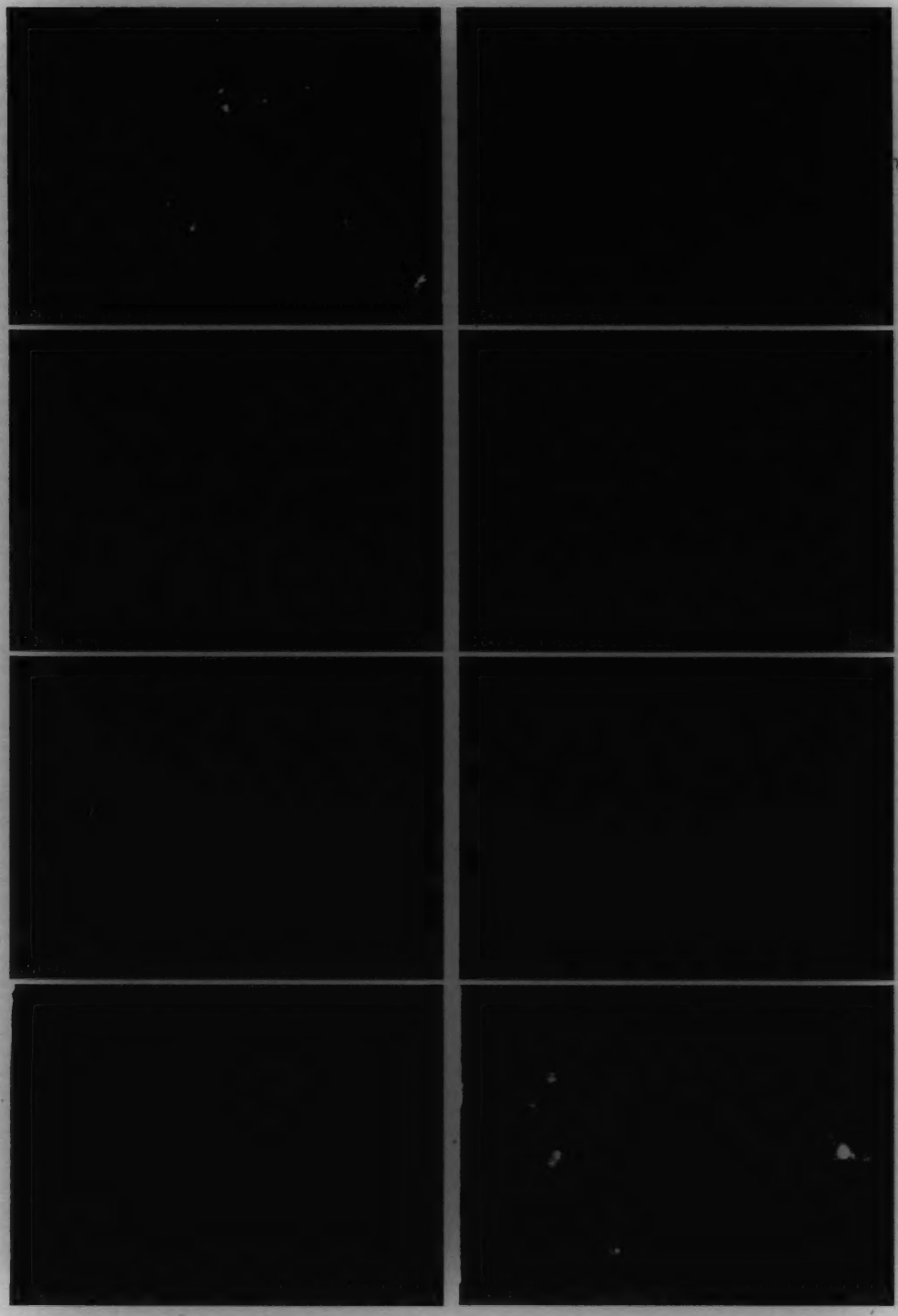

Figure 4.9 SEM images of various gold nanoparticles after 7 days incubation in human blood plasma at 37°C. a-b) short nanorods; c-d) 10 nm CTAB capped Au nanoparticles; e-f) long nanorods; g-h) 10 nm citrate capped Au nanoparticles.

Figure 4.10 shows the preliminary results of 4 hours incubation of gold nanoparticles with the whole blood or blood cells. We found that with the exception of the 10 nm nanoparticles (CTAB capped or citrate capped), other gold nanoparticles were not internalized into blood cells at all. Even for the 10 nm nanoparticles, the smallest ones, the cell uptake efficiency is very low; less than 10% of the red blood cells might have the particles inside, while others remain empty. According to the TEM results, there is no difference between using the whole blood and blood cells as the incubation media.

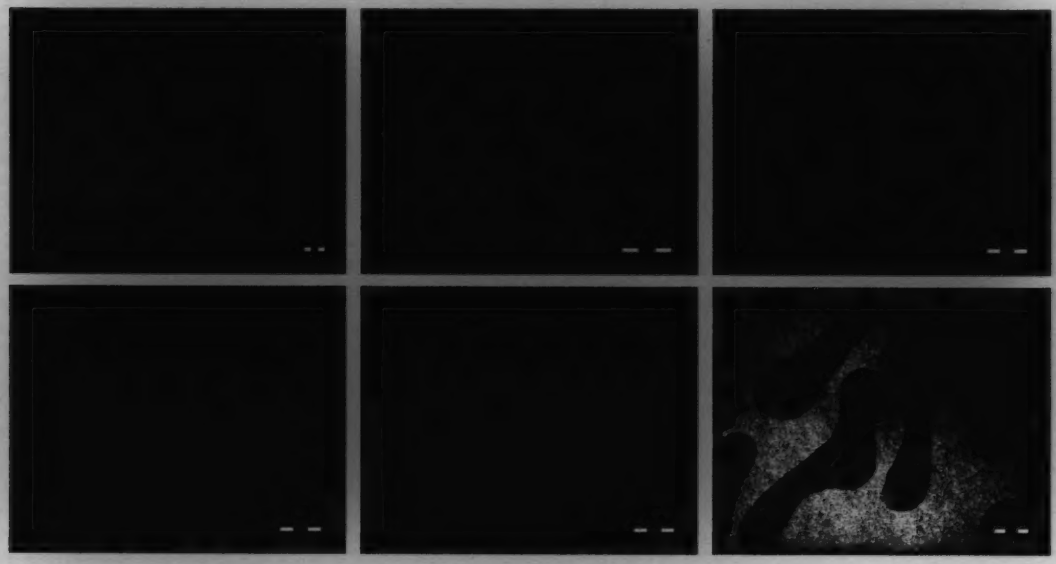

Figure 4.10 TEM images, after 4 hour incubation between gold nanoparticles and blood cells. a-c) Some 10 nm citrate capped Au nanoparticles were internalized by the red blood cells; d-e) more nanoparticles remained outside of the red blood cells; f) Au nanorods did not enter the red blood cells at all, all the cells were empty.

Our research exhibits a significant difference from some published results, in which the gold nanoparticles could be easily internalized by investigated tumor cells or macrophage cells. If further investigation reveals the red blood cells do not lose their activity after contacting with the gold nanoparticles, our results demonstrate selectivity between the normal red blood cells and tumor cells, providing a potential to gold

nanoparticles for tumor therapy. It is worth noting that the current research only demonstrates the interaction between gold nanoparticles and red blood cells. We are interested in extending the investigation to white blood cells, since they exhibit a stronger ability for particle internalization than red blood cells. Platelets might be the next investigated target due to their size similarity to nanoparticles, and potential ability to induce thrombosis while interacting with nanoparticles.

4.2.3 Conclusion

The gold nanoparticles exhibit high stability in human blood plasma and blood serum, which is similar to the results for interaction with SBP and BSA. Under current investigation conditions, very few Au nanoparticles had entered the red blood cell, most particles stayed outside. In the future, we would like to concentrate on the biological aspects of the research, including the possible effects the metal nanoparticles exert on blood proteins and possible interactions between the particles and other blood cells, such as white blood cells and platelets.

Chapter 5 Experimental Section

5.1 Synthesis of Nanocrystalline Gold Octahedra Generated from Thermal Decomposition of $HAuCl_4$ in Block Copolymers

Pretreatment of wafers. Si(111) wafers (*n*-type, P doped, 0.01-0.02 ohm-cm, 625μm thickness) purchased from Mitsubishi Silicon America were cleaned in an acetone ultrasonic bath for 10 min. The wafers were then immersed in a hot solution of H_2O_2/H_2SO_4 (1:2) for 20 min to remove organic contamination. After each cleaning step, the wafers were thoroughly rinsed with DI water (18 mega ohm, Barnstead Nanopure system) and blown dry with a nitrogen stream. The wafer was diced into small pieces for further use. Microscope slides (7.62 cm × 2.54 cm, ~1 mm thickness), purchased from Erie Scientific, were cleaned in a same way as for silicon wafers and cut into small pieces for further use.

Block copolymers. Block copolymers were purchased from Polymer Source, Inc. (www.polymersource.com) and were used without purification prior to use. In all cases, the PS-P4VP or PS-P2VP was dissolved in toluene at 70°C to make a 0.5 wt% solution and allowed to cool to room temperature.

Film preparation. In order to preload the polymers with $HAuCl_4$ (Aldrich), solid $HAuCl_4$ was dissolved in a toluene solution of the block copolymer (0.5 wt%) by stirring for at least for 12 h before use. The molar ratio of $[AuCl_4]^-$ to pyridyl groups ranges

from 0.1 to 0.7. Precursor thin films of block copolymer micelles were prepared by spin coating 50 μL of polymer solutions in toluene onto a 1 cm^2 silicon substrate (spin rate = 4000 rpm). For bulk preparation of gold nanoparticles, 50 μL of metal-loaded polymer solutions were dripped onto a 1 cm^2 silicon substrate and dried under ambient atmosphere in a fume hood.

Thermal decomposition of metal loaded polymer film. Samples were placed in an oven, in air, and dried at 150°C for 20 min to remove residual toluene. The samples were removed, and the oven temperature raised to the desired temperature. The sample was then placed in the oven and heated for the specified time.

Removal of residual block copolymer. For the bulk samples, much of the residual block copolymer can be removed via extraction with chloroform. The silicon wafer with the thermally treated bulk sample was immersed in chloroform in a glass vial and agitated in an ultrasonic bath for 20 min. The solution was then exposed to 4 cycles of centrifugation and repeated rinsing with chloroform.

Electron microscopy. Transmission electron microscopy (TEM) samples were prepared by placing a droplet of the purified gold nanocrystal solution (above, residual block copolymer removed) in chloroform onto carbon-coated 400-mesh copper grids for 25 s and then removing excess liquid using a tissue tip. TEM images were recorded on a JEOL 2010 microscope operating at 200 kV. Scanning electron microscopy (SEM) images of Au nanocrystals were recorded on a Hitachi S-4800 operating at 5-15 kV.

Surface plasmon spectroscopy of gold nanocrystals. Bulk samples purified by removal of residual block copolymers (above) were used for extinction measurements on an Agilent 8453E UV-Vis spectroscopy system.

X-ray diffraction (XRD). X-ray powder diffraction (XRD) of samples was performed on a Bruker D8 Discover equipped with a sealed Cu tube.

X-ray photoelectron spectroscopy (XPS). Spectra were taken with a Kratos Axis 165 was performed using a monochromatic Al Kα, with a photon energy of 1486.6eV. The instrument was calibrated by the measurement of C1s. The Au 4f metallic positions were also calibrated using sputtered Au films.

5.2 Block Copolymer Mediated Deposition of Metal Nanoparticles on Germanium Nanowires

Pretreatment of wafers. Si(100) wafers (*n*-type, P doped, 0.0080-0.0200 ohm-cm, 525 μm thickness) purchased from Mitsubishi Silicon America were cleaned in an acetone ultrasonic bath for 10 min. The wafers were then immersed in a hot solution of H_2O_2/H_2SO_4 (1:3) for 20 min to remove organic contamination. After each cleaning step, the wafers were thoroughly rinsed with DI water (18 MΩ, from a Barnstead Nanopure system) and blown dry with a nitrogen stream. The wafer was diced into small pieces for further use.

Block copolymers. Block copolymers were purchased from Polymer Source, Inc. (www.polymersource.com) and were used without purification prior to use. In all cases, the PS-P2VP or PS-P4VP was dissolved in toluene at 70°C to make a 0.5 or 1 wt% solution and allowed to cool to room temperature. In order to preload the polymers with $HAuCl_4$ (Aldrich) or $AgNO_3$ (Strem), solid $HAuCl_4$ or $AgNO_3$ was dissolved in a toluene solution of the block copolymer (0.5 wt%) by stirring for at least for 12 h before use.

Ge nanowire synthesis. Ge nanowires were prepared via supercritical fluid-liquid-solid (SFLS) processes described in related reference.[77a-c]

Ge nanowire (NW) dispersion. Ge NW powders (0.3 mg) were added to 20 g of toluene in a glass vial, followed by vigorous stirring. The dispersion was sealed and stored in the dark. Before each use, the dispersion was agitated in an ultrasonic bath for

20 min.

Removal of the oxide layer on Ge NWs. To a 1.5 mL microcentrifuge tube, 0.5 ml of Ge dispersion was added. The NWs were separated by centrifugation at 3000 rpm for 3 min and dried under a stream of nitrogen gas for 5 min. 0.5 ml of ethanol (95% in water) was then added to the microcentrifuge tube, and the tube was agitated in an ultrasonic bath for 5 min. The dispersion was then centrifuged again to remove the ethanol and residual toluene. This dispersion was exposed to two more cycles of rinsing with ethanol and centrifugation. The NWs were maintained in 0.5 mL of ethanol and agitated in an ultrasonic bath. Next, 0.5 mL of 10% HF (aq) was added into the 0.5 mL Ge nanowire dispersion and held for 1 min before centrifugation at 3000 rpm for 2 min. Immediately, the etched NWs were dried under a flow of nitrogen for 10 min to remove residual water and ethanol. The dried NWs were then redispersed in 0.5 mL of toluene and agitated before next step.

Galvanic Displacement on Ge NWs (no polymer; corresponds to Figure 1 in main text). A drop (~50 μL) of oxide-terminated (untreated) Ge NWs was placed onto a Si shard and allowed to dry in air. The shard was then immersed in the metal solutions for 1 min, followed by SEM analysis. For TEM analysis, 10 μL of Ge NWs solution was placed onto a copper TEM grid and allowed to dry in air. One drop of metal solution was placed on top of the grid allowed to sit for 1 min. Excess solution was removed with a corner of a tissue and allowed to dry.

Deposition Method 1 (corresponds to Scheme 1 in main text). As described in the main text, in method 1 of Scheme 1, 0.5 mL of a 0.5 wt% solution of PS-P2VP (MW = 91,500-105,000) or PS-P4VP (MW = 128000-33500), preloaded with the metal ion precursor ($HAuCl_4$ or $AgNO_3$) was mixed with 0.5 mL of a suspension hydride-terminated germanium nanowires (derived from a stock suspension of 0.3 mg of nanowires in 20 mL toluene) in a standard eppendorf, in ambient conditions. The mixture was allowed to react for one minute before centrifugation at 3000 rpm for 2 min to form a visible dark pellet. The toluene was replaced with fresh toluene, the nanowires re-dispersed with brief ultrasonication for 5 min, and the centrifugation process repeated twice to remove as much residual polymer as possible. Transmission electron microscopy (TEM) samples were prepared by placing a droplet of nanowire samples following block copolymer removal, re-suspended in ~1 mL of chloroform, onto carbon-coated 400-mesh copper grids for 25 s and then removing excess liquid using a Kimwipe tip.

Deposition Method 2 (corresponds to Scheme 1 in main text). 10 μL of the Ge NW suspension, either oxide-terminated (crude) or HF etched, were placed onto a Si substrate and dried under a stream of nitrogen. 10 μL of metal-loaded polymer solution was then spin coated onto the Si substrate (spin rate = 3000 rpm) for 1 min. The sample was then either heated, in air, in a preheated oven for the desired time, or immersed in Millipore grade water for 1 min.

Electron Microscopy. TEM images were recorded on a JEOL 2010 microscope

operating at 200 kV. Scanning electron microscopy (SEM) images were recorded on a Hitachi S-4800 operating at 5-15 kV.

X-ray photoelectron spectroscopy (XPS). XPS (Kratos Analytical, Axis-Ultra) was performed using a monochromatic Al Kα with a photon energy of 1486.6eV. Neutralizer was added to compensate the positive charging on the analyzing surface. The instrument was calibrated by the measurement of C 1s. The Ag 3d and Au 4f metallic positions were also calibrated by sputtered Ag and Au films, respectively.

Scanning Auger microcopy (SAM). SAM (JEOL, JAMP-9500F) was carried out with an electron accelerating voltage and emission current of 25 kV and 6 nA, respectively. The Auger peaks of Ge L3M45M45 (1147 eV), Ag M4N45N45 (350 eV), and Au M5N67N67 (2015 eV) were selected for the mapping. The Auger mapping for each element was obtained by plotting $(P - B)/B$, where P and B are peak and background intensities, respectively. The intensities were then scaled using the JEOL processing software for increased contrast.

5.3 Interactions between Metal Nanoparticles and Simulated Blood Plasma

Preparation of gold seeds. 250 μL 0.01 M $HAuCl_4$ was added to 7.5 mL 0.10 M CTAB solution. The mixture was then diluted to 10 mL and was stirred magnetically. To the stirred solution, 0.60 mL of ice-cold 0.010 M $NaBH_4$ was added at a time, which resulted in the formation of a brownish yellow solution. Vigorous stirring of the seed solution, which was kept at 25°C, was continued for 2 min, allowing the escape of the gas formed during the reaction.

Preparation of gold 10 and 60 nm gold nanoparticles. 200 μL 0.01 M $HAuCl_4$ was mixed with 1.6 mL of 0.10 M CTAB solution and then 1 mL of 0.060 M ascorbic acid before the solution was diluted to a total volume of 10 mL. After that, 500 μL original seed solution was diluted to 100 mL, from which 100 μL of solution was taken and injected into the growth solution to initiate the growth of 60 nm gold nanoparticles. The solution was gently mixed by inversion of the vial after the addition of every component and was aged overnight in air to ensure full formation of gold nanoparticles. If 100 μL original seed solution was injected to the growth solution instead of the dilution one, 10 nm gold nanoparticles would form in the solution.

Preparation of gold nanorods. Short and long gold nanorods were prepared in the seed mediated growth process described in the related references.[56,84b]

Preparation of silver nanoplates. Silver nanoplates were prepared in a thermal

transformation process described in the related references.[92]

Preparation of simulated blood plasma. 17.4 mg K_2HPO_4, 35.3 mg $NaHCO_3$, 27.7 mg $CaCl_2$, 30.5 mg $MgCl_2$, 22.4 mg KCl, and 805.3 mg NaCl were dissolved in water and then diluted to 100 mL. Tris (50 mM) and HCl (45 mM) were added later to adjust the final pH value to 7.4.

Surface functionalization of gold nanoparticles. According to the solubility, thiols were dissolved in either water or in CH_3OH to form a 1.0 wt% solution. The centrifuged gold nanoparticles were then dispersed in 1 mL thiol solution (1.0 wt%) for overnight reaction. After removing the unreacted thiols, the gold nanoparticles could be used for FT-IR characterization or incubation.

Incubation of gold nanoparticles in water. The centrifuged gold nanoparticles were dispersed in 1 mL water (for control experiments) and then incubated at 37°C. After 7 days incubation, the nanoparticles were purified by centrifugation for SEM imaging.

Incubation of gold nanoparticles in SBP. The centrifuged gold nanoparticles were dispersed in 1 mL SBP solution and then incubated at 37°C. 200 μL of solution were taken from the solution after 2, 7 and 22 days of incubation, and were purified by centrifugation for SEM imaging. When the thiol capped nanoparticles were incubated with SBP solution, SEM images were taken after 7 days interaction.

Incubation of gold nanoparticles in SBP and BSA. The centrifuged gold nanoparticles were dispersed in BSA containing (5 g/L) SBP solution and then incubated at 37°C. The UV-Vis spectroscopy for the solutions was taken after 3 and 7 days incubation. The SEM images were taken after 7 days incubation as well.

Incubation of silver nanoparticles. Similar experiments were carried out with silver nanoparticles. SEM images and UV-Vis spectra were taken to characterize the changes on such nanoparticles.

FT-IR spectroscopy of thiol capped gold nanoparticles. FT-IR spectra of were collected using a Nicolet Nexus 760 spectrometer with a DTGS detector and a nitrogen-purged sample chamber, with 32 scans at 4 cm^{-1} resolution.

UV-Vis spectroscopy of gold nanoparticles. The UV-Vis spectroscopy was carried out on an Agilent 8453E UV-Vis spectroscopy system.

Scanning Electron Microscopy. Typically 1.5 mL of the solution was centrifuged for 10 min to precipitate the solid. The supernatant was discarded. Then, the solid residue was redispersed in 1.5 mL water and centrifuged again. Finally the solid residue was redispersed in a suitable volume of water depending on the quantity of the residue. 50 μL of this solution was dropcast on cleaned silicon wafer and allowed to dry in open atmosphere. SEM images were recorded on a Hitachi S-4800 operating at 5-15 kV.

5.4 Interactions between Metal Nanoparticles and Human Blood

Separation of blood plasma and blood serum from whole blood. Newly donated blood was injected into four different blood collection tubes (BD Vacutainer®). While the EDTA tubes, sodium citrate tubes, and plasma separator tubes (PST) prevented blood from coagulation, the serum separation tubes (SST) accelerated the formation of clots. All the blood collection tubes were stored at 37°C for 30 min, allowing the separation between the plasma (or serum) and the blood cells in all tubes and complete formation of coagulation in SST. Centrifugation at 3000 rpm for 10 min helps to completely separate the blood plasma or serum, the top layer with a pale yellow color, from the blood.

Incubation of gold nanoparticles in human blood plasma and blood serum. The centrifuged gold nanoparticles (10 nm CTAB capped and citrate capped gold nanoparticles, CTAB capped short and long gold nanorods) were dispersed in 1 mL blood plasma or serum and then incubated at 37°C. After 7 days incubation, the gold nanoparticles were purified by centrifugation, and the SEM images were taken after that.

Incubation of gold nanoparticles in whole blood and blood cells. Citrate tubes were used to collect the donated blood in this case. Different centrifuged gold nanoparticles (10 and 60 nm CTAB capped gold nanoparticles, 10 nm citrate capped gold nanoparticles, and CTAB capped short and long gold nanorods) were dispersed in 1 mL such whole blood and then incubated at 37°C for 4 hours. The unused blood was centrifuged at 3000 rpm for 10 min and the bottom layer (blood cells) was collected. Centrifuged gold nanoparticles (same as above) were dispersed in 0.5 mL blood cells. The mixtures were

then diluted to 1 mL by phosphate buffered saline (PBS), followed with the incubation at 37°C for 4 hours.

Fixation and following treatment for blood cells. After 4 hours incubation, the cells were centrifuges at 300 g for 5 min, and the media was removed. The pelleted cells were then suspended in glutaraldehyde (2%) for 2 hours. After removing the glutaraldehyde, the cells were washed with three times PBS for 10 min each, and then were suspended in 250 μL osmic acid for 2 hours. The osmic acid was then removed and the cells were washed with three times PBS again. Ethanol with gradually increased concentrations (20% to 100%) was used to wash the cells. After rinsed with 1:1 propylene oxide/ethanol and pure propylene oxide respectively, the cells were suspended in a solution with 1:1 propylene oxide/spur resin for 24 hours. Finally, the cells were transferred to a micro centrifuge tube containing pure spur resin and were stored overnight at 60°C to allow the resin to harden. Using a microtome machine, the samples could be cut into slices and placed on carbon-coated copper TEM grids.

Electron microscopy. SEM images were recorded on a Hitachi S-4800 operating at 5-15 kV. TEM images were recorded on a Philips/FEI (Morgagni) Transmission Electron Microscope at 70 kV.

References

1. Feynman, R. P. Plenty of Room at the Bottom http://www.its.caltech.edu/~feynman/plenty.html (accessed April 10, 2007).

2. Taniguchi, N. *On the Basic Concept of Nanotechnology.* Proc. Intl. Conf. Prod. Eng., Part II; Tokyo: Japan Society of Precision Engineering, 1974; pp 18-23.

3. a) Drexler, K. E. *Nanosystems: Molecular Machinery, Manufacturing, and Computation*, 1st ed; Wiley: New York, 1992; b) Drexler, K. E. *Engines of Creation: The Coming Era of Nanotechnology*, 1st ed; Bantam Doubleday Dell: New York, 1986.

4. Mirkin C. A. *Small* **2005**, *1*, 14-16.

5. a) Creighton, J. A.; Eadon, D. GC. *J. Chem. Soc. Faraday Trans.* **1991**, *87*, 3881-3891; b) Link, S.; El-Sayed, M. A. *J. Phys.Chem. B* **1999**, *103*, 8410-8426; c) Xia, Y. N.; Halas, N. J. *MRS Bull.* **2005**, *30*, 338-348.

6. a) Qu, L. H.; Peng, X. G. *J. Am. Chem. Soc.* **2002**, *124*, 2049-2055; b) Pradhan, N.; Peng, X. G. *J. Am. Chem. Soc.* **2007**, *129*, 3339-3347.

7. a) Haruta, M.; Date, M. *Appl. Catal., A* **2001**, *222*, 427-437; b) Roucoux, A.; Schulz, J.; Patin, H. *Chem. Rev.* **2002**, *102*, 3757-3778; c) Chen, M. S.; Goodman, D. W. *Science* **2004**, *306*, 252-255.

8. Chen, C. C.; Hong, F. C. N. *Appl. Surf. Sci.* **2005**, *242*, 261-269

9. a) Alivisatos, A. P. *Science* **1996**, *271*, 933-937; b) Klimov, V. I.; Mikhailovsky, A. A.; Xu, S.; Malko, A.; Hollingsworth, J. A.; Leatherdale, C. A.; Eisler, H. J.; Bawendi, M. G. *Science* **2000**, *290*, 314-317.

10. Nanoscience and nanotechnologies: opportunities and uncertainties.

http://www.nanotec.org.uk/finalReport.htm (accessed July 29, 2004)

11. a) Whitesides, G. M.; Love, J. C. *Sci. Am.* **2001**, *285*, 38-47; b) Mijatovic, D.; Eijkel, J. C. T.; van den Berg, A. *Lab Chip*, **2005**, *5*, 492–500; c) Teo, B. K.; Sun, X. H. *J. Clust. Sci.* **2006**, *17*, 529-540

12. Wilbur, J. L.; Kumar, A.; Kim, E.; Whitesides, G. M. *Adv. Mater.* **1994**, *6*, 600- 604.

13. Kim, E.; Xia, Y. N.; Whitesides, G. M. *J. Am. Chem. Soc.* **1996**, *118*, 5722-5731.

14. Qiao, Y. H.; Wang, D.; Buriak, J. M. *Nano Lett.* **2007**, *7*, 464-469.

15. a) Piner, R. D.; Zhu, J.; Xu, F.; Hong, S. H.; Mirkin, C. A. *Science* **1999**, *283*, 661-663; b) Ginger, D. S.; Zhang, H.; Mirkin, C. A. *Angew. Chem. Int. Ed.* **2004**, *43*, 30-45.

16. Johnson, C. J.; Dujardin, E.; Davis, S. A.; Murphy, C. J.; Mann, S. *J. Mater. Chem.* **2002**, *12*, 1765-1770.

17. a) Anelli, P.-L.; Ashton, P. R.; Ballardini, R.; Balzani, V.; Delgado, M.; Gandolfi, M. T.; Goodnow, T. T.; Kaifer, A. E.; Philp, D.; Pietraszkiewicz, M.; Prodi, L.; Reddington, M. V.; Slawin, A. M. Z.; Spencer, N.; Stoddart, J. F.; Vicent, C.; Williams, D. J. *J. Am. Chem. Soc.* **1992**, *114*, 193-218; b) Fyfe, M. C. T.; Stoddart, J. F. F. *Acc. Chem. Res.* **1997**, *30*, 393- 401.

18. Percec, V.; Dulcey, A. E.; Balagurusamy, V. S. K.; Miura, Y.; Smidrkal, J.; Peterca, M.; Nummelin, S.; Edlund, U.; Hudson, S. D.; Heiney, P. A.; Hu, D. A.; Magonov, S. N.; Vinogradov, S. A. *Nature* **2004**, *430*, 764-768.

19. a) Leininger, S.; Olenyuk, B.; Stang, P. J. *Chem. Rev.* **2000**, *100*, 853-907; b) Wenz, G. *Angew. Chem. Int. Ed.* **1994**, *33*, 803-822.

20. a) Cho, A. Y. *J. Appl. Phys.* **1971**, *42*, 2074- 2081; b) Cho, A. Y. *J. Appl. Phys.* **1970**,

41, 2780- 2786.

21. a) Ulman, A. *Chem. Rev.* **1996**, *96*, 1533-1554; b) Love, J. C.; Estroff, L. A.; Kriebel, J. K.; Nuzzo, R. G.; Whitesides, G. M. *Chem. Rev.* **2005**, *105*, 1103-1169.

22. Iijima, S. *Nature* **1991**, *354*, 56-58.

23. a) Thostenson, E. T.; Ren, Z. F.; Chou, T. W. *Compos. Sci. Technol.* **2001**, *61*, 1899-1912; b) Kong, J.; Franklin, N. R.; Zhou, C. W.; Chapline, M. G.; Peng, S.; Cho, K. J.; Dai, H. J. *Science* **2000**, *287*, 622-625; c) Baughman, R. H.; Zakhidov, A. A.; de Heer, W. A. *Science* **2002**, *297*, 787-792; d) Collins, P. G.; Bradley, K.; Ishigami, M.; Zettl, A. *Science* **2000**, *287*, 1801-1804; e) Gudiksen, M. S.; Lauhon, L. J.; Wang, J.; Smith, D. C.; Lieber, C. M. *Nature* **2002**, *415*, 617-620.

24. a) Xia, Y. N.; Yang, P. D.; Sun, Y. G.; Wu, Y. Y.; Mayers, B.; Gates, B.; Yin, Y. D.; Kim, F.; Yan, Y. Q. *Adv. Meter.* **2003**, *15*, 353-389; b) Choi, H. J.; Seong, H. K.; Chang, J.; Lee, K. I.; Park, Y. J.; Kim, J. J.; Lee, S. K.; He, R. R.; Kuykendall, T.; Yang, P. D. *Adv. Meter.* **2005**, *17*, 1351-1356; c) Duan, X. F.; Huang, Y.; Cui, Y.; Wang, J. F.; Lieber, C. M. *Nature* **2001**, 409, 66-69.

25. a) Rajeshwar, K.; de Tacconi, N. R.; Chenthamarakshan, C. R. *Chem. Mater.* **2001**, *13*, 2765-2782; b) Schaller, R. D.; Klimov, V. I. *Phys. Rev. Lett.* **2004**, *92*, 186601; c) Bruchez, M.; Moronne, M.; Gin, P.; Weiss, S.; Alivisatos, A. P. *Science* **1998**, *281*, 2013-2016.

26. a) Lockman, P. R.; Mumper, R. J.; Khan, M. A.; Allen. D. D. *Drug Dev. Ind. Pharm.* **2002**, *28*, 1-13; b) Barratt. G. *Cell. Mol. Life Sci.* **2003**, *60*, 21-37; c) Moghimi, S. M.; Hunter, A.C.; Murray, J. C. *FASEB J.* **2005**, *19*, 311-330; d) Michalet, X.; Pinaud, F. F,; Bentolila, L. A.; Tsay, J. M.; Doose, S.; Li, J. J.; Sundaresan, G.; Wu, A. M.; Gambhir, S.

S.; Weiss, S. *Science* **2005**, *307*, 538-544; e) Klostranec, J. M; Chan, W, C. W. *Adv. Mater.* **2006**, *18*, 1953-1964.

27. a) Colvin, V. L. *Nat. Biotechnol.* **2003**, *21*, 1166-1170; b) Service, R. F. *Science* **2003**, *300*, 243; c) Hett, A. Nanotechnology-Small Matter, Many Unknowns. http://www.swissre.com (accessed July 5, 2005); d) Oberdorster, G.; Oberdorster, E.; Oberdorster, J. *Environ. Health Perspect.* **2005**, *113*, 823-839; e) Nel, A.; Xia, T.; Madler, L.; Li, N. *Science* **2006**, *311*, 622-627.

28. a) Pekkanen, J.; Timonen, K. L.; Ruuskanen, J.; Reponen, A.; Mirme, A. *Environ. Res.* **1997**, *74*, 24–33; b) Penttinen, P.; Timonen, K. L.; Tiittanen, P.; Mirme, A.; Ruuskanen, J.; Pekkanen, J. *Eur. Resp. J.* **2001**, *17*, 428–435; c) Peters, A.; Doring, A.; Wichmann, H. E.; Koenig, W. *Lancet* **1997**, *349*, 1582–1587; d) Peters, A.; Wichmann, H. E.; Tuch, T.; Heinrich, J.; Heyder, J. *Am. Respir. Crit. Care Med.* **1997**, *155*, 1376–1383; e) von Klot, S.; Wolke, G.; Tuch, T.; Heinrich, J.; Dockery, D. W.; Schwartz, J.; Kreyling, W. G.; Wichmann, H. E.; Peters, A. *Eur. Respir. J.* **2002**, *20*, 691–702.

29. a) Elder, A. C. P.; Gelein, R.; Finkelstein, J. N.; Cox, C.; Oberdörster, G. *Inhal. Toxicol.* **2000,** *12*, 227-246; b) Zhou, Y. M.; Zhong, C. Y.; Kennedy, I. M.; Leppert, V. J.; Pinkerton, K. E. Toxicol *Appl. Pharmacol.* **2003**, *190*, 157-169; c) Oberdörster, G.; Sharp, Z.; Atudorei, V.; Elder, A.; Gelein, R.; Kreyling, W.; Cox, C. *Inhal. Toxicol.* **2004**, *16*, 437-445; d) Oberdörster, G.; Sharp, Z.; Atudorei, V.; Elder, A.; Gelein, R.; Lunts, A.; Kreyling, W.; Cox, C. *J. Toxicol. Environ. Health* **2002**, *65A*, 1531-1543.

30. International Commission on Radiological Protection. *Ann. ICRP* **1994**, *24*, 1-300.

31. Warheit, D. B.; Overby, L. H.; George, G.; Brody, A. R. *Exp. Lung Res.* **1988**, *14*, 51-66.

32. a) Kreyling, W. G.; Semmler, M.; Erbe, F.; Mayer, P.; Takenaka, S.; Schulz, H.; Oberdörster, G.; Ziesenis, A. *J Toxicol Environ Health* **2002**, *65A*, 1513-1530; b) Oberdörster, G.; Finkelstein, J. N.; Johnston, C.; Gelein, R.; Cox, C.; Baggs, R.; et al. *Res. Rep. Health Eff. Inst.* **2000**, 96, 5-74; c) Semmler M, Seitz J, Erbe F, Mayer P, Heyder J, Oberdörster G, Kreyling, W. G. *Inhal. Toxicol.* **2004**, *16*, 453-459.

33. Schürch, S.; Gehr, P.; Hof, V. I.; Geiser, M.; Green, F. *Respir. Physiol.* **1990**, *80*, 17-32.

34. Oberdörster, G. *Philos. Trans. R. Soc. Lond. A* **2000**, 358, 2719-2740.

35. a) Nel, A. *Science* **2005**, *308*, 804-806; b) Nemmar, A.; Hoet, P. H. M.; Vanquickenborne, B.; Dinsdale, D.; Thomeer, M.; Hoylaerts, M. F.; Vanbilloen, H.; Mortelmans, L.; Nemery, B. *Circulation* **2002**, *105*, 411-414; c) Brook, R. D.; Franklin, B.; Cascio, W.; Hong, Y. L.; Howard, G.; Lipsett, M.; Luepker, R.; Mittleman, M.; Samet, J.; Smith, S. C.; Tager, I. *Circulation* **2004**, *109*, 2655-2671.

36. Gianutsos, G.; Morrow, G. R.; Morris, J. B. *Fundam. Appl. Toxicol.* **1997**, *37*, 102-105.

37. Blundell, G.; Henderson, W. J.; Price, E. W. *Ann. Trop. Med. Parasitol.* **1989**, *83*, 381-385.

38. Tinkle, S. S.; Antonini, J. M.; Rich, B. A.; Roberts, J. R.; Salmen, R.; DePree, K.; Adkins, E. J. *Environ. Health Perspect.* **2003**, *111*, 1202-1208.

39. Kim, S.; Lim, Y. T.; Soltesz, E. G.; De Grand, A. M.; Lee, J.; Nakayama, A.; Parker, J. A.; Mihaljevic, T.; Laurence, R. G.; Dor, D. M.; Cohn, L. H.; Bawendi, M. G.; Frangioni, J. V. *Nat. Biotechnol.* **2004**, *22*, 93-97.

40. a) Li, N.; Sioutas, C.; Cho, A.; Schmitz, D.; Misra, C.; Sempf, J.; Wang, M. Y.;

Oberley, T.; Froines, J.; Nel, A. *Environ. Health Perspect.* **2003**, *111*, 455–460; b) Rodoslav, S.; Laibin, L.; Eisenberg, A.; Dusica M. *Science* **2003**, *300*, 615–618.

41. Donaldson, K.; Tran, C. L. *Inhal. Toxicol.* **2002**, *14*, 5-27.

42. Somasundaran, P.; Chakraborty, S.; Qiang, Q.; Deo, P.; Wang, J.; Zhang, R. *J. Cosmet. Sci.* **2004**, *55*, S1.

43. Johnston, C. J.; Finkelstein, J. N.; Mercer, P.; Corson, N.; Gelein, R.; Oberdorster, G. *Toxicol. Appl. Pharmacol.* **2000**, *168*, 208–215.

44. a) Sayes, C. M.; Fortner, J. D.; Guo W.; Lyon, D.; Boyd, A. M.; Ausman, K. D.; Tao, Y. J.; Sitharaman, B.; Wilson, L. J.; Hughes, J. B.; West, J. L.; Colvin, V. L. *Nano Lett.* **2004**, *4*, 1881-1887; b) Dugan, L. L.; Turetsky, D. M.; Du, C.; Lobner, D.; Wheeler, M.; Almli, C. R.; Shen, C. K. F.; Luh, T. Y.; Choi, D. W.; Lin, T. S. *Proc. Natl. Acad. Sci. U.S.A.* **1997**, *94*, 9434-9439; c) Shvedova, A. A.; Castranova, V.; Kisin, E. R.; Schwegler-Berry, D.; Murray, A. R.; Gandelsman, V. Z.; Maynard, A.; Baron, P. *J. Toxicol. Environ. Health Part A* **2003**, *66*, 1909-1926; d) Monteiro-Riviere, N. A.; Nemanich, R. J.; Inman, A. O.; Wang, Y. Y. Y.; Riviere, J. E. *Toxicol. Lett.* **2005**, *155*, 377-384; e) Magrez, A.; Kasas, S.; Salicio, V.; Pasquier, N.; Seo, J. W.; Celio, M.; Catsicas, S.; Schwaller, B.; Forro, L. *Nano Lett.* **2006**, *6*, 1121-1125; f) Chen, X.; Tam, U. C.; Czlapinski, J. L.; Lee, G. S.; Rabuka, D.; Zettl, A.; Bertozzi, C. R. *J. Am. Chem. Soc.* **2006**, *128*, 6292-6293.

45. Beckett, W. S.; Chalupa, D. F.; Pauly-Brown, A.; Speers, D. M.; Stewart, J. C.; Frampton, M. W.; Utell, M. J.; Huang, L. S.; Cox, C.; Zareba, W.; Oberdorster, G. *Am. J. Respir. Crit. Care Med.* **2005**, *171*, 1129-1135.

46. a) Derfus, A. M.; Chan, W. C. W.; Bhatia, S. N. *Nano Lett.* **2004**, *4*, 11-18; b)

Kirchner, C.; Liedl, T.; Kudera, S.; Pellegrino, T.; Javier, A. M.; Gaub, H. E.; Stolzle, S.; Fertig, N.; Parak, W. J. *Nano Lett.* **2005**, *5*, 331-338; c) Cho, S. J.; Maysinger, D.; Jain, M.; Roder, B.; Hackbarth, S.; Winnik, F. M. *Langmuir*, **2007**, *23*, 1974-1980.

47. a) Shukla, R.; Bansal, V.; Chaudhary, M.; Basu, A.; Bhonde, R. R.; Sastry, M. *Langmuir*, **2005**, *21*, 10644-10654; b) Connor, E. E.; Mwamuka, J.; Gole, A.; Murphy, C. J.; Wyatt, M. D. *Small*, **2005**, *1* 325-327; c) Takahashi, H.; Niidome, Y.; Niidome, T.; Kaneko, K.; Kawasaki, H. Yamada, S. *Langmuir*, **2006**, *22*, 2-5; d) Chithrani, B. D.; Ghazani, A. A.; Chan, W. C. W. *Nano Lett.* **2006**, *6*, 662-668; e) Huff, T. B.; Hansen, M. N.; Zhao, Y.; Cheng, J. X.; Wei, A. *Langmuir*, **2007**, *23*, 1596-1599.

48. a) Burda, C.; Chen, X. B.; Narayanan, R. M.; El-Sayed, A. *Chem. Rev.* **2005**, *105*, 1025-1102; b) El-Sayed, M. A. *Acc. Chem. Res.* **2004**, *37*, 326-333; c) Alivisatos, A. P. *Science* **1996**, *271*, 933-937; d) Mulvaney, P. *Langmuir* **1996**, *12*, 788-800; e) Kelly, K. L.; Coronado, E.; Zhao, L. L.; Schatz, G. C. *J. Phys. Chem. B.* **2003**, *107*, 668-677; f) Liz-Marzan, L. M. *Langmuir* **2006**, *22*, 32-41. g) Murphy, C. J.; Sau, T. K.; Gole, A. M.; Orendorff, C. J.; Gao, J.; Gou, L.; Hunyadi, S. E.; Li, T. *J. Phys. Chem. B* **2005**, *109*, 13857-13870.

49. a) Kim, F.; Connor, S.; Song, H.; Kuykendall, T.; Yang, P. D. *Angew. Chem. Int. Ed.* **2004**, *43*, 3673-3677; b) Chen, Y.; Gu, X.; Nie, C. G.; Jiang, Z. Y.; Xie, Z. X.; Lin, C. J. *Chem. Commun.* **2005**, *33*, 4181-4183; c) Sau, T. K.; Murphy, C. J. *J. Am. Chem. Soc.* **2004**, *126*, 8648-8649.

50. a) Im, S. H.; Lee, Y. T.; Wiley, B. Y.; Xia, N. *Angew. Chem. Int. Ed.* **2005**, *44*, 2154-2157; b) Wiley, B.; Sun, Y. G.; Mayers, B.; Xia, Y. N. *Chem. Eur. J.* **2005**, *11*, 454-463; c) Sun, Y. G.; Xia, Y. N. *Science* **2002**, *298*, 2176-2179.

51. a) Ahmadi, T. S.; Wang, Z. L.; Green, T. C.; Henglein, A.; El-Sayed, M. A. *Science* **1996**, *272*, 1924-1926; b) Herricks, T.; Chen, J. Y.; Xia, Y. N. *Nano Lett.* **2004**, *4*, 2367-2371.

52. a) Puntes, V. F.; Krishnan, K. M.; Alivisatos, A. P. *Science* **2001**, *291*, 2115-2117; b) Puntes, V. F.; Zanchet, D.; Erdonmez, C. K.; Alivisatos, A. P. *J. Am. Chem. Soc.* **2002**, *124*, 12874-12880.

53. a) Jana, N. R.; Gearheart, L.; Murphy, C. J. *J. Phys. Chem. B* **2001**, *105*, 4065-4067; b) Kim, F.; Song, J. H.; Yang, P. D. *J. Am. Chem. Soc.* **2002**, *124*, 14316-14317; c) Yu, Y. Y.; Chang, S. S.; Lee, C. L.; Wang, C. R. C. *J. Phys. Chem. B* **1997**, *101*, 6661-6664; d) Link, S.; Mohamed, M. B.; El-Sayed, M. A. *J. Phys. Chem. B* **1999**, *103*, 3073-3077.

54. a) Sun, Y. G.; Gates, B.; Mayers, B.; Xia, Y. N. *Nano Lett.* **2002**, *2*, 165-168. b) Jana, N. R.; Gearheart, L.; Murphy, C. J. *Chem. Commun.* **2001**, *7*, 617-618. c) Murphy, C. J.; Jana, N. R. *Adv. Mater*. **2002**, *14*, 80-82.

55. a) Jin, R. C.; Cao, Y. C.; Hao, E. C.; Metraux, G. S.; Schatz, G. C.; Mirkin, C. A. *Nature* **2003**, *425*, 487-490; b) Jin, R. C.; Cao, Y. W.; Mirkin, C. A.; Kelly, K. L.; Schatz, G. C.; Zheng, J. G. *Science* **2001**, *294*, 1901-1903.

56. Gou, L. F.; Murphy, C. J. *Chem. Mater.* **2005**, *17*, 3668-3672.

57. Davis, D. M. *The Nature and Power of Mathematics.* Princeton University Press, 1993.

58. a) Aizawa, M.; Buriak, J. M. *J. Am. Chem. Soc*. **2005**, *127*, 8932-8933; b) Aizawa, M.; Buriak, J. M. *J. Am. Chem. Soc.* **2006**, *128*, 5877-5886.

59. Porel, S.; Singh, S.; Radhakrishnan, T. P. *Chem. Commun*. **2005**, *18*, 2387-2389.

60. Newman, J. D. S.; Blanchard, G. J. *Langmuir* **2006**, *22*, 5882.

61. a) Peng, Z. A.; Peng, X. G. *J. Am. Chem. Soc.* **2001**, *123*, 1389-1395; b) Shevchenko, E. V.; Talapin, D. V.; Rogach, A. L.; Kornowski, A.; Haase, M.; Weller, H. *J. Am. Chem. Soc.* **2002**, *124*, 11480-11485.

62. Murphy, P. J.; Stevens, G.; LaGrange, M. S. *Geochim. Cosmochim. Acta* **2000**, *64*, 479-494.

63. Cho, K.S.; Talapin, D.V.; Gaschler, W.; Murray, C.B. *J. Am. Chem. Soc.* **2005**, *127*, 7140-7147.

64. Wang, Z.L. In *Characterization of nanophase materials*; Wang, Z.L.; Ed.; Wiley-VCH Verlag GambH: Weinheim, Germany, 2000; Vol. 3, pp 45-51.

65. a) Moffitt M.; Mcmahon, L.; Pessel, V.; Eisenberg, A. *Chem. Mater.* **1995**, *7*, 1185-1192; b) Mossmer, S.; Spatz, J.P.; Moller, M.; Aberle, T.; Schmidt. J. *Macromolecules* **2000**, *33*, 4791-4798; c) Youk, J. H.; Park, M.; Locklin, J.; Advincula, R.; Yang, J.; Mays, J. *Langmuir* **2002**, *18*, 2455-2458; d) Bennett, R.D.; Xiong, G.Y.; Ren, Z.F.; Cohen, R.E. *Chem. Mater.* **2004**, *16*, 5589-5595.

66. Lofton, C.; Sigmund, W. *Adv. Funct. Mater.* **2005**, *15*, 1197-1208.

67. a) Kosonen, H.; Valkama, S.; Nykänen, A.; Toivanen, M.; Brinke, G.; Ruokolainen, J.; Ikkala, O. *Adv. Mater.* 2006, *18*, 201-205; b) Carotenuto, G.; Nicolais, L. In *Metal-polymer nanocomposites;* Nicolais, L.; Carotenuto, G.; Ed.; John Wiley & Sons, Inc.: Hoboken, NJ, 2005; Vol. 5, pp 178-179.

68. a) Orendorff, C. J.; Sau, T. K.; Murphy, C. J. *Small*, **2006**, *2*, 636-639; b) Leonhardt, U. *Nat. Photon.* **2007**, *1*, 207-208.

69. a) Geoghegana, M.; Krausch, G. *Prog. Polym. Sci.* **2003**, *28*, 261–302; b) Green, P. F.; Limary, R. *Adv. Colloid Inter. Sci.* **2001**, *94*, 53-81.

70. a) M. Y. Efremov, E. A. Olson, M. Zhang, Z. Zhang, L. H. Allen, *Phys. Rev. Lett.* **2003**, 91, 085703; b) B. H. Sohn, B. W. Seo, S. I. Yoo, *J. Mater. Chem.* **2002**, *12*, 1730-1734.

71. Haynes, C. L.; McFarland, A. D.; Zhao, L. L.; Van Duyne, R. P.; Schatz, G. C.; Gunnarsson, L.; Prikulis, J.; Kasemo, B.; Kall, M. *J. Phys. Chem. B.* **2003**, *107*, 7337-7342.

72. a) Oskam, G.; Long, J. G.; Natarajan A.; Searson, P. C. *J. Phys. D: Appl. Phys.* **1998**, *31*, 1927-1949; b) Porter, L. A.; Choi, H. C.; Ribbe, A. E.; Buriak, J. M. *Nano Lett.* **2002**, *2*, 1067-1071.

73. a) Magagnin, L.; Maboudian, R.; Carraro, C. *J. Phys. Chem. B* **2002**, *106*, 401-407; b) Aizawa, M.; Cooper, A. M.; Malac, M.; Buriak, J. M. *Nano Lett.* **2005**, *5*, 815-819.

74. a) Goldberger, J.; Hochbaum, A. I.; Fan, R.; Yang, P. D. *Nano Lett.* **2006**, *6*, 973-977; b) Wu, Y.; Xiang, J.; Yang, C.; Lu, W.; Lieber, C. M. *Nature* **2004**, *430*, 61-65.

75. a) Yasseri, A. A.; Sharma, S.; Kamins, T. I.; Li, Z.; Williams, R. S. *Appl. Phys.A: Mater. Sci. Process.* **2006**, *82*, 659-664; b) Sun, X. H.; Li, C. P.; Wong, H. B.; Lee, C. S.; Lee, S. T.; *Inorg. Chem.* **2002**, *41*, 4331-4336; c) Kim, Y. T.; Ohshima, K.; Higashimine, K.; Uruga, T.; Takata, M.; Suematsu, H.; Mitani, T. *Angew. Chem., Int. Ed.* **2006**, *45*, 407-411; d) Qin, L. D.; Park, S.; Huang, L.; Mirkin, C. A. *Science* **2005**, *309*, 113-115.

76. a) Qu, L. T. Dai, L. M. *J. Am. Chem. Soc.* **2005**, *127*, 10806-10807; b) Qu, L. T.; Dai, L. M.; Osawa, E. *J. Am. Chem. Soc.* **2006**, *128*, 5523-5532.

77. a) Hanrath, T.; Korgel, B. A. *J. Am. Chem. Soc.* **2002**, *124*, 1424-1429; b) Hanrath, T.; Korgel, B. A. *Adv. Mater.* **2003**, *15*, 437-440; c) Lu, X.; Fanfair, D. D.; Johnston, K. P.; Korgel, B. A. *J. Am. Chem. Soc.* **2005**, *127*, 15718-15719; d) Hanrath, T.; Korgel, B. A. *J.*

Am. Chem. Soc. **2004**, *126*, 15466-15472; e) Adhikari, H.; Marshall, A. F.; Chidsey, C. E. D.; McIntyre, P. C. *Nano Lett.* **2006**, *6*, 318-323; f) Kamins, T. I.; Li, X.; Williams R. S.; Liu, X. *Nano Lett.* **2004**, *4*, 503-506.

78. R. Glass, M. Moller and J. P. Spatz, Nanotechnology, 2003, 14, 1153.

79. Zhang, J.; Gao, Y.; Alvarez-Puebla, R.; Buriak J. M.; Fenniri, H. *Adv. Mater.* **2006**, *18*, 3233-3237.

80. Zsigmondy, R.; Thiessen, P. A. *Das Kolloide Gold*; Veragsges.: Leipzig, 1925.

81. Turkevich, J.; Stevenson, P. C.; Hillier, J. *Discuss. Faraday Soc.* **1951**, *11*, 55-75.

82. a) Brown, K. R.; Natan, M. J. *Langmuir* **1998**, *14*, 726-728; b) Brown, K. R.; Walter, D. G.; Natan, M. J. *Chem. Mater.* **2000**, *12*, 306-313.

83. a) Henglein, A.; Meisel, D. *Langmuir* **1998**, *14*, 7392-7396; b) Henglein, A.; Giersig, M. *J. Phys. Chem. B* **1999**, *103*, 9533-9539; c) Henglein, A. *J. Phys. Chem. B* **2000**, *104*, 1206-1211.

84. a) Busbee, B. D.; Obare, S. O.; Murphy, C. J. *Adv. Mater.* **2003**, *15*, 414-416; b) Gole, A.; Murphy, C. J. *Chem. Mater.* **2004**, *16*, 3633-3640.

85. Jana, N. R.; Gearheart, L.; Murphy, C. J. *Chem. Mater.* **2001**, *13*, 2313-2322.

86. a) Nemmar, A.; Hoylaerts, M. F.; Hoet, P. H. M.; Dinsdale, D.; Smith, T.; Xu, H. Y.; Vermylen, J.; Nemery, B.; Nemery, B. *Am. J. Respir. Crit. Care Med.* **2002**, *166*, 998-1004; b) Nemmar, A.; Hoet, P. H. M.; Dinsdale, D.; Vermylen, J.; Hoylaerts, M. F.; Nemery, B. *Circulation* **2003**, *107*, 1202-1208; c) Radomski, A.; Jurasz, P.; Alonso-Escolano, D.; Drews, M.; Morandi, M.; Malinski, T.; Radomski, M. W. *Br. J. Pharmacol.* **2005**, *146*, 882–893; d) Schwalbe, M.; Pachmann, K.; Hoeffken, K.; Clement, J. H. *J. Phys.:Condens. Matter* **2006**, *18*, S2865-S2876; e) Bhattacharya, R.; Patra, C. R.;

Verma, R.; Kumar, S.; Greipp, P. R.; Mukherjee, P. *adv. Mater.* **2007**, *19*, 711-716.

87. a) Mehta, D.; Bhattacharya, J.; Matthay, M. A.; Malik, A. B. *Am. J. Physiol. Lung Cell Mol. Physiol.* **2004**, *287*, L1081-L1090; b) Heckel, K.; Kiefmann, R.; Dorger, M.; Stoeckelhuber, M.; Goetz, A. E. *Am. J. Physiol. Lung Cell Mol. Physiol.* **2004**, *287*, L867-L878.

88. Kato, T.; Yashiro, T.; Murata, Y.; Herbert, D. C.; Oshikawa, K.; Bando, M.; Ohno, S.; Sugiyama, Y. *Cell Tiss. Res.* **2003**, *311*, 47-51.

89. Rejman, J.; Oberle, V.; Zuhorn, I. S.; Hoekstra, D. *Biochem. J.* **2004**, *377*, 159-169.

90. a) Perez, J. M.; Josephson, L.; Weissleder, R. *ChemBioChem* **2004**, *5*, 261-264; b) Saleh, A.; Schroeter, M.; Jinkmanns, C.; Hartung, H. P.; Modder, U.; Jander, S. *Brain* **2004**, *127*, 1670-1677; c) Dardzinski, B. J.; Schmithorst, V. J.; Holland, S. K.; Boivin, G. P.; Imagawa, T.; Watanabe, S.; Lewis, J. M.; Hirsch, R. *Magn. Res. Imaging* **2001**, *19*, 1209-1216.

91. a) Moghimi, S. M.; Hunter, A. C.; Murray, J. C. Pharmacol. Rev. 2001, 53, 283-318; b) Adams, M. L.; Lavasanifar, A.; Kwon, G. S. *J. Pharm. Sci.* **2003**, *92*, 1343-1355; c) Allen, T. M.; Cullis, P. R. *Science* **2004**, *303*, 1818-1822.

92. Metraux, G. S.; Mirkin, C. A. *Adv. Mater.* **2005**, *17*, 412-415.

93. a) Nikoobakht, B.; El-Sayed, M. A. *Langmuir* **2001**, *17*, 6368-6374; b) Sau, T. K.; Murphy, C. J. *Langmuir* **2005**, *21*, 2923-2929.

94. Shukla, S.; Priscilla, A.; Banerjee, M.; Bonde, R. R.; Ghatak, J.; Satyam, P. V.; Sastry, M. *Chem. Mater.* **2005**, *17*, 5000-5005; b) Chen, J.; Saeki, F.; Wiley: B. J.; Cang, H.; Cobb, M. J.; Li, Z. Y.; Au, l.; Zhang, H.; Kimmey, M. B., Li, X.; Xia, Y. *Nano Lett.* **2005**, *5*, 473-477.

95. Yang, P. H.; Sun, X.; Chiu, J. F.; Sun, H.; He, Q. Y. *Bioconjugate Chem.* **2005**, *116*, 494-496.

96. a) Hirsch, L. R.; Stafford, R. J.; Bankson, J. A.; Sershen, S. R.; Rivera, B.; Price, R. E.; Hazle, J. D.; Halas, N. J.; West, J. L. *Proc. Natl. Acad. Sci. U.S.A.* **2003**, *100*, 1549-1554; b) Loo, C.; Lin, A.; Hirsch, L.; Lee, M. H.; Barton, J.; Halas, N.; West, J.; Drezek, R. *Technol. Cancer Res. Treat.* **2004**, *3*, 33-40; c) Hainfeld, J. F.; Slatkin, D. N.; Smilowitz, H. M. *Phys. Med. Biol.* **2004**, *49*, N309-N315.

97. Kokubo, T.; Kushitani, H.; Sakka, S.; Kitsugi, T.; Yamamuro, T. *J. Biomed. Mater. Res.* **1990**, 24, 721-734.

98. a) Canham, L. T.; Reeves, C. L.; Newey, J. P.; Houlton, M. R.; Cox, T. I.; Buriak, J. M.; Stewart, M. P. *Adv. Mater.* **1999**, *11*, 1505-1507; b) Dorozhkina, E. I.; Dorozhkin, S. V. *Colloids and Surf. A* **2002**, 210, 41-48; c) Dorozhkina, E. I.; Dorozhkin, S. V. *Colloids and Surf. A* **2003**, 223, 231-237; d) Dorozhkin, S. V.; Dorozhkina, E. I. *J. Mater. Sci.* **2005**, *40*, 6417-6422.

99. Dorozhkin, S. V.; Dorozhkina, E. I. *Colloids and Surf. A* **2003**, 215, 191-199.

100. a) Burt, J. L.; Gutierrez-Wing, C.; Miki-Yoshida, M.; Jose-Yacaman, M. *Langmuir* **2004**, *20*, 11778-11783; b) Singh, A. V.; Bandgar, B. M.; Kasture, M.; Prasad, B. L. V.; Sastry, M. *J. Mater. Chem.* **2005**, *15*, 5115-5121.

101. Gao, J. X.; Bender, C. M.; Murphy, C. J. *Langmuir* **2003**, *19*, 9065-9070.

102. Gole, A.; Orendorff, C. J.; Murphy, C. J. *Langmuir* **2003**, *20*, 7117-7122.

103. a) Shipway, A. N.; Lahav, M.; Gabai, R.; Willner, I. *Langmuir* **2000**, *16*, 8789-8795; b) Cumberland, S. L.; Strouse, G. F. *Langmuir* **2001**, *18*, 269-276; c) Cheng, W. L.; Dong, S. J.; Wang, E. K. *Angew. Chem., Int. Ed.* **2003**, *42*, 449-452; d) Li, D.; Huang Y. J.; Li, J.

H. *J. Colloid Interface Sci.* **2005**, *283*, 440-445.

104. a) Weisbecker, C. S.; Merritt, M. V.; Whitesides, G. M. *Langmuir* **1996**, *12*, 3763-3772; b) Mayya, K. S.; Patil, V.; Sastry, M. *Langmuir* **1997**, *13*, 3944-3947; c) Aslan, K.; Perez-Luna, V. H. *Langmuir* **2002**, *18*, 6059-6065; d) Lin, S. Y.; Tsai, Y. T.; Chen, C. C.; Lin, C. M.; Chen, C. H. *J. Phys. Chem. B* **2004**, *108*, 2134-2139.

105. a) Chang, J. Y.; Wu, H. M.; Chen, H.; Ling, Y. C.; Tan, W. H. *Chem. Commun.* **2005**, 1092-1094; b) Thomas, K. G.; Barazzouk, S.; Ipe, B. I.; Joseph, S. T. S.; Kamat, P. V. *J. Phys. Chem. B* **2004**, *108*, 13066-13068; c) Sudeep, P. K.; Joseph, S. T. S.; Thomas, K. G. *J. Am. Chem. Soc.* **2005**, *127*, 6516-6517.

106. Curry, S.; Mandelkow, H.; Brick, P.; Franks, N. *Nat. Struct. Biol.* **1998**, *5*, 827-835.

107. *The Oxford Companion to the Body*; Blakemore, C. Jennett S.; Eds.; Oxford University Press: New York, NY, 2002.

108. Morel, F. M. M.; Baker, R. F.; Wayland, H. *J. Cell Biol.* **1971**, *48*, 91-100.

109. Bratosin, D.; Estaquier, J.; Petit, F.; Arnoult, D.; Quatannens, B.; Tissier, J. P.; Slomianny, C.; Sartiaux, C.; Alonso, C.; Huart, J. J.; Montreuil, J.; Ameisen, J. C. *Cell Death Differ.* **2001**, *8*, 1143-1156.

110. a) Brewer, S. H.; Glomm, W. R.; Johnson, M. C.; Knag, M. K.; Franzen, S. *Langmuir* **2005**, 21, 9303-9307; b) Ao, L. M.; Gao, F.; Pan, B. F.; Cui, D. X.; Gu, H. C. *Chin. J. Chem.* **2006**, *24*, 253-256; c) Shang, L.; Wang, Y. Z.; Jiang, J. G.; Dong, S. J. *Langmuir* **2007**, *23*, 2714-2721.